ADDIS ABABA UNIVERSITY

INSTITUTE OF TECHNOLOGY

SCHOOL OF CIVIL AND ENVIRONMENTAL ENGINEERING

Investigation of the potential use of wire mesh-epoxy composite for flexural retrofitting of reinforced concrete beams

A thesis in structural engineering

By Girma Kebede

June 2019

Addis Ababa

A thesis

Submitted in the partial fulfillment of the requirements for the degree of Master of Science

Declaration

I certify that this research work entitled “investigation of the potential use of wire mesh-epoxy composite for flexural retrofitting of reinforced concrete beams” is my own work. The work has not been presented elsewhere for assessment and award of any degree or diploma. Any external material that has been used from other sources has been duly acknowledged.

Name: Girma Kebede

Signature: _____

Addis Ababa Institute of technology

Date of submission: June 2019

Acknowledgement

Above all else, I would like to praise the almighty lord for giving me the strength and patience to see the end of this task. He has never left my side my entire life and for that, I am eternally grateful.

My paramount gratitude goes to my esteemed advisor, Dr-Ing Adil Zekaria for his relentless concern towards this thesis, helpful guidance and pushing me to do my best at every step. He has inspired me immensely throughout the program and it has been such a privilege to be taught by him and work with him on this thesis.

I would like to extend a great deal of gratitude and appreciation towards Mr. Biniam Fantahun, Mrs. Wubet G/Eyesus, Mr. Demis Melaku and Mr. Fikiru Bedada of AAiT Material Test Laboratory, for their support during the laborious experimental setups and works.

I would also like to thank Mr. Abenezer Nigussie and Mr. Samuel Tilahun, my friends and colleagues, for their support and assistance throughout my time at AAiT. I cherish every single moment I have spent with them.

Finally yet importantly, my deepest gratitude goes to my family and Ms. Eyerusalem Beyene for their encouragement and love. I am forever indebted to them.

Contents

List of figures

List of tables

Notations

Chapter 2

$\mu_\epsilon = strain\ ductility$

$\Delta_y = yield\ displacement$

$\epsilon = total\ strain$

$U = Linear\ deformation\ in\ the\ x\text{-}direction$

$\epsilon_y = yield\ strain$

$\sigma = normal\ stress$

$\epsilon_m = maximum\ strain$

$E = young's\ modulus$

$\mu_\emptyset = curvature\ ductility$

$dx = differential\ dimension\ in\ the\ x - direction$

$\mu_\Delta = displacement\ ductility$

$dy = differential\ dimension\ in\ the\ y - direction$

$\emptyset_m = maximum\ curvature$

$dz = differential\ dimension\ in\ the\ z - direction$

$\emptyset_y = yield\ curvature$

U = strain energy density

$\Delta_p = full\ plastic\ displacement$

$e_x = strain\ in\ the\ x - direction$

$mm = millimeter$

$MPa = mega\ Pascal$

$kN = kilo\text{-}newton$

$f_{cm} = mean\ compressive\ strength\ of\ concrete$

$f_{ci} = principal\ compressive\ stress$

$f_s = reinforcement\ stress$

$\varepsilon_{ci} = compressive\ principal\ strain$

$E_S = young's\ modulus\ of\ reinforcement$

$\varepsilon_p = peak\ compressive\ strain$

$\varepsilon_s = reinforcement\ strain$

$f_p = peak\ compressive\ stress$

$\varepsilon_y = reinforcement\ yield\ strain$

$f'_c = unconfined\ uniaxial\ concrete\ cylinder\ strength$

$\varepsilon_{sh} = strain\ at\ the\ onset\ of\ strain\ hardening$

$\varepsilon_u = reinforcement\ ultimate\ strain$

$\varepsilon_0 = unconfined\ uniaxial\ concrete\ cylinder\ strength$

$f_y = yield\ strength\ of\ steel$

$f_u = ultimate\ strength\ of\ steel$

$P = strain\ hardening\ parameter$

$P_s(x) = steel\ tensile\ force\ at\ a\ distance\ x\ from\ a\ crack$

$E_{sh} = strain\ hardening\ modulus$

$P_c(x) = concrete\ tensile\ force\ at\ a\ distance\ x\ from\ a\ crack$

$E_c = initial\ tangent\ modulus\ of\ elasticity$

$As = cross\ sectional\ area\ of\ steel\ bar$

$\sigma_1^c = smeared\ (average) concrete$

$\rho = reinforcement\ steel\ ratio\ tensile\ strength$

$\varepsilon_1^c = smeared\ (average) concretetensile\ strain$

$\bar{\varepsilon}_s(x) = steel\ strain\ at\ a\ distance\ x\ from\ a\ crack$

$f_{so} = steel\ tensile\ stress$

$Ac = area\ of\ net\ concrete\ section$

$f_s(x) = steel\ stress\ at\ a\ distance\ x\ from\ a\ crack$

$\varepsilon_c(x) = concrete\ strain\ at\ a\ distance\ x\ from\ a\ crack$

$\sigma_c(x) =\ concrete\ tensile\ stress\ at\ \ a\ distance\ x\ from\ a\ crack$

$M = bending\ moment$

$T_C = critical\ section\ reinforcing\ bar\ tension$

$V = shear\ force\ acting\ on\ a\ shear\ span$

$v_c = shear\ stress\ in\ the\ critical\ zone$

$y = distance\ from\ the\ neutral\ axis\ to\ the\ bottom\ of\ the\ beam$

$v_{max} = maximum\ shear\ stress$

$v_{avg} = average\ shear\ stress$

$I = moment\ of\ inertia$

$m_b = magnification\ factor\ defined\ by\ the\ \ ratio\ of\ v_{max}\ and\ v_{avg}$

$v = shear\ flow\ (average\ shear\ stress)$

$z_0 = lever\ arm\ calculated\ from\ conventionalflexural\ theory$

$b = width\ of\ a\ beam$

$z_c = actual\ moment\ arm\ at\ the\ cricitcal\ section$

$a_C = span\ length\ between\ two\ cracks$

$m_a = magnification\ factor\ defined\ by\ the\ ratio\ of\ z_0\ and\ z_c$

$dA = differential\ area$

$f'_t = limiting\ tensile\ stress$

$Q = first\ moment\ of\ area$

$d_s = depth\ to\ level\ of\ bottom\ reinforcement$

$T = tension\ force\ in\ the\ reinforcement$

$f_{ck} = chracterstic\ compressive\ strength$

$V_{cr,s} = inclined\ shear\ cracking\ load$

$\tau_{pes} =\ plate\ end\ shear\ stress$

$f'_r = modulus\ of\ rupture$

$S = section\ modulus$

$b_{red} = web\ breadth$

$k_1 = coefficient\ of\ constant\ factors$

$\tau_{com} = composite\ end\ shear\ stress$

$\rho = steel\ reinforcement\ ratio$

$V_{com} =\ composite\ end\ shear\ force.$

$d = effective\ depth$

$a_c = distance\ of\ outer\ flexural\ cracks\ from\ the\ support$

$a = actual\ shear\ span$

$a_L = fictitious\ shear\ span$

Acronyms

RC = reinforced concrete

RCC = reinforced cement concrete

FRP = fiber reinforced polymer

CFRP = carbon fiber reinforced polymer

GFRP = glass fiber reinforced polymer

AFRP = aramid fiber reinforced polymer

FEA = finite element analysis

FEM = finite element method

NLFEA = nonlinear finite element analysis

LVDT = linear variable differential transducer

ACI = American concrete institute

DSFM = disturbed stress field model

MCFT = modified compression field theory

CESM = composite end shear model

AAIT=Addis Ababa institute of technology

ABSTRACT

When a structural element is found to be inadequate, it can either be demolished and replaced or modified with retrofitting. Considering the economic loss and inconvenience that can be incurred from demolition, it is ideal to retrofit structural elements whenever possible. In this thesis, the possibility of using a relatively new technique (i.e. wire mesh-epoxy composite) for flexural retrofitting of reinforced concrete beams is investigated. The investigation was carried out through experimental study, numerical simulations and analytical study on undamaged and predamaged specimens. Furthermore, the effect of the technique on the ductility and energy absorption capacity of reinforced concrete beams has been studied.

The experimental investigation was carried out on undamaged and predamaged specimens. The experimental program was designed to scrutinize and understand the effect of the wiremesh-epoxy composite on the flexural capacity of reinforced concrete beams. Ductility and energy absorption capacity of the retrofitted specimens were also particular interests in the experimental investigation.

In addition to the experimental investigation, this thesis incorporates a nonlinear finite element analysis of undamaged and predamaged specimens using a finite element software named VecTor. Furthermore, based on the results obtained from the experimental investigation and the non-linear finite element analysis, an analytical investigation was carried out on a peculiar kind of failure that occurred due to the attachment of the wire mesh-epoxy composite.

The experimental and nonlinear finite element analysis revealed that the wire mesh-epoxy composite has the potential to enhance the flexural capacity of reinforced concrete beams considerably. However, a considerable loss of ductility and energy absorption capacity was observed in the retrofitted specimens. Finally yet importantly, the analytical model adopted after the analytical investigation proved to be effective and accurate in predicting the failure load.

1. Introduction

1.1 General

Reinforced concrete structures often have to face modification and improvement of their performance during their service life. The main contributing factors are change in their use, new design standards, deterioration due to corrosion in the steel caused by exposure to an aggressive environment and accidental events such as earthquakes. In such circumstances, there are two possible solutions: replacement or retrofitting. Full structure replacement might have detrimental disadvantages such as high costs for material and labor, a stronger environmental impact and inconvenience due to interruption of the function of the structure. When possible, it is often better to repair or upgrade the structure by retrofitting. (Heiza et.al, 2014)

In the last few decades, the development of strong epoxy glue has led to a technique, which has great potential in the field of upgrading structures. The technique involves gluing steel plates or fibre reinforced polymer (FRP) to the surface of the concrete. The plates then act compositely with the concrete and help to carry the loads. In some circumstances, Existing components can be modified to improve the performance of elements that are connected to them.(Heiza.et.al,2014)

The necessity to upgrade structural elements may arise from unexpected load increment due to unforeseen incidents, damage of structural parts, improvement of existing structural elements so as to improve serviceability, etc. (Aalto,2016)

In general strengthening can be achieved through either of the following methods.

- ✓ Replacing poor quality or defective material by better quality material
- ✓ Attaching additional load-bearing material

When selecting between these methods of strengthening, the following factors need to be considered.

- ✓ Magnitude of strength increment required.
- ✓ Effects of changes in relative member stiffness.
- ✓ Size of project.
- ✓ Environmental condition.
- ✓ In-place concrete strength and substrate integrity.

- ✓ Dimensional/clearance constraints.
- ✓ Availability
- ✓ Operational constraints
- ✓ Availability of materials, equipment and qualified man power.
- ✓ Construction cost, maintenance cost and life cycle cost.

There are many literatures concerning the structural feasibility of the above retrofitting techniques. They all emphasize that these methods can provide satisfactory results up on application. Most of these literatures direct their focus towards specific set of structural loads; especially towards flexural and shear loads. The reason behind this is the fact that building structures are mainly subjected to these kinds of loads. Furthermore, these studies tend to focus only on the strengthening of undamaged specimens. As a result, the outcome of these studies can be reproached on the basis that structural elements always incur certain degree of damage during their service life. When it comes to their economic or environmental feasibility, there is a lot that has to be done. This on its own shows that there is still a possibility of coming up with methods that can be as effective as these techniques and that are also an improvement in a multitude of aspects. In addition to this, analytical investigation need to be included in the studies so that incorporating the retrofitting schemes in design codes becomes a possibility.

The invention of epoxy glue has made it possible to use different kinds of plates and fibers for retrofitting purposes. Wire mesh materials have been used for retrofitting purposes mainly as ferrocement laminates. Although this method is applicable, it still has its own drawbacks. Many researches that have been conducted in relation to ferrocement laminates have indicated that the technique has shortcomings when it comes to resistance against delamination or long-term use. The low tensile strength of mortar subjects the laminates to an early stage cracking which exposes the wiremesh to environmental moisture that results in corrosion. These shortcomings can be mitigated by using epoxy as a laminating and bonding agent instead of mortar. The higher tensile strength of epoxy resin makes it an ideal choice for replacing mortar as a binding or laminating agent.

In this thesis, the capability of wire mesh-epoxy composite for flexural retrofitting of beams is investigated. The investigation is intended to be carried out through experimental tests, non linear

finite element analysis and analytic models. Along with the flexural capacity, the effect of the technique on aspects like ductility and energy absorption capacity will be investigated.

1.2 Statement of the problem

In recent decades, many techniques have been developed for flexural retrofitting of RC beam elements. Although these techniques have proven to be effective, there are still shortcomings when it comes to their applicability. These shortcomings are usually inherent to their cost, unavailability or structural behavior. Furthermore, most researches do not include analytical studies in their investigation which makes it difficult to incorporate these techniques in design schemes. Another factor that studies usually tend to overlook is the damage reinforced concrete beams incur from service. In this thesis, the possibility of using wire mesh-epoxy composite for flexural retrofitting of RC beams has been investigated. In the investigation, both damaged and undamaged specimens have been used.

1.3 Objective of the study

1.3.1 General objective

The general objective of this study is to investigate the structural capability of wire mesh-epoxy composite in flexural retrofitting of reinforced concrete beams. In doing so, the technique's capability in strengthening as well as rehabilitating is examined independently.

1.3.2 Specific objectives

The specific objectives of this thesis are:

- investigating the effect of attaching the wire mesh-epoxy composite on the ductility of reinforced concrete beams;
- investigating the impact of attaching wire mesh-epoxy composite on the energy absorption capacity of reinforced concrete beams;
- investigating the failure mechanism of retrofitted beams with wire mesh-epoxy composite;

1.4 Scope

The scope of this study is limited to flexural retrofitting only. The flexural investigations are carried out through a three point monotonic flexural test. Moreover, the study does not include any comparative studies with other retrofitting techniques. It focuses on investigating the capability of wire mesh-epoxy composite in flexural enhancement of reinforced concrete beams.

1.5 Methodology

The research is carried out through experimental, numerical and analytical investigations. The literature review conducted on previous works lays the foundation for the development of the experimental, numerical and analytical programs. The experimental investigation is conducted independently for strengthening and rehabilitating scheme. The results obtained are used for all the subsequent comparisons depending on flexural performance, ductility and energy absorption capacity. A nonlinear finite element analysis is carried out with VecTor2, a non linear finite element analysis software designed for reinforced concrete elements. The analysis is conducted for the strengthening and rehabilitating scheme independently and the outputs are validated with the experimental results. At last, an analytical study is carried out to explain failure behavior of specific group of specimens.

1.6 Organization and Layout of chapters

In the second chapter ,literature review of previous research works is carried out. This review on literatures served as a foundation over which the current study will be built up on while trying to fill some of the gaps that have been left in previous works.

The third chapter discusses about the experimental program designed in order to carry out the investigations. It discusses about the material mobilization, specimen preparation and testing conducted at AAiT material testing laboratory.

The fourth chapter discusses about the nonlinear finite element analysis conducted on predamaged and undamaged specimens using VecTor2, a simulation software specifically designed for reinforced concrete elements.

The fifth chapter is the chapter where all the results obtained from the experimental tests and nonlinear finite element analysis are interpreted, analyzed, discussed and compared.

The sixth chapter is the chapter where the analytical model is adopted, analyzed and compared against experimental and FEM results for verification. This chapter also presents the verifications conducted to examine the accuracy of the adopted model.

The seventh chapter is the last chapter where the conclusions are depicted and recommendations for future works are forwarded.

2. Literature review

2.1 General introduction

Reinforced concrete beams are non-homogeneous in that they are made of two entirely different materials. The methods used in the analysis of RC beams are therefore different from those used in the design or investigation of beams composed of entirely steel, wood, or any other structural material. The fundamental principles involved are, however, essentially the same. At any cross section, there exists internal forces that can be resolved into components normal and tangential to the section. Those components that are normal to the section are the bending stresses (tension on one side of the neutral axis and compression on the other). Their function is to resist the bending moments at the section. The tangential components are known as the shear stresses and they resist the transverse or shear forces**.** (Nilsson et.al, 2010)

Although the flexural analysis and design of reinforced concrete beams are well known and common for most codes, beams tend to be deficient in some way in many circumstances. When a structural element is found to be deficient, there are two possible ways of mitigating the problem. It can either be demolished and replaced or repaired and strengthened i.e. retrofitted. Considering the economic loss, inconvenience and complications incurred from replacing structural elements, retrofitting is the ideal solution. Extensive research works have been conducted when it comes to retrofitting reinforced concrete beam elements flexurally. Due to this fact, recent studies have shifted their focus towards coming up with better and cheaper techniques rather than concentrating on as to how the techniques work. This thesis can be taken as one among such kinds of works with the specific difference being; it also examines as to how the technique works by studying the failure mechanism through experimental investigation, nonlinear finite element analysis and analytical model.

Literatures usually tend to focus on the strength parameters when studying insufficiency in structural elements, which is a rather incorrect approach. Not seldom, catastrophes occur in building structures while having a sufficient amount of strength but due to deficiency of other structural behaviors like ductility. Especially, in regions where threats from dynamic loads are imminent, a great deal of concern need to be directed towards structural properties like ductility and energy dissipation capacity.

2.2 Ductility of beams

Ductility is the ability of a section to deform beyond its yield point without a significant strength loss. The ductility of structures can be quatified using one of the following parameters.

2.2.1 Strain ductility

The fundamental source of ductility is the ability of the constituent materials to sustain plastic strains without significant reduction of stress.it can be simply defined

$$\mu_\epsilon = \frac{\epsilon}{\epsilon_y} \tag{2.1}$$

Where ϵ-total strain

ϵ_y-yield strain

- Imposed strain shall not exceed the dependable maximum strain capacity, ϵ_m.
- Significant ductility in a structural member can be achieved only if inelastic strains can be developed over a reasonable length of that member. If inelastic strains are restricted to a very small length, extremely large strain ductility demand may arise.

2.2.2 Curvature ductility

The most common and desirable sources of inelastic structural deformations are rotational in potential plastic hinges. Therefore, it is useful to relate section rotations per unit length (curvature) to causative bending moments. The maximum curvature ductility is expressed thus;

$$\mu_\emptyset = \frac{\emptyset_m}{\emptyset_y} \tag{2.2}$$

- Where $\emptyset_m$ is the maximum curvature expected to be attained or relied on and $\emptyset_y$ is the yield curvature.

2.2.3 Displacement (deflection) ductility

The most convenient quantity to evaluate either the ductility imposed on the structure by an earthquake μ_m or the structure's capacity to develop ductility μ_u, is displacement. Displacement ductility is

$$\mu_\Delta = \frac{\Delta}{\Delta_y} \tag{2.3}$$

Where, $\Delta = \Delta_y + \Delta_p$

- Δ_y implies the yield displacement and Δ_p implies the fully plastic displacement. (seismic design of reinforced concrete and masonry buildings) (Paulay & priestly, 1992)

2.3 Energy in structural elements

It is a known fact that work done by surface and body forces on an elastic solid are stored inside the body in the form of strain energy.

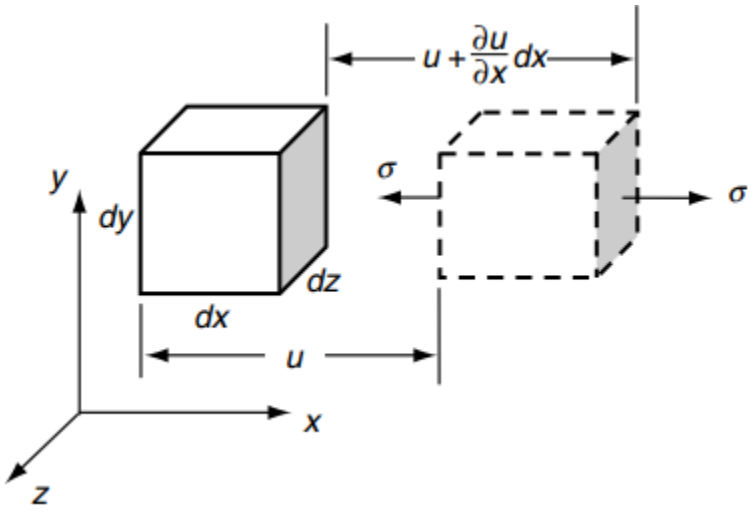

Figure 2-1 Deformation under uniform uniaxial stress, (Saad,M.H.,2009)

$$\int_0^{\sigma_x} \sigma d\left(u+\frac{\partial u}{\partial x}dx\right)dydz - \int_0^{\sigma_x} \sigma dudydz = \int_0^{\sigma_x} \sigma d\left(\frac{\partial u}{\partial x}\right)dxdydz \quad (2.4)$$

Using the strain displacement relations and hooke's law,

$$\frac{\partial u}{\partial x} = e_x = \frac{\sigma_x}{E} \quad (2.5)$$

And thus the above equation reduces to

$$dU = \int_0^{\sigma_x} \sigma \frac{d\sigma}{E} dxdydz = \frac{{\sigma_x}^2}{2E} dxdydz \quad (2.6)$$

The strain energy per unit volume, or strain energy density, is specified by

$$U = \frac{dU}{dxdydz} \quad (2.7)$$

And thus for this case we find

$$U = \frac{{\sigma_x}^2}{2E} = \frac{E{e_x}^2}{2} = \frac{1}{2}\sigma_x e_x \quad (2.8)$$

Moreover, this can easily be shown that it is the area under the stress strain curve for a linear material. (Saad, M.H., 2009)

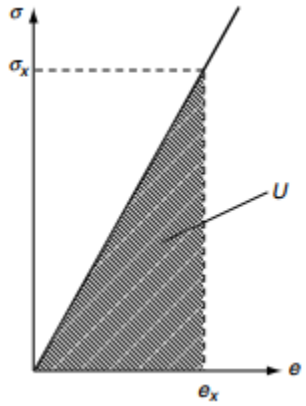

Figure 2-2 Area under stress-strain diagram (Saad,M.H.,2009)

From this, we can deduce that the area under the stress-strain diagram or the load-deflection diagram can be taken as the energy absorbed by the material upon load imposition.

2.4 Flexural Retrofitting of beams

The generic meaning of the term "retrofitting" is the modification of a certain physical system by adding a part that was not the integral part of the system originally. In this sense, the term serves to describe the condition where additional material will be installed to an already existing structural element, i.e. beam in this case, in order to improve the flexural capacity and investigate if certain specific properties like ductility, and energy dissipation are modified as well. Furthermore, it will also be used to describe the mechanism in which the beam can be repaired from an already incurred damage through the addition of new external element.

When strengthening is going to be undertaken, all failure modes must be evaluated. Strengthening a structure for flexure may lead to shear failure instead of giving the desired increased flexural capacity. It should also be noted that not only the failure mode of the strengthened member is important. If a critical member in a structure is strengthened, another member can become the critical one. Because of stiffness change in an undetermined structural system, the whole structure must be investigated. The strengthening should also be designed with consideration to minimize the maintenance and repair needs. (Heiza.et.al,2014)

Hereunder, a brief overview of different retrofitting techniques and related research works is presented.

2.4.1 Steel plates

In earlier times, steel plates were used to retrofit beams by attaching them to the soffit of beams. Although the beams show an enhanced capacity after the deployment of the technique, there are certain shortcomings, which made the method inefficient. To mention a few,

- ✓ Low strength to weight ratio i.e. compare to other recent techniques, it gives a lower added strength for a larger weight.
- ✓ Unwanted stiffening of structural elements.
- ✓ Long-term problems like corrosion and deterioration.
- ✓ Debonding of the plate due to its heavy weight, etc.

Although the technique has these shortcomings, it still finds its use in some structural works like bridges and continues to be one of the most common strengthening techniques. It has proven to be very effective for increasing the flexural and shear capacity of reinforced concrete beam. Strengthening by steel plate is a popular method due to its availability, cheapness, uniform materials properties (isotropic), ease of application, high ductility and high fatigue strength. Investigations into the performance of members strengthened by this technique were started in the 1960s. This method had been used to strengthen both buildings and bridges in countries such as Belgium, France, Japan, Poland, South Africa, Switzerland and United Kingdom (Jones et al., 1998). The most common form of plating is to glue steel plates to the tension faces of beams. In this position, the plate is at its furthest extremity from the compression region and, as a result, the composite flexural action is at its maximum (Oehlers, 1997). Furthermore, the composite action between the plate, glue, and concrete will be maintained until failure (Swamy et al., 1987). However, the effectiveness of this method depends on the surface preparation and bonding methods between existing beam and steel plates. Thus, the surface preparation of existing beam as well as steel plate has to be carried out effectively. Adhikary et al. (2000) has described the roughening process of the beam surface before placing the plates. The roughening process is carried out using a mechanical grinding until the laitance was removed and the surfaces were then brushed and cleaned thoroughly with acetone. The bonding faces of the steel plates can also be sandblasted and then cleaned with acetone. After surface preparation epoxy adhesive is placed on the roughened surface and then steel plate is positioned on top.

As mentioned earlier, steel plates are one of the most studied and applied techniques in flexural retrofitting of beams. Starting form earlier ages, researchers dedicated their efforts in understanding the behavior of reinforced concrete beams that have been plated with steel plates. Arslan, et.al. (2006), conducted an experimental and a non-linear finite element analysis investigation to gain an understanding on the contribution of steel plates in the load carrying capacity of RC beams retrofitted with steel plates. From the investigation, it has been confirmed that the attachment of the steel plates enhances the cracking load as well as the flexural capacity considerably. However, a premature failure has also been observed in the retrofitted specimens due to what has been referred by prior investigators as, shear peeling. It was reported that the separation cannot be attributed to the non-homogeneity of friction between the concrete and steel plate as the experiment was conducted meticulously.

In an effort to investigate the potential flexural repairing capability of steel plates glued to the soffit of RC beams, Sevuk & Arslan (2005) witnessed that the technique is capable of not only repairing but also strengthening the predamaged specimens. In the study, the specimens are repaired using different plate configurations as defined by variations in plate curtailment length. From the investigation, it was proved that externally bonded longitudinal steel plates can improve the ultimate load carrying capacities of RC damaged beams and can enhance their flexural strength as compared to reference beams. It is observed that the more strength in flexure increases, the more shear failure increases in repairing and strengthening of RC beams. Moreover, it was confirmed that the variation of the curtailment length of the steel plates has a significant role in the flexural capacity of the retrofitted specimens. The specimens with the least unplated length i.e. distance from support to plate end, showed the largest increment in flexural load capacity.

Furthermore, existing experimental research works show that the hypothetical high ultimate capacity of externally bonded strips used for strengthened RC beams often cannot be achieved because of the externally plate debonding or diagonal cracking. The debonding of plates significantly reduces the strength enhancement provided by the externally bonded plate and can create brittle failures.

Figure 2-3 steel plated structural elements,(Heiza et.al,2014)

2.4.2 Ferrocement laminates

Ferrocement is a type of thin composite materials made of cement mortar reinforced with uniformly distributed layers of continuous, relatively small diameter, wire meshes. Ferrocement, being of the same cementitious material as reinforced concrete, is ideally suited as an alternative strengthening component for the rehabilitation of reinforced concrete Structures. The ferrocement laminate possesses higher tensile strength to weight ratio and a degree of toughness, ductility, durability and cracking resistance that is considerably greater than those found in other conventional cement based materials. Romuldi and Irons (1987) first introduced the use of ferrocement laminates in repair in the early 1980s mainly as relining membranes for the repair of liquid retaining structures, such as pools, sewer lines, tunnels, etc. For flexural strengthening, the ferrocement laminates were cast onto the soffits (tension face) of the beams without any change in width of the beams, while in shear strengthening the ferrocement laminates were formed onto the three exposed faces of the beams, except for the top compression face. Before placing the ferrocement laminates proper surface preparation should be ensured. Several research works have been conducted on ferrocement laminates.

Ganapathy and Sakthieswaran (2015) studied the behavior of reinforced concrete beams Strengthening by using fibrous Ferrocement Laminates composites, which were directly glued into the cracked tension face of the beam by epoxy adhesives. Beams were cast and tested under two point's loads. Five beams were kept as perfect beam and the remaining beams are cracked under overloading by applying 70% ultimate load. The cracked beams were strengthened by polymer modified fibrous ferrocement composites with two different volume fractions (4.94%, 7.41%).

Eldeen (2015) studied this paper concerned with strengthening and retrofitting of reinforced concrete beams completely damaged due to flexural failure. The strengthening technique consists of steel wire mesh with and without additional longitudinal steel angles, cast and tested under two point loading. All beams were tested and loaded monotonically to failure, and then cracks were filled with grout mortar. The beams were strengthened and retrofitted under the existing deformation using two and three external plies of expanded galvanized steel wire mesh with square grids in the form of U-jacket. The investigated parameters were the size of longitudinal steel angles, which were added at the bottom corners of beams inside the steel wire mesh. In addition, numbers of vertical steel clamps (2, 4 and 6) were used to fix the jacket to eliminate the debonding. The strengthened and retrofitted beams were again tested under two points loading. The results shows the increasing numbers of steel wire mesh plies fixed with 2, 4 and 6 vertical clamps without external steel angles increase the beam carrying capacity from 26.59% to 49.55%.

Sridhar et al. (2014) probed the flexural behavior of reinforced concrete (RC) beams strengthened with ferrocement laminates using steel slag from the steel industry as a partial replacement material for fine aggregate. The parameter varied in this study includes volume fraction of mesh reinforcement 1.88% and 2.35% and percentage replacement of steel slag (0% and 30%) to fine aggregate in ferrocement laminate. The observations were focused on first crack load, ultimate load and mid span deflection. From the investigation result, it was concluded that the beams strengthened with ferrocement having a volume fraction of 2.35% and 30% replacement of steel slag increases the load carrying capacity significantly under flexural load. Incorporation of steel slag in ferrocement laminates with volume fraction 2.35% and steel slag replacement 30% have highly reduced the deflection when compared to other specimens. The addition of ferrocement laminate to the tension face of the RC beams substantially delays the first crack load.

Besides studying the structural feasibility of ferrocement as a strengthening means, researchers have engaged themselves in optimizing the technique. Bansal et.al conducted test on beams retrofitted with ferrocement laminates under different orientation of wire mesh. The laminates were prepared using three different wire mesh orientations i.e. 0^0, 45^0 and 60^0. It was observed that wire mesh oriented at 45^0 for retrofitting the stressed beam has the highest load carrying capacity as compared to the control beams as well as the other beams retrofitted using different orientation,

additionally, the beams retrofitted with wire mesh oriented at zero degree were most efficient as their cost to strength ratio is the lowest.

Neeladharan et.al. Investigated the performance of RC beams strengthened by ferrocement and phenolic. Phenol formaldehyde resins (PF) or phenolic resins are synthetic polymers obtained by the reaction of phenol or substituted phenol with formaldehyde. These resins have been replaced with epoxy resins largely these days. From the experimental investigation, the following results were obtained. The strengthened beam gives higher strength when compared to the conventional concrete beam. The flexural strength of preloaded beams are higher (>70%, >80%, >85%, >90%). Hence, the existing damaged beams can be strengthened up to 83% of failure or collapse using ferrocement & phenolic resin.

2.4.3 Fiber reinforced polymers

There are three most commonly used fiber reinforced polymers that have been used extensively for retrofitting works namely, carbon fibre reinforced polymer (CFRP), glass fibre reinforced polymer (GFRP) and aramid fibre reinforced polymer (AFRP).

Carbon Fiber Reinforced Polymer

Neeladharan (2018) investigated the flexural strength of beams that have been damaged and retrofitted after using CFRP wraps for different damage degree. The behavior of the beams were studied using experimental investigation and finite element modeling. Six beams were casted and tested for the investigation. The study was carried out in such a way that the beams are first damaged and then injected with epoxy after which they are wrapped with CFRP for the second round testing. The study revealed that the retrofitted beams showed a considerable 125% increase of flexural capacity when compared with the control groups. Additionally, the retrofitted beams also showed less deflection than the control groups.

In addition to studying the capability of the technique for retrofitting structural elements, many researchers have engaged themselves in optimizing the technique for better results. Khan and Fareed (2013) conducted an experimental investigation focusing on the behavior of RC beams strengthened with CFRP wraps instead of strips. The investigation was carried out using six beams in two sets. On one set of the beams, the wrap has an end anchorage while the other set was tested without end anchorage. At the end of the investigation, the wrapped beams showed a far better performance than the controls in terms of stiffness, load carrying capacity and ductility. In

addition, the set with end anchorage exhibited a stiffer load deflection diagram. Unlike most researches previously conducted on CFRP strips, the wrapped beams showed better ductility.

Pham and Almahaidi (2005) used non-linear finite element modeling technique to study the debonding failure of RC beams retrofitted with CFRP using a non-linear finite element software named DIANA. In order to verify the outputs, they compared their results with an experimental data they acquired from their own previous investigation. At the end of their investigation, they were able to prove that non-linear finite element analysis can simulate the beams' behavior within an acceptable range of accuracy. Their analysis accurately predicted the ultimate capacity, crack pattern and CFRP strain distributions. Three failure modes were observed among the analyzed beams as end debond, intermediate span debond and combination of both end and intermediate span debond.

Glass Fiber Reinforced Polymer

The second type of FRP that has found its place in structural retrofitting is GFRP (glass fiber reinforced polymer). Even if the mechanical properties of GFRP is not as outstanding as CFRP for the aforementioned structural retrofitting purposes, several conducted researches indicate its convenient applicability for the strengthening purpose.

Meried,R., (2016) is pioneer when it comes to research works related to GFRP that have been conducted in AAiT. In his thesis, he investigated the capability of the technique for flexural retrofitting of beams by varying the number of layers used. He tested 12 beams in four groups, one being the control and the rest being the modified. At the end, his findings indicated that the technique can be used effectively for flexural retrofitting of beams. The retrofitted beams have showed an improved yield and failure load capacity. A flexural capacity that mounted up to 50% was observed in his findings. In addition to the experimental investigation, he also carried out a numerical study using a finite element software and compared the results with the experimental findings. There is a good agreement between the two, which makes it easier for future research works that are going to be conducted in relation to the topic.

All these mentioned techniques and many others have been considered in researches or practical application for flexural retrofitting of beams. Besides their merits, there are shortcomings that can be raised against the discussed techniques. This means that there is a gap that needs to be filled. This thesis work aims at investigating a flexural retrofitting technique that is expected to fill some

of these gaps. A retrofitting technique that deploys composite of wire mesh and epoxy resin is used and tested in order to investigate the general performance of the beams under a three point load lest. The pre-peak behavior i.e. cracking and deflection, yield load capacity, post-peak behavior i.e. ductility and energy dissipation capacity of the beams is investigated.

2.4.4 Wire mesh-epoxy composite

Thanks to epoxy glues' capacity to absorb considerable tensile and shearing stresses, it is possible to reinforce concrete constructions, for example a bridge deck, so that they can withstand heavier loads. The method involves gluing steel plates or carbon fibre to the concrete to increase the reinforcement area. It is possible to reinforce for both bending forces and shear forces. These properties make epoxy ideal for retrofitting works. As mentioned in earlier articles, epoxy has been used as a glue for other retrofitting material like steel and FRPs. In these circumstances, the epoxy serves only as a glue, which renders its high tensile strength unexploited to full extent.

Recently however, an ideology was raised by Qeshta et.al (2015) to combine it with wiremesh as a composite and use it as a laminate in flexural retrofitting of beams. In the investigation, in addition to the ability of the technique, the effect of increasing layers was studied and it was observed that the flexural capacity increased as the number of the layers increased. Although this work is a pioneer when it comes to applying the technique, it was only limited to the strength investigation of unloaded specimens and did not carry out analytic or finite element investigation to examine any additional characteristics.

Ealias and Binu (2015) carried out a finite element analysis depending on Qeshta's experimental program using the finite element analysis software ANSYS. Their analysis covered the pre-peak region of the load deflection response. Although their result showed a good agreement in the pre peak region with Qeshta's findings, they could not study the post peak characteristics of the beams retrofitted with wiremesh-epoxy composite laminates. These are the only available literatures in relation to the subject. Although there is a huge potential in the technique, it is apparent that the potentials are being overlooked.

3. Experimental program

3.1 Aim of experimental program

The main goal of the experimental program is to gain evidence of and insight into the capability of the wire mesh-epoxy composite for the flexural retrofitting of RC beams. Aspects like flexural behavior, deflection behavior, ease of application and failure mode are of particular interest for the experimental study. Most researches conducted on retrofitting techniques focus on strengthening aspect rather than repairing. Considering this, the experimental program is designed to be carried out in two schemes i.e. strengthening of undamaged beams and rehabilitation of predamaged beams.

The experimental evidence obtained on this new technique will provide the first and foremost insight on the capability of the wire mesh-epoxy composite technique in overcoming the aforementioned issues from both strengthening and repairing perspective. It also lays the foundation for further numerical and analytical investigations.

The experimental investigation is carried out in the following three phases.

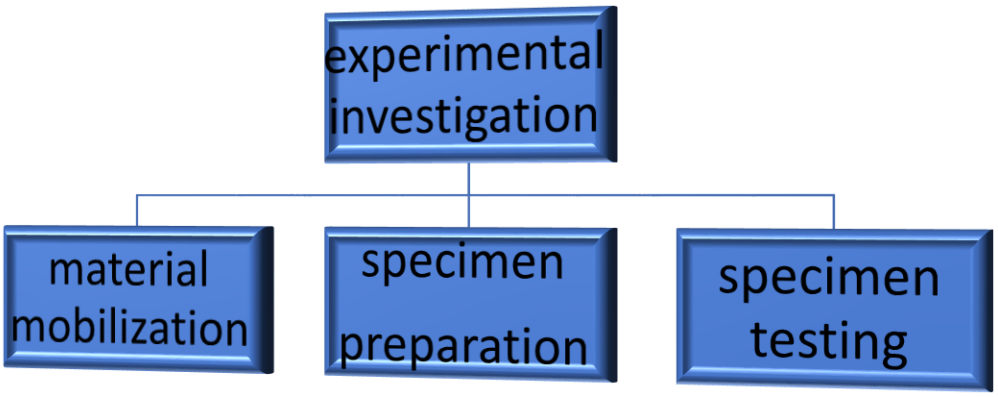

Figure 3-1 Experimental program phase layout

3.2 Material mobilization

In this phase, all the necessary materials required for the preparation of the samples were purchased and mobilized. This includes input materials like sand, aggregate, cement, reinforcement bar, wire mesh, epoxy, gypsum, timber, etc. that are necessary for the fabrication of the specimens and the subsequent tests. Since most of the experimental work took place during the summer, a great deal of caution was taken in order to at most prevent or at least minimize any detrimental effect of excessive moisture in the surrounding. Especially, highly susceptible materials like cement were given due care.

3.3 Specimen preparation

This is the phase where the specimens were prepared. A total of twelve beams were cast for the investigation. In order to attain a reliable output, all the necessary inputs and molding equipment need to be at their possible best condition. Therefore, the assurance of these necessary conditions was given paramount precedence. This includes storing the materials and equipment in a safe environment, conducting all the necessary tests on the input materials before using, measuring the quantity of the mixing materials meticulously, outsourcing the tasks that require skillful touch to skilled personnel and handling the specimens with care to obtain the desired results. In addition to these, caution was taken in order to avoid dangerous and hazardous incidents while working.

3.3.1 specimen description

In order to carry out the investigation, twelve specimens were prepared. These specimens were categorized in four groups.in the first group; there were three specimens, labeled as “GK-CT”, with similar geometric as well as structural specifications. These were the control items, whose test results serve as a comparison reference for the rest of the modified groups. The second group consisted of three specimens as well, that were labeled as “GK-RET3”-1, 2 & 3. These specimens were similar to the first group in all aspects, i.e. geometrical and structural specifications, except the fact that they were retrofitted with three layers of wire mesh-epoxy composite. The third group of specimens consisted of three items that were retrofitted with five layers of the composite, otherwise the same as the aforementioned groups. The items in this group were labeled as “GK-RET5”-1, 2 & 3. The fourth and the last group of items consisted of three beams with the label “GK-REP-RET”-1, 2, 3 and with the same geometric and structural specifications as that of the above groups. However, the samples were subjected to a specific amount of loading prior to any

retrofitting. In this case, the beams were repaired rather than being strengthened. The figures below illustrate the geometrical and structural specifications of the specimens.

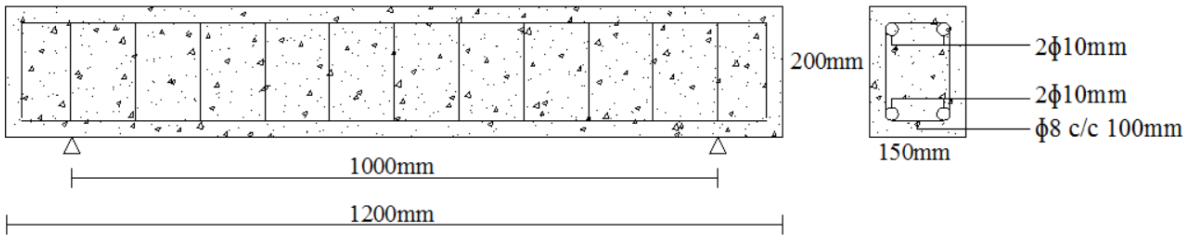

Figure 3-2 configuration of control beams

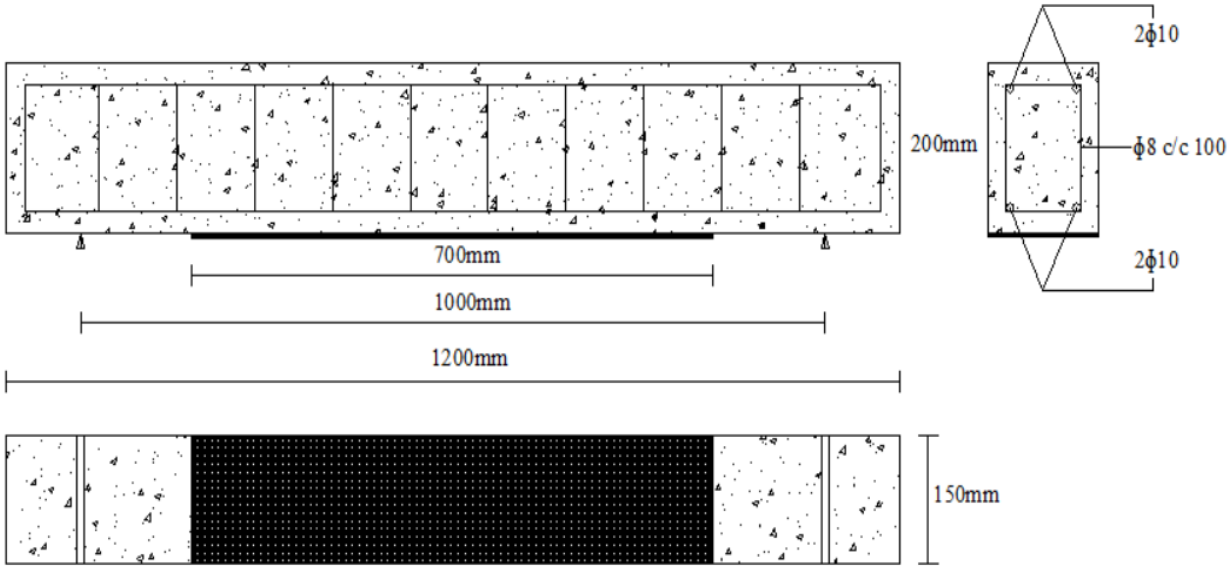

Figure 3-3 configuration of retrofitted beams

3.3.2 Material preparation and tests

In this experimental investigation, a conventional RCC beams were casted for the control as well as the retrofitted samples. All the necessary inputs used for the concrete i.e. sand, aggregate and cement were all locally available materials. The reinforcement bars are locally manufactured as well by Abyssinia integrated steel PLC. The material selection was carried out in such a way that it is a compromise among the ideal for the purpose, the material readily available and the relative costs.

3.3.2.1 Coarse aggregate

An aggregate, for concrete making, is any hard, inert material composed of fragments in a wide gradational range of sizes, which is mixed with a cementing material and water to form concrete. Aggregates should be clean, sound, tough, durable and uniform in quality. Aggregates make up 65 to 75% of the volume of concrete. Therefore, the quality of concrete produced is highly influenced by the properties of its aggregates. Considering these facts, the grading of aggregates shall be given due consideration. The nominal size of aggregates in the present investigation was found to be 25 mm. Figure3-4 summarizes the results of the sieve analysis.

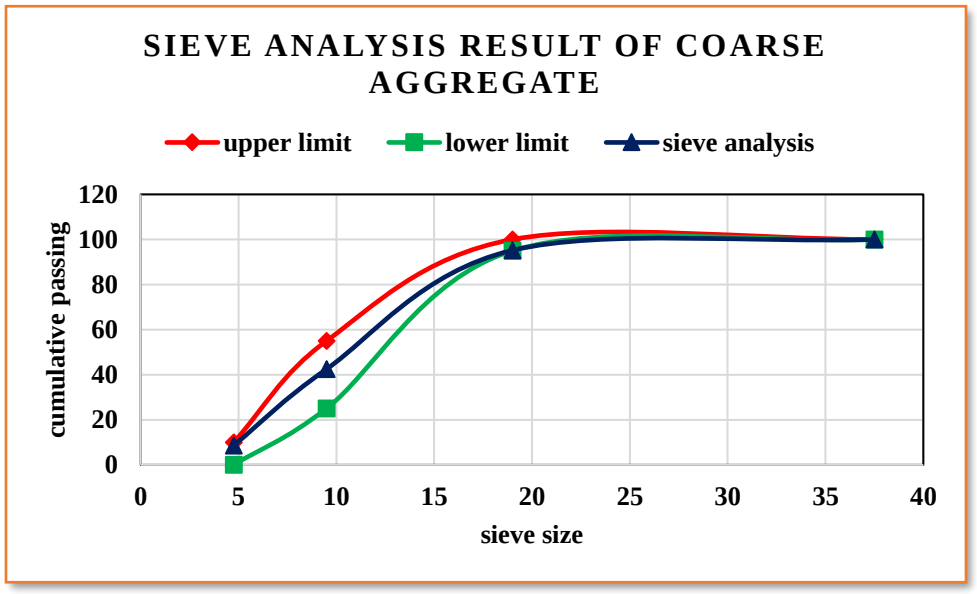

Figure 3-4 gradation curve of coarse aggregate

3.3.2.2 Fine aggregate, sand

Naturally occurring sand is usually used as fine aggregate in the preparation concrete. This Sand is obtained from glacial, river, lake, marine, residual and wind-blown (very fine sand) deposits. These deposits, however, do not provide pure sand. The presence of such materials in sand makes concrete or mortar decrease the bond between the materials to be bound together and hence the strength of the mixture. The finer particles do not only decrease the strength but also the quality of the mixture produced resulting in fast deterioration. Bearing this in mind, the sand that was used in the mixture has passed through a serious of tests.

Silt content

Determination of the silt content of sand is a simple test that can be conducted in a graduated jar. The measured sand is mixed with water in a graduated jar for a minute and was let to settle for at least an hour after which the amount of the settled fine material on the top of the sand is compared with the rest of the sand in a rather simple procedure**.**

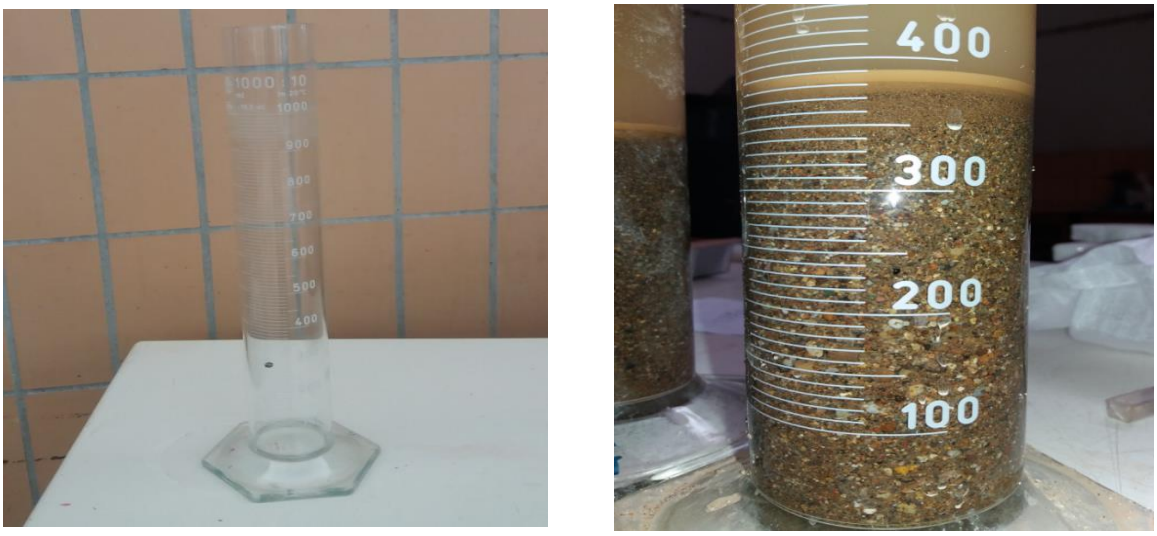

Figure 3-5 silt content test on fine aggregate

The table below summarizes the results.

Table 3-1 Summary of silt content test results

specimen	**Silt content, ml**	**Pure sand, ml**	**Silt content, %=$\frac{silt\ content}{pure\ sand} * 100$**
1	14	370	3.78
2	13	362	3.59
3	17	373	4.56

The test showed that, the sand has a silt content of 3.98% (average) of silt material. According to Ethiopian standards, if the silt content in a sand sample exceeds 6%, it shall be either washed or discarded. From the test result, it can be observed that it is safe to use the sand. Nevertheless, the sand has been washed in order to get rid of porous materials and organic materials that might compromise the quality of the end results. Furthermore, sieve analysis has been carried out in order to assure that the grading is within the allowable limits (see figure 3-7).

Figure 3-6 washing treatment of fine aggregates

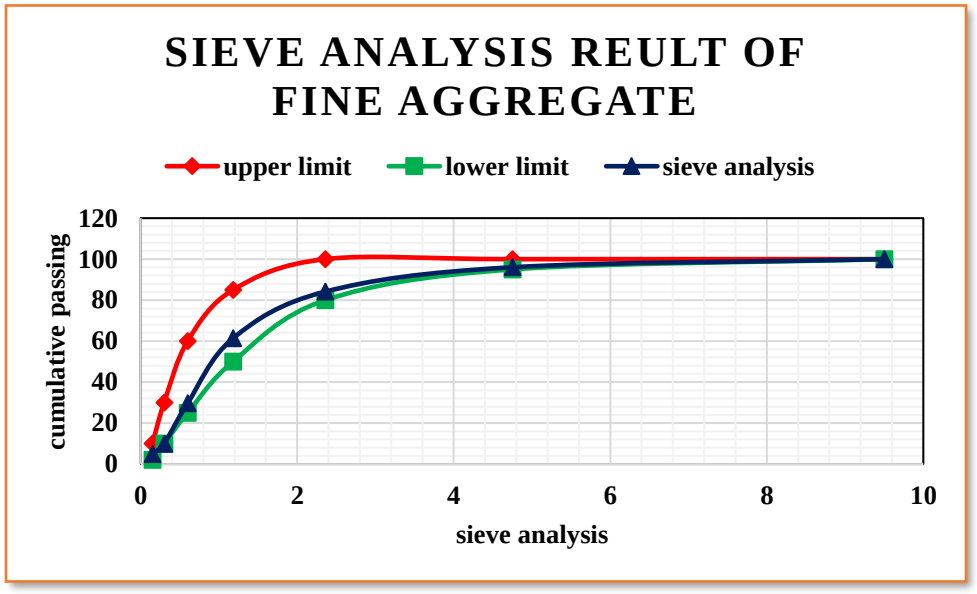

Figure 3-7 gradation curve of fine aggregate i.e. sand

The fineness modulus has been calculated as follows.

$$fineness\ modulus = \frac{\sum cumulative\ coarser(\%)}{100} = \frac{310.564}{100}$$

From the computation, it can be clearly seen that the fineness modulus is **3.10.**

In order to adjust moisture content discrepancies, the sand was tested for its moisture content and determined to be **9.89%.** the aggregate was surface dried to a state in which the moisture content can be igonred.

3.3.2.3 Reinforcement bars

Two diameters of reinforcement bars i.e. diameter 8 and diameter 10 were used in this experimental investigation. The diameter 8 ribbed bar was used for shear reinforcement while the diameter 10 was used for longitudinal reinforcement. the tensile strength of the reinforcement bars was conducted using the universal testing machine in AAiT material laboratory. Six samples were taken, three for each bar size.

Figure 3-8 Universal testing machine test set up at AAiT

Table 3-2 Tensile strength test results of reinforcement bars

Type of reinforcement	Diameter, mm	Yield capacity, MPa	Ultimate capacity, MPa	Ultimate strain
Shear reinforcement	8	445	592	30%
Flexural reinforcement	10	545	632	24%
wiremesh	0.77	290	350	-

3.3.2.4 Concrete mix proportion

It is imperative that the strength of the concrete is at the desired level of strength so that reliable outputs can be attained at the end of the experimental program. Bearing this in mind, The target compressive strength at the 28^{th} day was set to be 25MPa. The mix design was done using ACI

specifications. For the determination of the compressive strength of the concrete, twelve cube samples were taken from four mix, three from each mix.

Table 3-3 C25/30 mix proportions of concrete

Max aggregate size	25mm
Fineness modulus	3
w/c ratio	0.61
Concrete unit mass/m^3	2380
Weight of water/m^3	193Kg
Weight of cement/m^3	316.4Kg
Weight of aggregate/m^3	1040Kg
Weight of fine aggregate/m^3	830.6Kg

Using this ratio, a trial batch was prepared at first which gave acceptable results. In order to facilitate the mixing process, the coarse aggregate as well as the sand was weighed in a quantity sufficient enough for a single mix i.e. one beam, and packed in order to preserve conditions like moisture content in a consistent state up to the day of the mix. Slump test was conducted on the concrete mix in order to assure the workability of the mixture.

Figure 3-9 Slump test on mixed fresh concrete

The slump was measured to be 60mm which is an acceptable range for concrete mix prepared for beams. The table below summarizes the end results of the concrete mix.

Table 3-4 Compression test results of the sample concrete cubes

Beam type	Designation of sample	description	crushing compressive strength (MPa)	Mean copressive strength,fcm(MPa)
control	GK-CT-1	Control specimen	27.18	26.75
	GK-CT-2	Control specimen	26.33	
	GKCT-3	Control specimen	26.75	
Retrofitted with three layers	GK-RET3-1	3layer wiremesh	24.33	24.11
	GK-RET3-2	3layer wiremesh	23.43	
	GK-RET3-3	3layer wiremesh	24.57	
preloaded and retrofitted	GK-REP-RET-1	Preloaded beam	28.13	27.41
	GK-REP-RET-2	Preloaded beam	28.22	
	GK-REP-RET-3	Preloaded beam	25.88	
Retrofitted with five layers	GK-RET5-1	5layer wiremesh	25.53	24.9
	GK-RET5-2	5layer wiremesh	24.66	
	GK-RET5-3	5layer wiremesh	24.52	
Trial beam	*TRL1*	*Trial beam*	*29.65*	*29.65*
average				***26.56***

3.3.2.5 Wire mesh

The wiremesh used in the experimental program was a common welded wiremesh which is commonly used for sieve fabrication, fences, glass reinforcement, etc. the transversal and longitudinal wires have a diameter of 0.77mm and are welded with each other at a spacing of 13mm. the mesh was cut into a dimension of 700x150mm^2. After this, the desired number layers was attained by tying each layer together using a common fabric thread. This helps the layers to act as one. The wires in the longitudinal direction carry the load. The transversal wires tie the longitudinal bars which inturn helps the load carrying side to act as one.

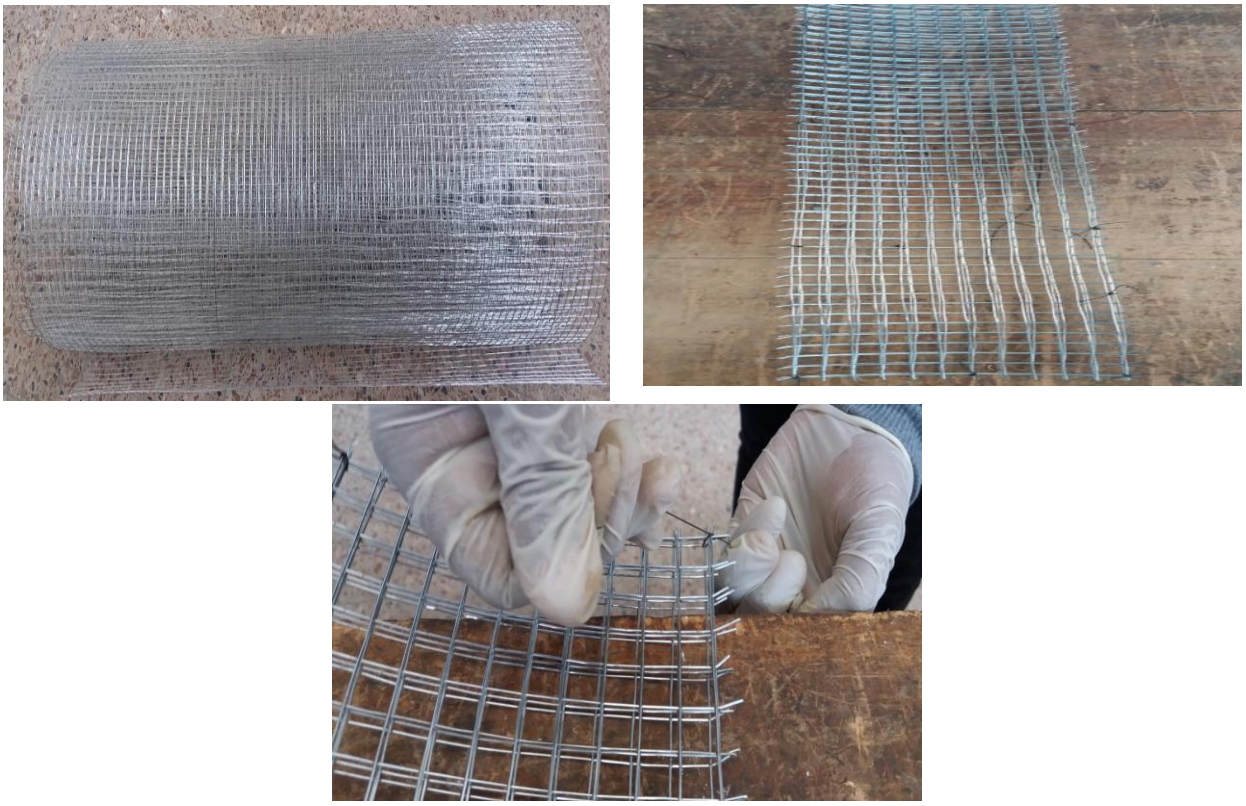

Figure 3-10 Preparation of wiremesh layers

3.3.2.6 Epoxy

Two brands of epoxy were used in this investigation. The initial intention was to use only Sikadur-32P for the entire specimen preparation. however, due to shortage of supply in the market, another brand of epoxy i.e. Forsoc Nitobond EP, was used for second layer coating i.e lamination stage of the composite. The two brands had similar mechanical properties for the most part.

Table 3-5 Mechanical properties of epoxy adhesive

Mechanical property	**Sikadur-32P**	**Forsoc Nitobond EP**
Compressive strength	60-70 N/mm^2	70 N/mm^2
Flexural strength	30-35 N/mm^2	-
Tensile strength	18-20 N/mm^2	30 N/mm^2
Bond strength to concrete	2.5-3 N/mm^2(concrete failure)	-
Bond strength to steel	18-20 N/mm^2	-

3.3.3 Specimen fabrication

The fabrication of the specimens was carried out in two phases.

Phase 1- after the completion of the reinforcement bar settup and formwork preparation, the casting of the concrete commenced.

(a)

(b)

(c)

(d)

Figure 3-11 (a) & (b) Final setup for casting (c) casted specimen (d) final state of specimens

phase 2- this is the phase where the strengthening and repairing of the samples was carried out. Before the commencement of the strengthening, the samples need to go through surface preparation in order to assure strong bond strength between the epoxy and the beam surface. The surface preparation was done based on the manufacturer's instructions for the application of epoxy resin. The surface was abraded to remove loose materials and weak cement layer to expose the textured smooth surface of the concrete. The surface was then cleaned to remove the dust and remaining loose materials using wet sponge and towel.

Once the surface is ready, a thin layer of epoxy was spread on the concrete surface in order to make sure that the epoxy completely covered the concrete surface and filled some surface voids. The wire mesh layers were laid on the mid 70% of the soffit of the specimen and were coated with a thin overlay of epoxy. After this, it was covered with plastic films and loaded with weight in order to assure strong adherence between the wiremesh layers and the concrete. It also helps create a strong bond between the wiremesh layers themselves. The specimens were kept in this condition for 24 hours afterwhich they were overlaid with a third layer of epoxy. This will laminate the composite effectively. Again they were loaded with weight for similar reason mentioned earlier and kept in that condition for eight days before testing.

Figure 3-12 Laminating the bonded wiremesh with epoxy

3.4 Specimen testing

The specimens were all subjected to a three point flexural test from which the necessary data for the analysis and interpretation is collected. Nevertheless, not all of them were tested under the same condition. The testing was carried out in two schemes. In the first scheme, unloaded specimens were tested after being strengthened. In this scheme, three and five layers of the composite were used for strengthening. In the second scheme, preloaded (damaged) specimens were tested after being retrofitted with five layers of the composite.

3.4.1 Instrumentation

The arrangement for the three point flexural test is showed in figure 3.13(d). A mechanical hydraulic jack was used to impose the concentrated load. The load applied was measured using a load cell placed beneath the hydraulic jack while the deflection was measured using an LVDT. The data acquired from the load cell and the LVDT was recorded with a digital data logger.

(a)

(b)

(c)

(d)

Figure 3-13 Data collecting and recording devices (a) LVDT (b) load cell (c) data logger (d)three point flexural test setup at AAiT

4. Nonlinear finite element analysis (NLFEA)

4.1 Theoretical background of VecTor2

VecTor suits are computer programs for a nonlinear finite element analysis of reinforced concrete. The VecTor suits include VecTor2, VecTor3, VecTor4, VecTor5, and VecTor6. Among these programs, VecTor2 has been used for the non linear finite element analysis program of this thesis.

The theoretical bases of VecTor2 are the Modified Compression Field Theory (Vecchio and Collins, 1986) and the Disturbed Stress Field Model (Vecchio, 2000). These are analytical models for predicting the response of reinforced concrete elements subject to in-plane normal and shear stresses. VecTor2 models cracked concrete as an orthotropic material with smeared and rotating cracks. The program utilizes an incremental total load, iterative secant stiffness algorithm to produce an efficient and robust nonlinear solution. (Wong et.al, 2013)

4.2 Nonlinear finite element analysis of undamaged specimens

In this strengthening scheme of undamaged specimens, three simulations have been conducted on control specimen, retrofitted specimen with three layers of the composite, and specimen with five layers of the composite.

The table below summarizes the specifications of the items in the simulation.

Table 4-1 Specifications of the specimens in the simulation program

Specimen designation	description	Longitudinal reinforcement	Transverse reinforcement	Retrofitting scheme
SIM-CTRL	Control specimen	2Φ10 top 2Φ10 bottom	Φ8 c/c 100mm	none
SIM-RET3	Retrofitted specimen	2Φ10 top 2Φ10 bottom	Φ8 c/c 100mm	Three layers of composite
SIM-RET5	Retrofitted specimen	2Φ10 top 2Φ10 bottom	Φ8 c/c 100mm	Five layers of composite

4.2.1 Constitutive and behavioral models for nonlinear analysis

The first step in creating the VecTor2 input is to define the Job Data. This is the stage where information on the job data, structure data, loading data and analysis parameter is inserted to the software. In addition to these, the material constitutive and behavioral models are selected in this stage of the modeling. These constitutive and behavioral models are paramount to the accuracy of the VecTor2 results. At each load step, the structure stiffness is determined from the stresses and strains calculated from the constitutive models. Table 4-2 presents the constitutive and behavioral models used in this analysis. VecTor2 has a library of different built in models that helps capture the different behaviors of reinforced concrete material that ultimately lead to complex non-linear analysis. This makes it easier for users to define and try different combinations of models that provide outputs that simulates actual results from experimental investigations.

Table 4-2 Summary of models used in VecTor2

Aspect/parameter	***model***
Convergence criteria	Displacement-weighted
Compression base curve/pre-peak	Hogenstad (parabola)
Compression post peak	Modified park-kent
Compression softening	Vecchio 1992-A
Tension stiffening	Modified Bentz-2003
Tension softening	Non-linear Yamamoto
Confinement strength	Montoya/ottosen
Concrete dilatation	Montoya w/limit-iso
Cracking criterion	Mohr-coulomb (stress)
Crack stress calculation	Basic (DSFM-MCFT)
Crack width check	Crack limit (agg/2.5)
Crack slip calculation	walraven
Concrete bond	Elighausen
Geometric non-linearity	considered
Cracking spacing	CEP-FIP-1978-deformed

4.2.2 Modeling of specimens

The compressive and tensile strength of the concrete for each specimen were directly taken from the experimental program. The mechanical behavior of longitudinal and transverse reinforcements was also taken from the tests conducted in the material testing laboratory of AAiT. Besides the strength of the concrete and the reinforcement materials, additional properties are left for the program to calculate depending on the previously selected material models.

- ✓ Initial tangent modulus $E_C = 5500\sqrt{f_c}$
- ✓ Cylinderical strain at peak strength $\varepsilon_o = 3.5\ millistrain$
- ✓ Poisson's ratio 0.15
- ✓ Thermal expanssion coefficient $10x10^{-6}/℃$
- ✓ Density $2400kg/m^3$
- ✓ Maximum aggregate size 25mm

One aspect that makes the VecTor2 suit versatile is the ability it grants users to model the reinforcements either as discrete or smeared entity. Both techniques have been used in these simulations to model the shear reinforcements as smeared and the flexural reinforcements as discrete elements. Another feature that makes VecTor2 convenient is the fact that it has a mechanism to define nodes, elements, restraints, and assign material types without having to manually create and number the nodes and elements automatically.

The wire mesh is modeled as a ductile reinforcement that is attached to the soffit of the beams with a perfect bond,taking the collective area of each wire in every layer and summing it up to model it as a single reinforcement package. Since no delamination occurred, at the interface between the wiremesh and the beam, the perfect bond asumption is a feasible and acceptable way of modeling their interaction. The experimental programs were planned to have a loading scenario controlled by displacement. As a result, to capture the post-peak behavior and to properly compare the results, a displacement controlled loading of 1 mm per load step is applied in the finite element simulation. The displacement control loading was applied at a node situated at the center of the beams. The specimens are modeled as a simply supported reinforced concrete beams. The figures below show the modeled beams using these material and analysis modeling schemes.

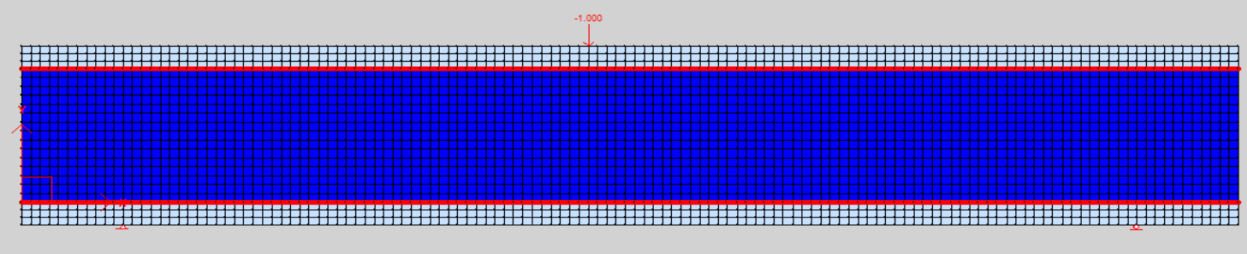

(a) SIM-CTRL; control specimen

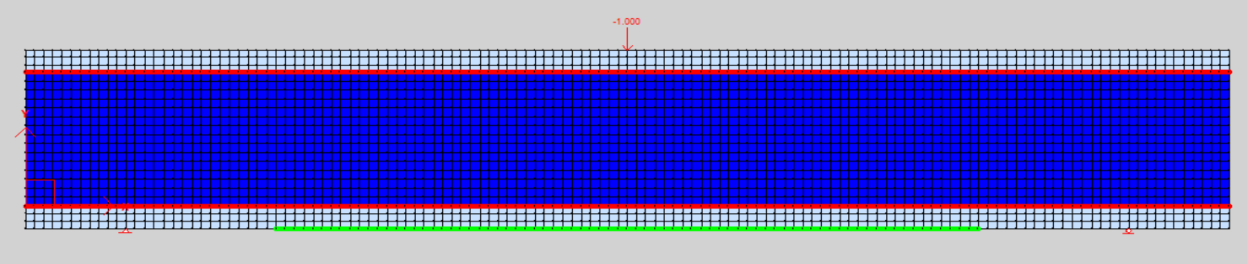

(b) SIM-RET3; retrofitted specimens with three layers of wire mesh-epoxy composite

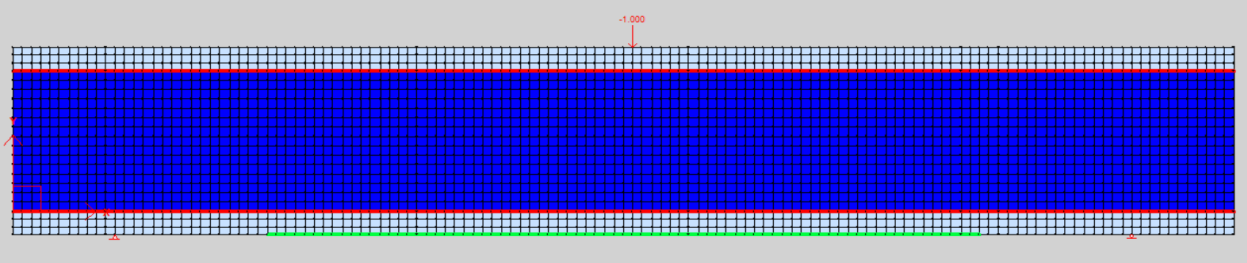

(c) SIM-RET5; retrofitted specimens with five layers of wire mesh-epoxy composite

Figure 4-1 Physical model of the simulated specimens

In the figures, the red lines at the top and bottom are discrete reinforcement bars. The middle part, which has deep blue color, is the part of the concrete that has transversal reinforcement. The transversal reinforcement has been smeared over the concrete. The outer most part with light cyan color is the unreinforced concrete i.e. concrete cover. In figure 4.1 b & c, a green line can be seen at the bottom of the beams. It is the wire mesh-epoxy composite layer. Just as the case of the experimental specimens, the layer has been attached to the middle 70% of the span length. The support conditions have been specified by the pin support on one edge and a roller support on the other end.

4.3 Nonlinear finite element analysis of predamaged specimens

4.3.1 Theoretical basis of damage modeling

Defining a concrete with its nonlinearity in entirety is a very difficult and sophisticated task. The existence of micro cracks and the fact that different materials with different sets of mechanical properties combine to act as one makes it difficult. Different models have been formulated in order to capture this nonlinearity and the additional softening and degradation that is incurred as loading progresses; concrete damaged plasticity comes to mind. This task becomes even more difficult when it comes to defining an already damaged concrete. As a results, simplistic techniques of capturing damage need to be used. In these techniques, assumptions are taken to simplify the modeling. However, these assumptions must be logical and have a solid theoretical background. In this NLFEA, the damage is captured by integrating the cracks developed due to the preload into the finite element model.

Figure 4-2 simulates a condition where one steel bar is surrounded by concrete and subjected to a tensile force P. After cracking, a portion of the tensile member is isolated which includes two cracks as shown in the figure.

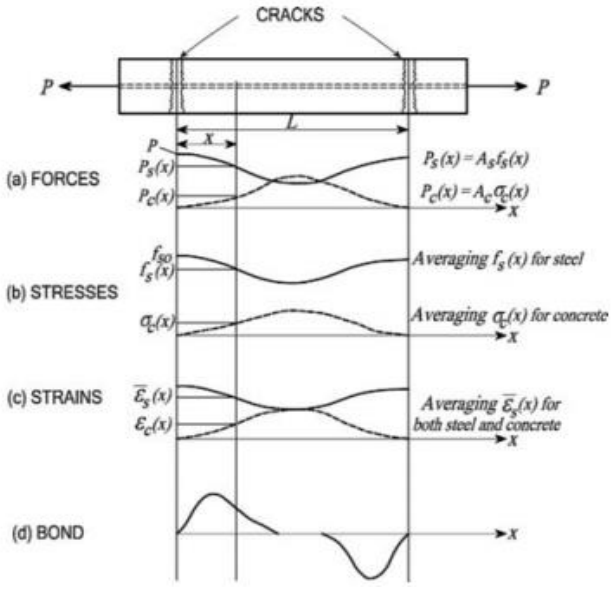

Figure 4-2 stresses and strain between cracks, (Hsu & Mo, 2010)

At the two cracks indicated there is stress only on the steel and is designated by *fso*. At any section a distance *x* from the first left crack, however, the steel stress will be less than *fso*, and the concrete in tension will carry the difference. When it comes to the strains, the steel strain decrease from a

maximum at the crack to a minimum at midpoint between the cracks. In contrast, the concrete strain should be zero at the crack and increase to a maximum at the midpoint between the cracks. This ideology of Hsu & Mo serves as a basis for the crack modeling in the preloaded beams to capture the damage incurred due to the imposed preload. At the cracks, both the concrete stress and strain are taken to be zero. The reinforcement bar in between this cracks will be subjected to all the stress and strain that could have been carried by the concrete. As a result, modeling the cracks as geometric gaps in the middle of the specimen could be a viable way of simulating the damage incurred due to the preloading.After meticulous observation of the crack in the preloaded specimens, they are modeled as geometric entities in the reinforced concrete.

Figure 4-3 state of specimens after preloading

4.3.2 Modeling of specimens

In an attempt to understand the relation between degree of damage and cracks in RC beams, Sharif et al. Reported that in RC beams with 85 % damage, the cracks height approached 75 % of the beam height with a maximum width of 1.5 mm. additionally, he also implied that there are no certain rules for crack width, length and interval. First, parametric values are assigned to these three geometric entities and results of numerical models are compared with the results of real experiments to obtain the modeling values for defining cracks. As a result, information about the crack depth is acquired from the experimental observation. From the final state of the beams after preloading, the maximum number of visible cracks was observed to be five. Furthermore, the cracks grew as deep as 150mm towards the compression zone. In the model, the cracks are distributed in the mid 500 mm span length at a spacing of 125 mm.

In the finite element modeling, the concrete between the cracks is assumed to have the same mechanical properties as that of the concrete in the crack free zones. Additionally, the cracks also are incepted in the model under the assumption that they all have progressed to a similar height.

The experimental program was planned to have a loading scenario controlled by displacement. As a result, to capture the post-peak behavior and to properly compare the results, a displacement controlled loading of 0.5 mm per load step is applied in the finite element simulation. The displacement control loading was applied at a node situated at the center of the beam. The figures below show the modeled beam using the discussed modeling schemes.

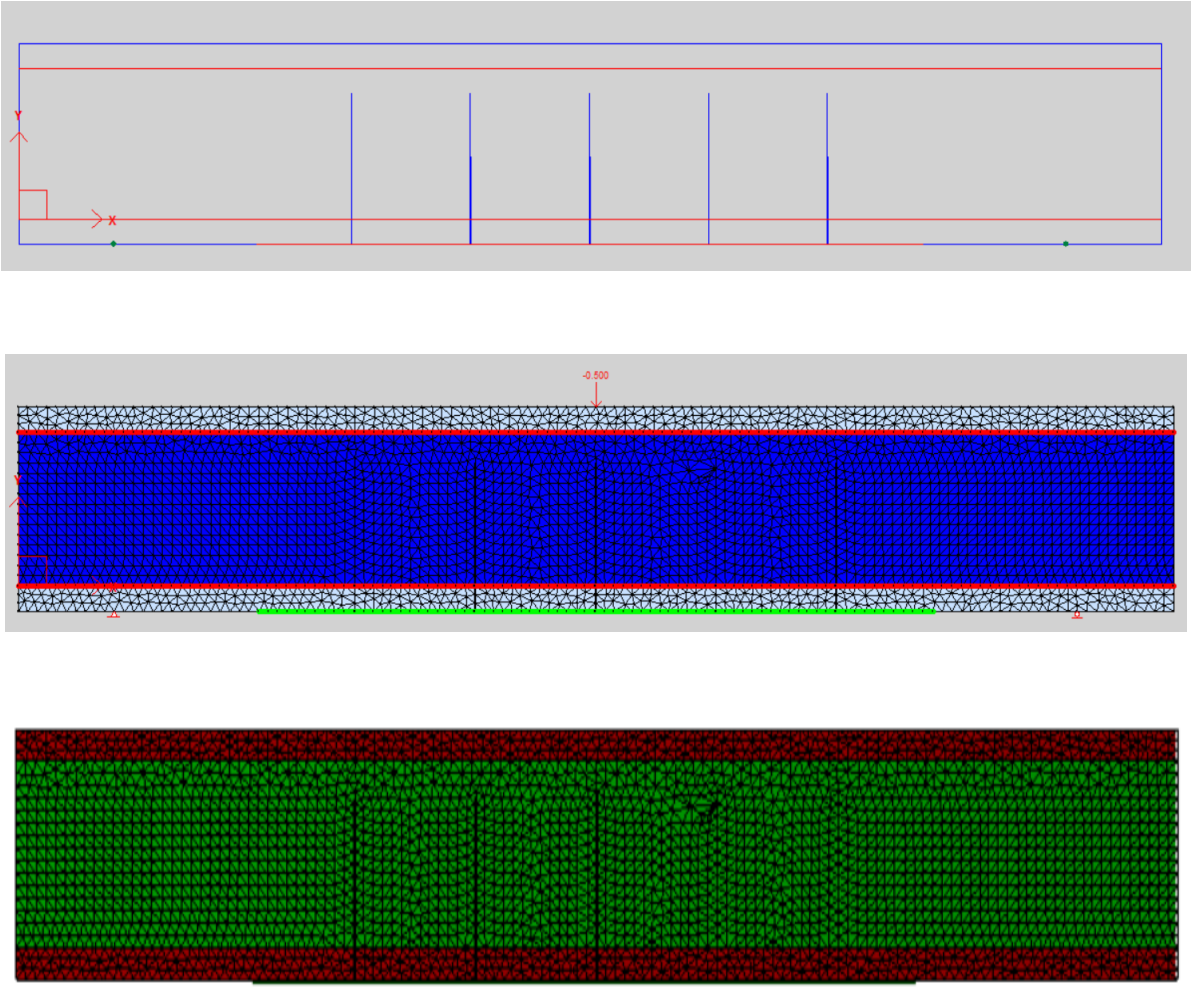

Figure 4-4 Modeling of repaired beams

5. Results and discussion

5.1 Experimental results of undamaged specimens

The experimental testing was done in three groups; control specimens, undamaged strengthened specimens and predamaged repaired specimens. Three items are tested for each specific case. The average of the three results is used for the comparison.

5.1.1 Control specimens (GK-CT-1, 2, 3)

All the three control specimens showed a ductile behavior up to failure.

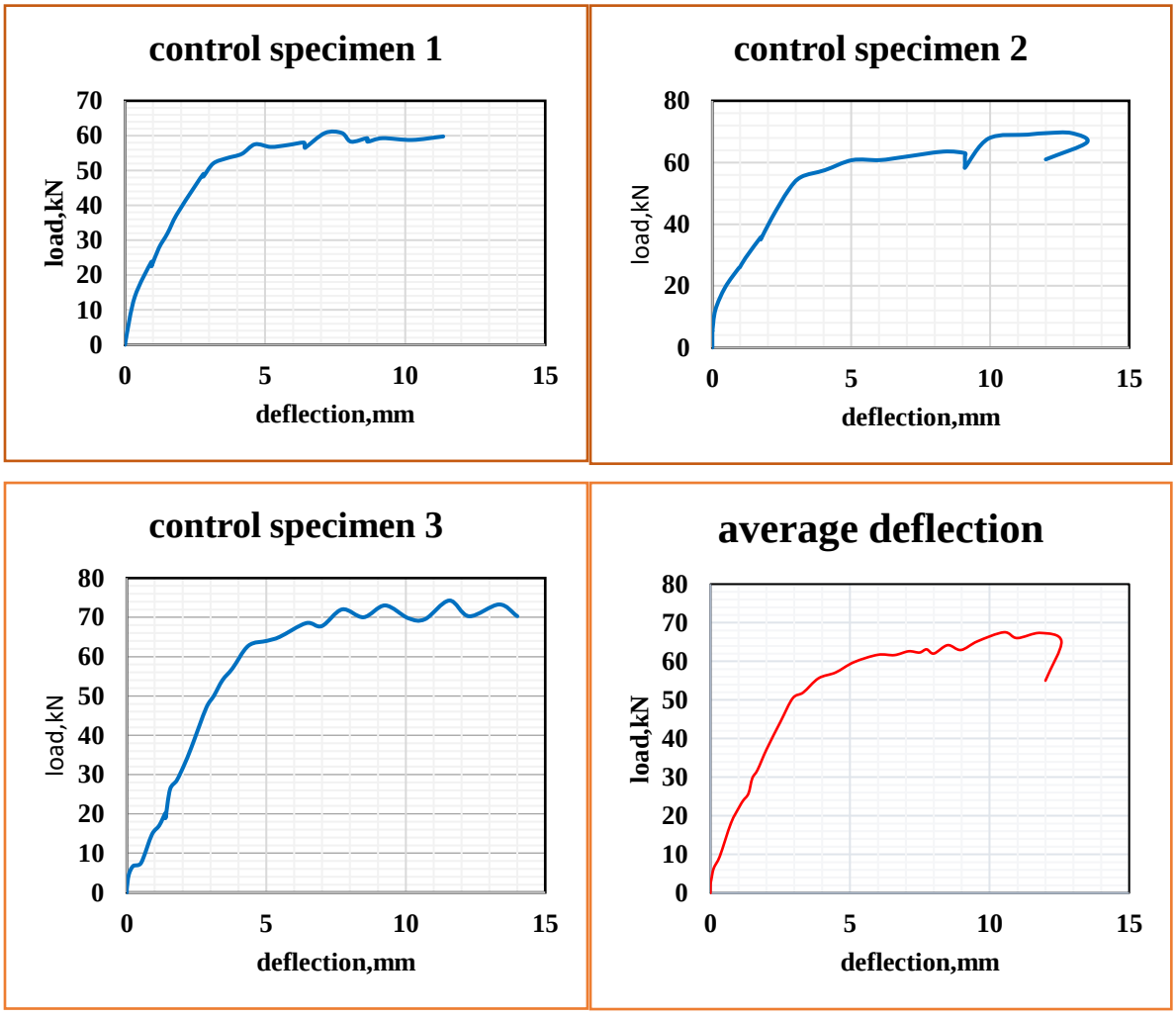

Figure 5-1 Load deflection response of control specimen

The control specimens exhibited a typical reinforced concrete beam behavior during the testing sessions. As it can be clearly seen in the load-deflection response diagrams, they all exhibited a ductile behavior prior to failure. At about 6 kN, the beam softened i.e. the stiffness degraded by certain amount, which can be owed to the formation of cracks. The slope of the load-deflection diagram shows a clear change of slope. The beams yielded at about 51 kN and also showed a uniform crack distribution. Once, the beams reached to their yield point, the cracks stopped growing and instead they were widening to their ultimate failure point i.e. crushing of the compression concrete.

Figure 5-2 final state of control specimen

5.1.2 Retrofitted specimens with three layers (GK-RET3-1, 2, 3)

These specimens have been modified in such a way that three layers of wire mesh-epoxy composite have been attached to the soffit of the beam over the middle 70% of the span length. From the load-deflection diagrams (Figure 5-3), it can be observed that the bonding of the wire-mesh epoxy composite has resulted in a different load-deflection response from that of the control specimens. The control specimens, once they reached at their yield strength, they showed an increment of deflection without a major increment in load. This is expected from ordinary reinforced concrete beam elements. Nevertheless, it is observed that this is not the case for these strengthened beam specimens. As it can be seen in the load-deflection diagram, the load reached at a maximum of 74 kN (average) before dropping down instantaneously. The epoxy acts as a matrix that binds the wire mesh together so that the wire elements act together in carrying the load as a single unit. It also has the same effect on the layers. Due to this fact, at ultimate load, the composite ruptured in an almost straight cut (see Figure 5.4).

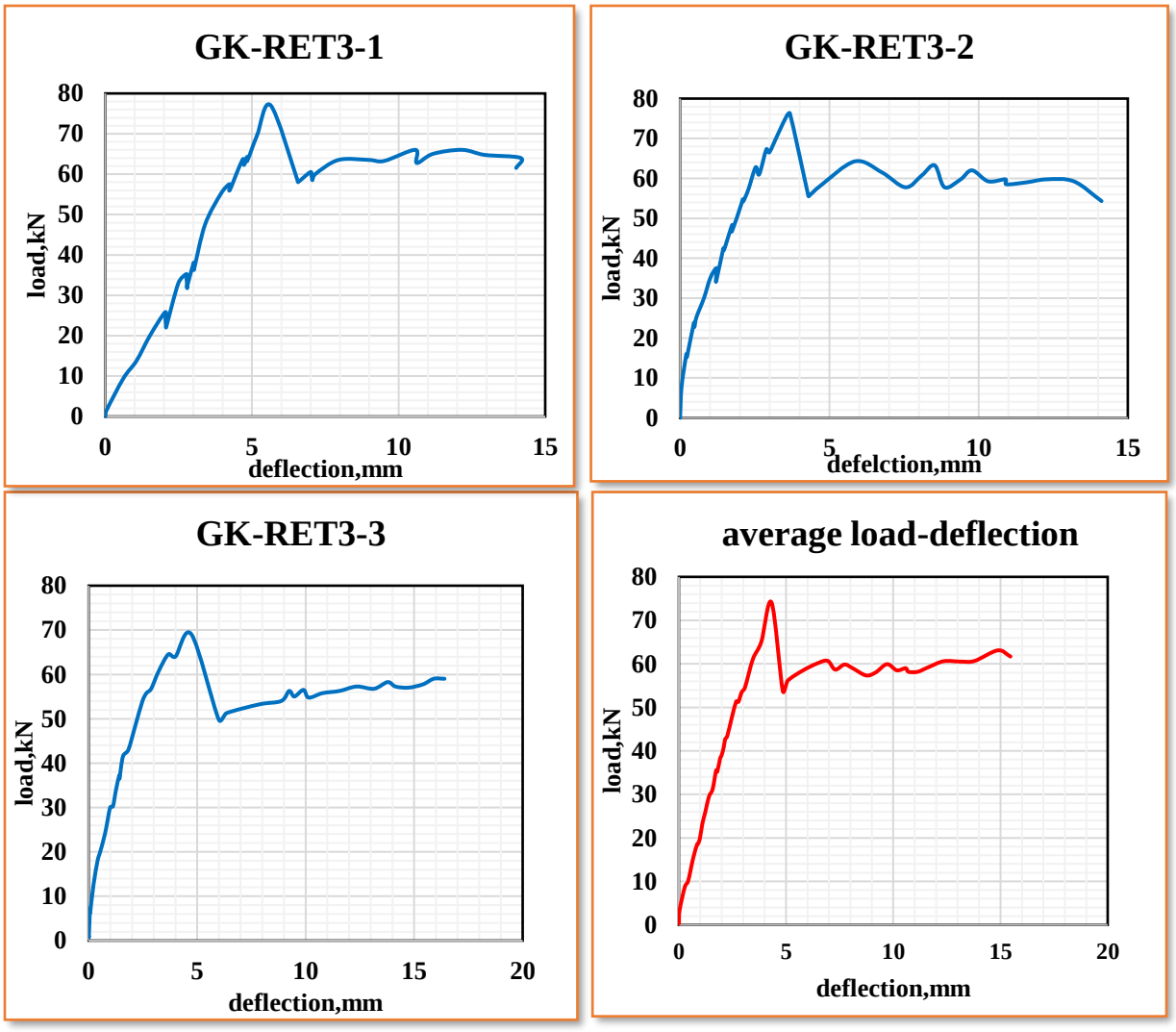

Figure 5-3 Load deflection diagram of retrofitted beam with three layers of the composite

The instantaneous rupture and loss of the action of the composite triggers an immediate transfer of load towards the reinforcement bars. This means, the beams become a conventional reinforced concrete beam without any externally bonded reinforcement. This causes the drop observed in the load deflection diagrams. After dropping instantaneously, the load-deflection response went on in such a way that the deflection increases without any major increment to the load. Besides these facts, the specimens showed a typical reinforced concrete beam behavior before failing due to the crushing of the compression concrete.

Figure 5-4 state of the GK-RET-3 series specimens at failure

5.1.3 Retrofitted specimen with five layers (GK-RET5-1, 2, 3)

These specimens have been modified in such a way that five layers of wire mesh-epoxy composite have been attached to the soffit of the beam over 70% of the span length. This resulted in 6.5mm increment on the overall depth of the beam. Unlike the three layer specimens, these specimens showed a behavior that deviates from the normally anticipated norm. Through the course of loading, it started out behaving like a typical reinforced concrete beam. As the loading progressed though, the deviations started to emerge. After the formation of the flexural cracks, it went on responding in the same expected manner until the first shear cracks occurred. The shear cracks occurred at the end of the attached layer of the wire mesh. These cracks started out vertical and as they stretched up to the compression zone turned to diagonal cracks. This indicates that the interruption of the layers in the middle of the shear span has resulted in a shear concentration at the end of the composite. After their formation, the cracks progressed to grow for a while. Under normal circumstances, it is expected that the flexural cracks widen and eventually lead to the failure of the beam. As the loading progressed though, a sudden and brittle peeling of the concrete at the bottom reinforcement level disrupted the shear cracks from widening to a level that result in failure. The peeling occurred at a maximum load of 88.01kN (average) with a high popping sound, which indicates the suddenness of the failure.

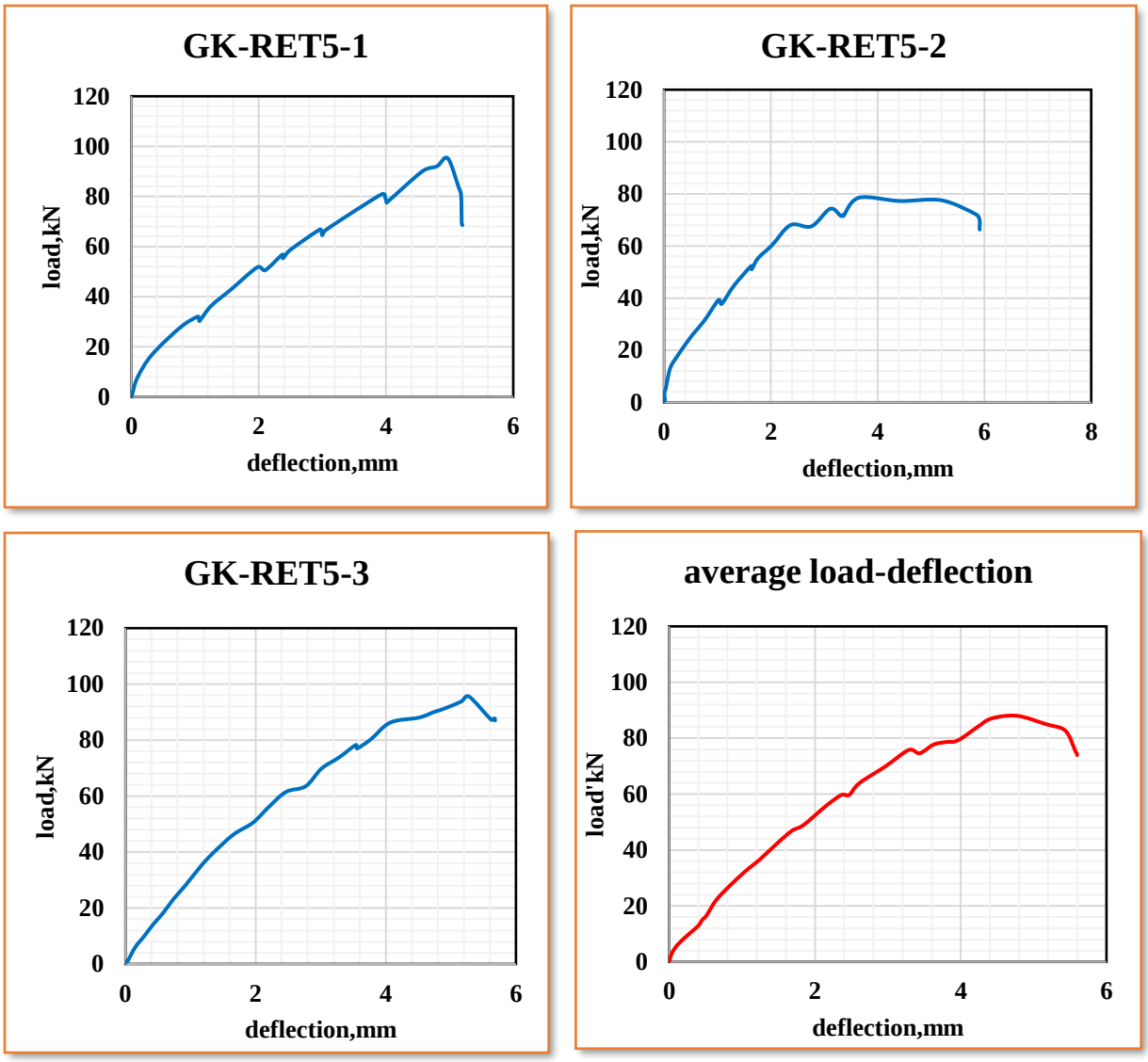

Figure 5-5 load deflection diagram of specimens retrofitted with five layers

Figure 5-6 (a) to (c) shows the beams at different loading stages. As it can be seen in figures 5-6 (a) and (b), the shear cracks started vertical and progressed to a diagonal crack as they developed towards the compression zone. However, before reaching the flexural capacity, the beams fail due to a sudden and brittle peeling at the bottom flexural reinforcement level. Figure 5-6(c) shows this peeling separation.

(a)

(b)

(c)

Figure 5-6 State of specimens retrofitted with five layers

5.1.4 Comparison of control (GK-CT-1,2,3) and three layered specimens (GK-RET3-1,2,3)

Throughout the course of the experimental investigation, it was observed that the attachment of the wire mesh-epoxy composite has modified the beams' flexural capacity. Figure 5-7 illustrates the comparison between the load-deflection response of the control specimens and the retrofitted specimens with three layers of wire mesh-epoxy composite. The average load-deflection response diagrams have been used for the comparison.

From the figure, it is apparent that the retrofitted beams have exhibited an increased flexural capacity than the control specimens. The control specimens experienced yielding around 51.9 kN while this figure rises to 74.1 kN when it comes to the retrofitted specimens. This shows 42.77% increment in the yield load i.e. flexural capacity, due to the wire-mesh epoxy composite.

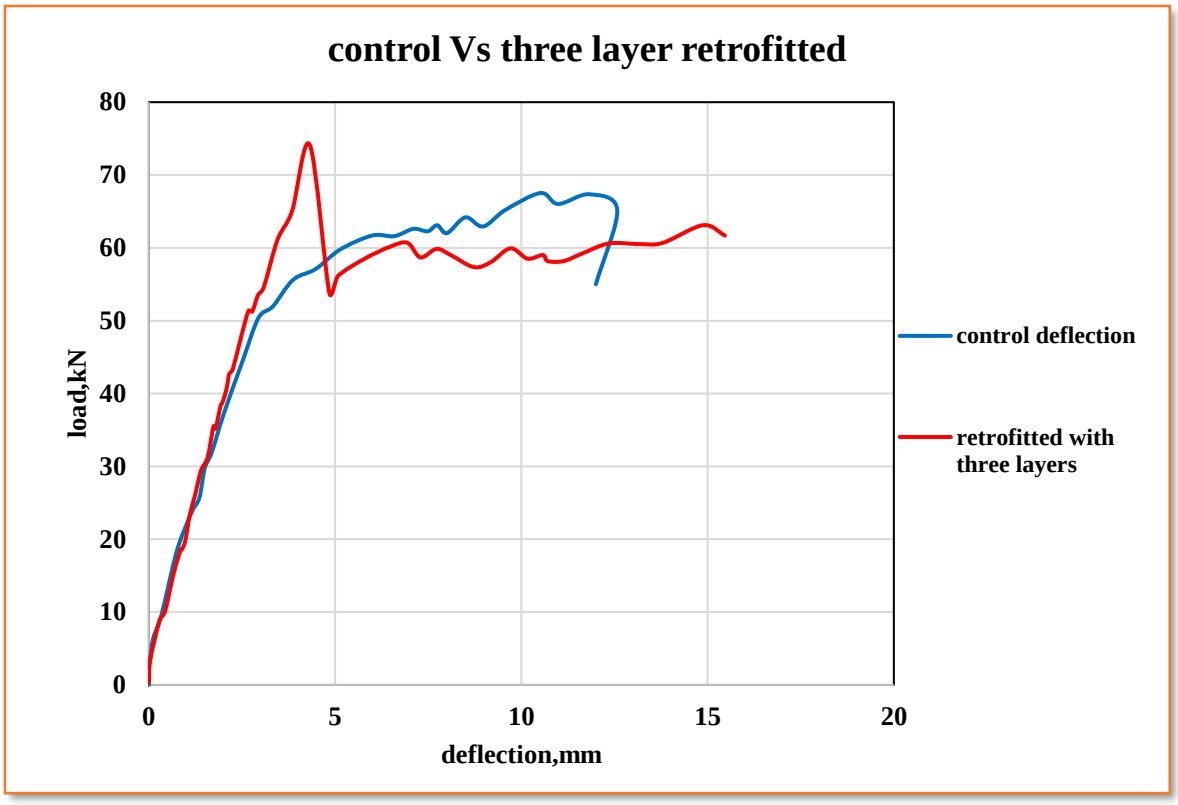

Figure 5-7 Comparison of control specimens and retrofitted specimens with three layers of the composite

Under the prevailing arrangement, although the technique boosted up the flexural capacity of the beam considerably, it did not have a noticeable impact on the stiffness of the beam in the serviceability limits. Prior to yielding, both specimens respond to the loading in a similar manner i.e. the slope of their load deflection diagram remain similar to their yielding point. In addition to the flexural capacity, the retrofitted specimens also showed an enhanced deflection capacity at failure. Other aspects like ductility and energy dissipation capacity can also be studied from the load-deflection diagrams. The information than can be inferred from these aspects helps to determine if the technique has an adverse effect on the dynamic load resistance capacity of the specimens. Calculating the deflection ductility index gives a value of 3.79 for the control specimens and 3.58 for the retrofitted specimens. This clearly shows a decrement in the ductility of the beams due to the attachment of external material that enhances the flexural capacity.

The area under the load-deflection diagram gives the total energy absorbed by the element (section 2.3). As a result, by using the load deflection diagram of the control specimen and the

retrofitted specimen with three layers, the effect of the technique on the energy absorption capacity of the members can be examined. Using the points on the chart, a formulation can be derived to determine the area under the charts. The average load-deflection charts are used in this case either. Calculating the area under the control specimen load-deflection diagram, the total energy absorbed is calculated to be 684.8 Joules.

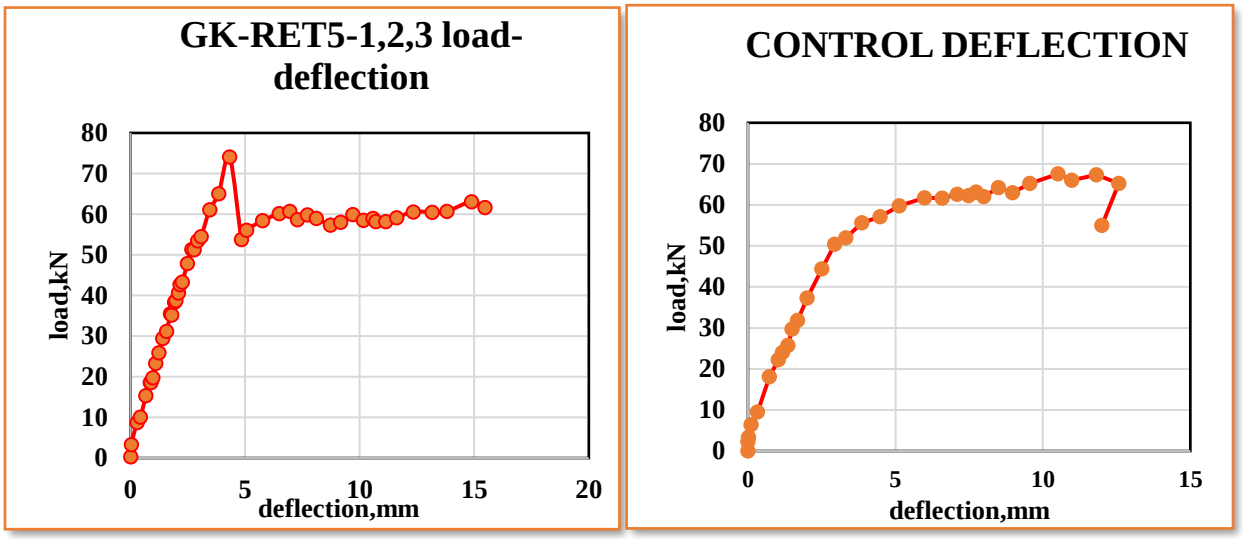

Figure 5-8 area under load deflection diagram of control and retrofitted specimens with three layers

Similar calculations carried out on the load-deflection diagram of the retrofitted sample with three layers i.e. area under the load-deflection diagrams in figure 5-8, estimate the total absorbed energy to be 854.09 Joules. In this case, the retrofitted samples have showed a considerable increment. More specifically, there is a 24.7% increment in the total absorbed energy.

5.1.5 Comparison of control(GK-CT-1,2,3) and five layered specimens(GK-RET5-1,2,3)

The attachment of five layers of wire mesh-epoxy composite has affected the properties of the reinforced concrete beam immensely. Figure 5.9 illustrates the comparison between the load-deflection response of the control specimens and the specimens that are retrofitted with five layers of wire mesh-epoxy composite. The average load-deflection diagrams are used in the comparison. Based on these diagrams, the modification in the flexural capacity, ductility and energy absorption capacity is examined.

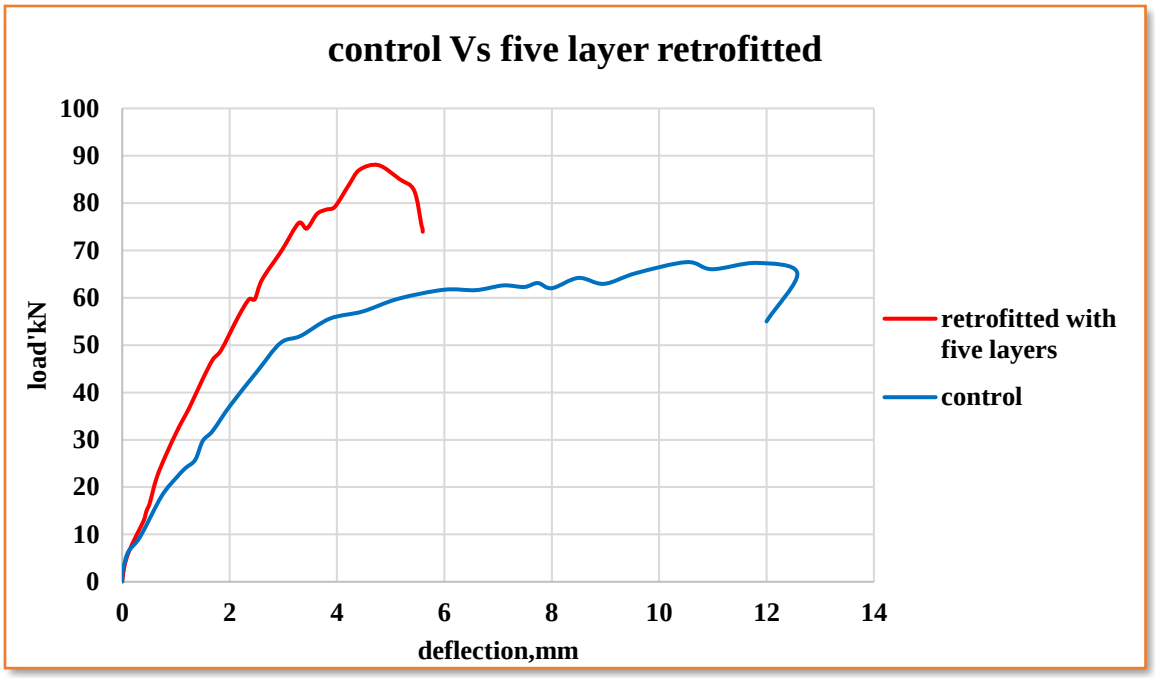

Figure 5-9 comparison of control specimen and retrofitted specimens with five layers of the composite

From figure 5-9, it can be clearly seen that the retrofitted specimens have showed an increment in their flexural capacity. The control specimens experienced yielding around 51.9 kN. This number increases to 88 kN for the retrofitted beams. This means there is a 69.6% increment in the flexural capacity of the beams. Additionally, unlike the specimens retrofitted with three layers, these specimens exhibit a stiffer response prior to yielding. However, the failure observed in these specimens is a rather brittle failure. Before reaching their ultimate flexural capacity, a sudden and brittle peeling occurred at the bottom reinforcement level (cover rip off). This indicates that the full strengthening potential of the technique has not been exploited. Further, the sudden and brittle failure hindered the beams from experiencing a ductile response in the post-yield regime. The loading was immediately interrupted once the peeling occurred in order to avoid any incidents that might endanger the safety of the working personnel or testing equipment. As a result, these specimens have a very low deflection ductility index of 1.17. Comparing this value with the specimens examined previously, one can infer that the ductility of the specimens in the GK-RET5 series has fallen considerably.

Here again, the energy absorption capacity can be examined from the area of the load-deflection diagrams using the points on the chart. Previously, the total energy absorbed in the control specimens through the course of the loading was determined to be 684.8 joules. For the GK-RET5 series, the area under the load-deflection diagrams give the total energy to be 335.2 Joules. In this case, there is a large fall in the energy absorption capacity, 51.11% decrement from the control specimens to be exact. The ductility of the specimens reduced too much that a large amount of energy that can be sustained through plastic deformation i.e. irrecoverable deflection in the post yield region, is lost.

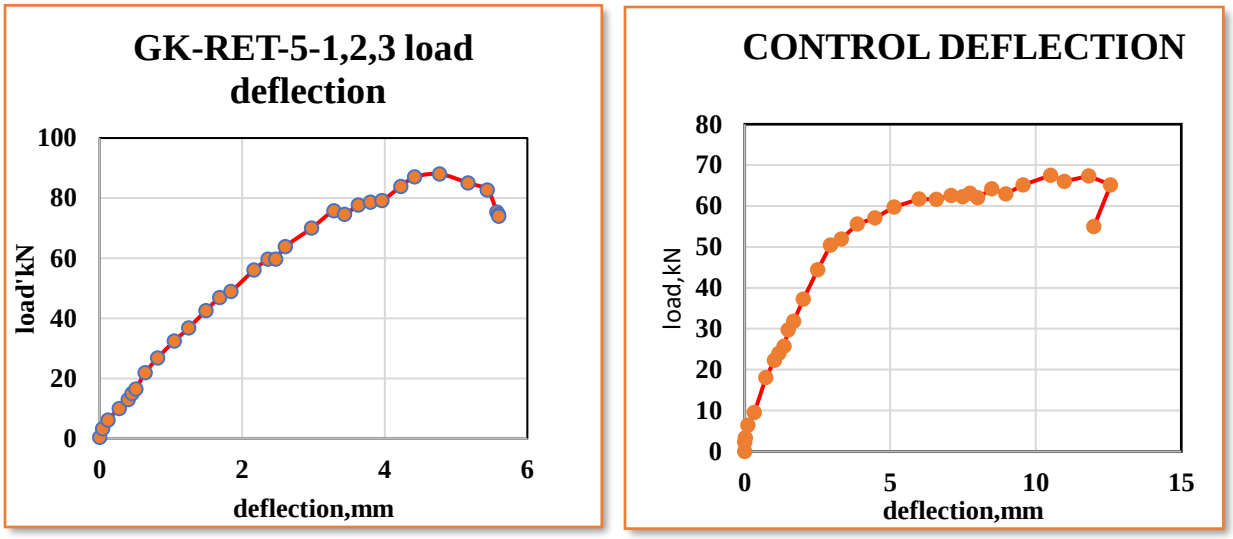

Figure 5-10 area under load deflection diagram of specimens retrofitted with five layers of the composite

5.1.6 Summary of strengthened specimens

Figure 5.11 shows the comparison in the response of the specimens towards the imposed load. The "GK-RET5" series specimens showed a stiffer response towards the load prior to yielding and showed a larger increment in flexural load capacity than the "GK-RET3" series specimens before experiencing a sudden and brittle failure due to flexural-shear peeling at the bottom reinforcement level. They failed prior to reaching their flexural capacity due to the sudden peeling failure.

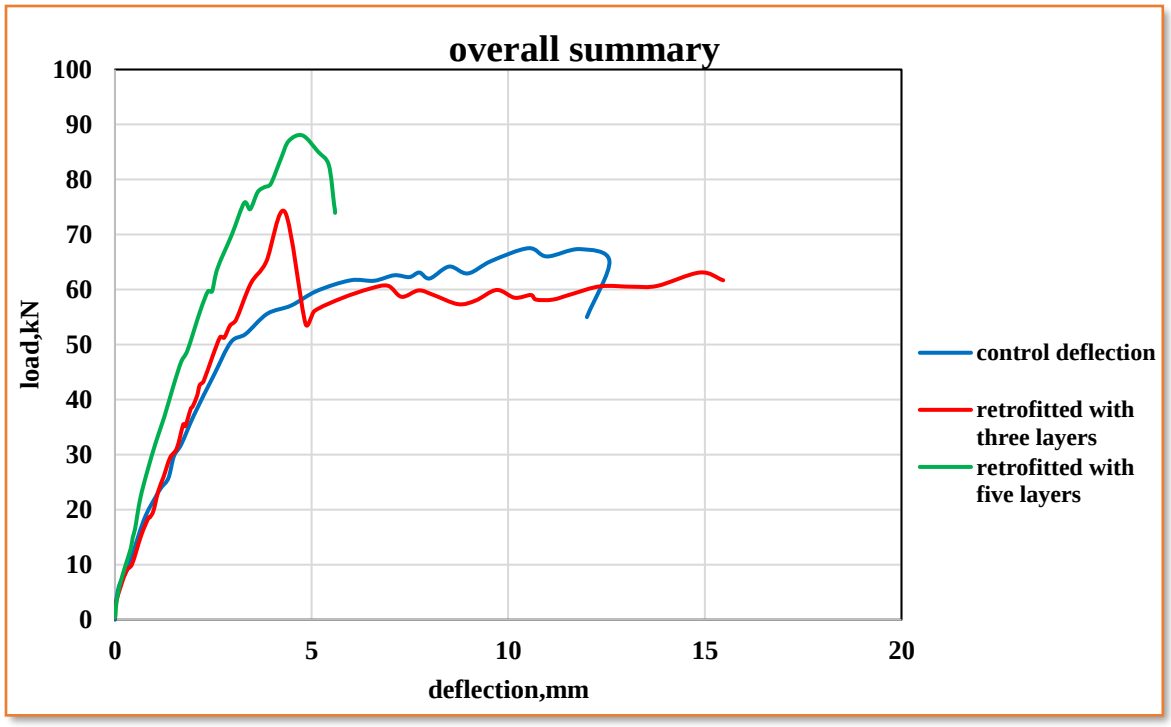

Figure 5-11 overall comparison among control specimens, retrofitted specimens with three layers and five layers of the composite

Table 5-1 summarizes the results of the different test series in the strengthening regiment.

Table 5-1 Summary of test outputs for strengthening scheme

specimen	Maximum load, kN		Mid-span deflection mm		Deflection ductility index		Total energy absorbed, Joule	
	load	%increase	At yield	failure	value	%change	value	%change
GK-CT-1,2,3	51.9	-	3.32	12.57	3.79	-	684.8	-
GK-RET3-1,2,3	74.1	42.77 ↑	4.32	15.47	3.58	5.5 ↓	854.09	24.72 ↑
GK-RET5-1,2,3	88	69.55 ↑	4.77	5.6	1.17	69.1 ↓	335.2	51.11 ↓

↑-*increment*
↓-*decrement*

5.2 Experimental results of predamaged specimens

Most research works related to retrofitting tend to focus only on strengthening of undamaged members, which is a rather incorrect approach since all structures that are in need of strengthening are preloaded to some extent. In order to address this shortcoming of previous researches, this thesis has incorporated a test series of preloaded specimens.

5.2.1 Extent of preloading

Figure 5-12 presents the level of the preload in the specimens.

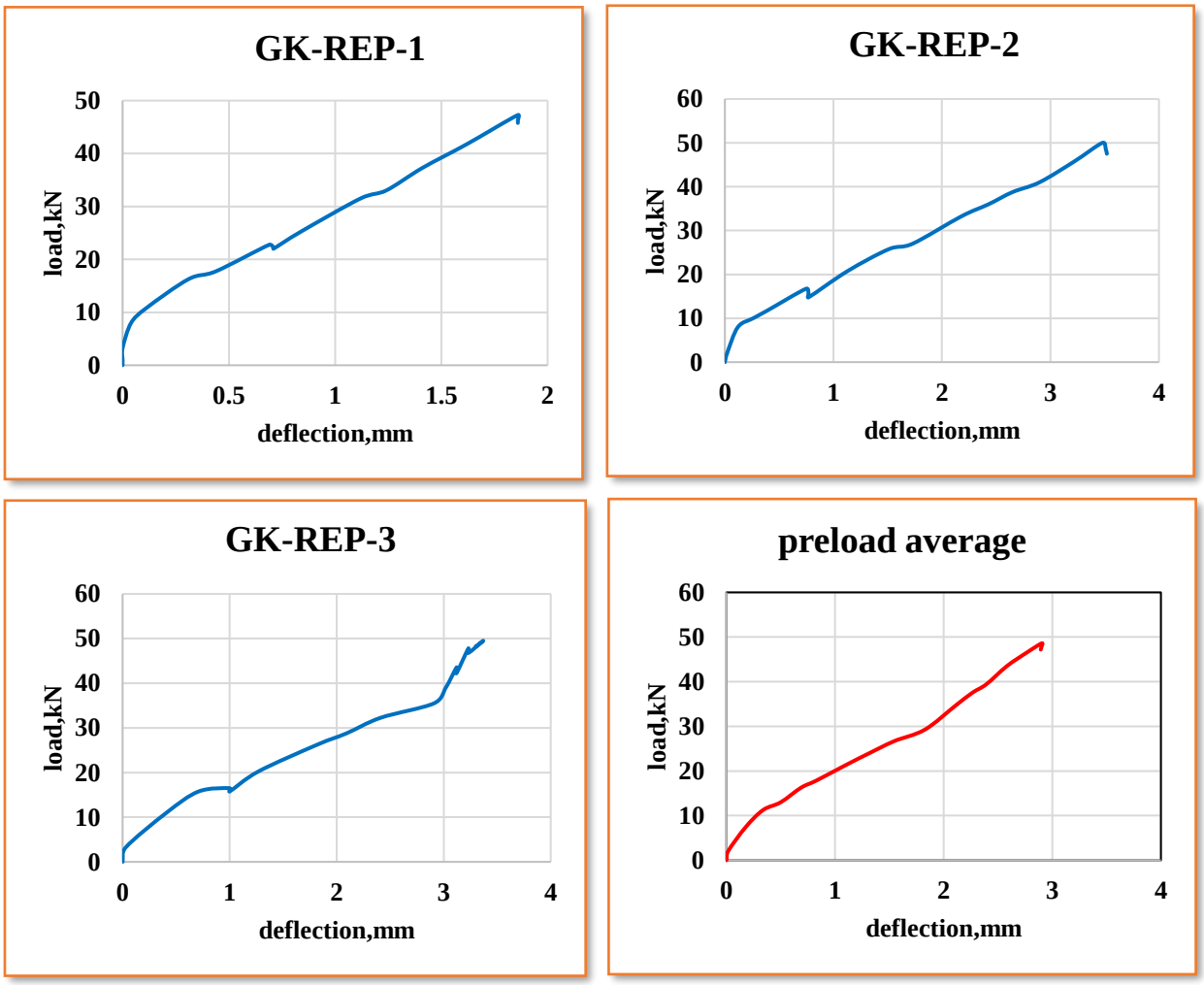

Figure 5-12 preloading extent of repaired specimens

All the necessary caution was taken so that the specimens will not be loaded beyond their yield load since the purpose of the test is to investigate the capability of the technique to retrofit damaged

elements. As a result, care needed to be taken in order to avoid yielding of the reinforcement since the composite is not intended to replace actual reinforcement but rather to assist.

The intention was to load the specimens up to at least 85%, at most 95% of their actual capacity. Since the loading was carried out manually, (i.e. without the help of load actuator), a certain margin of error must be taken into consideration. During the course of the loading, the progress of the cracks was recorded carefully for the numerical simulation parts. The actual level of loading in the specimens is determined from the comparison between these specimens and the previously discussed control specimens.

From figure 5-13, it is apparent that the "GK-REP-RET" series specimens were unloaded prior to reaching their yield load. The specimens have been loaded up to 93.6% their yield load capacity. This is few moments earlier before the yielding of the reinforcement. This means most of the damage that can be incurred on the beams in the pre-yield state has already occurred.

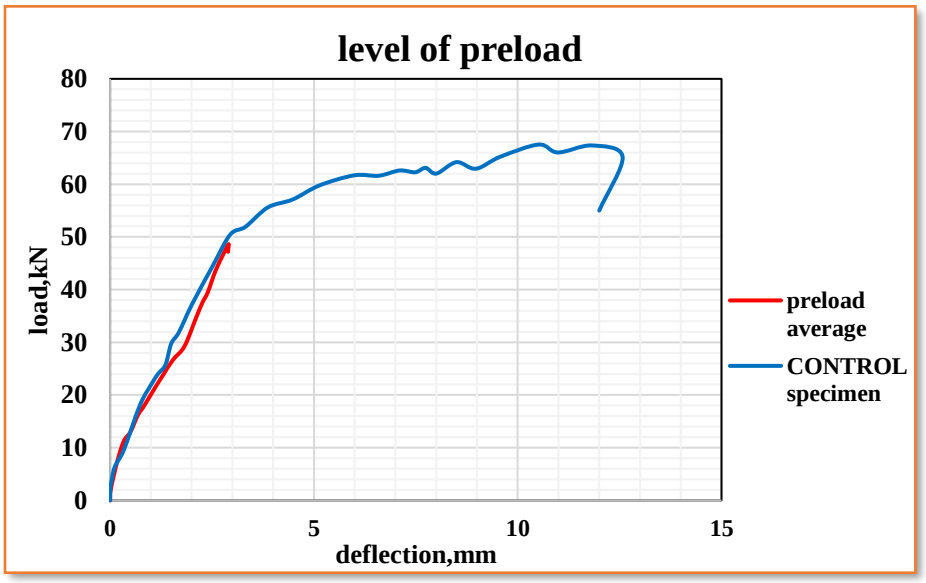

Figure 5-13 level of preloading in the GK-REP series specimens

Figure 5-14 state of beams after preloading

Figure 5.14 shows the final states of the preloaded specimens prior to repair measures. Uniformly distributed cracks in the mid 50% of the span length were observed in all the three specimens. These cracks are vertical cracks that have progressed a little further above the middle of the beams' section. Taking approximate results, they have progressed up to a maximum 75% of the beams' depth.

5.2.2 Results of repaired specimens

Once the preloading is carried out, five layers of the wire-mesh epoxy composite were attached to the mid 70% of the span length. After that, the repaired specimens were tested again and their results' examination and comparison is carried out in subsequent sections.

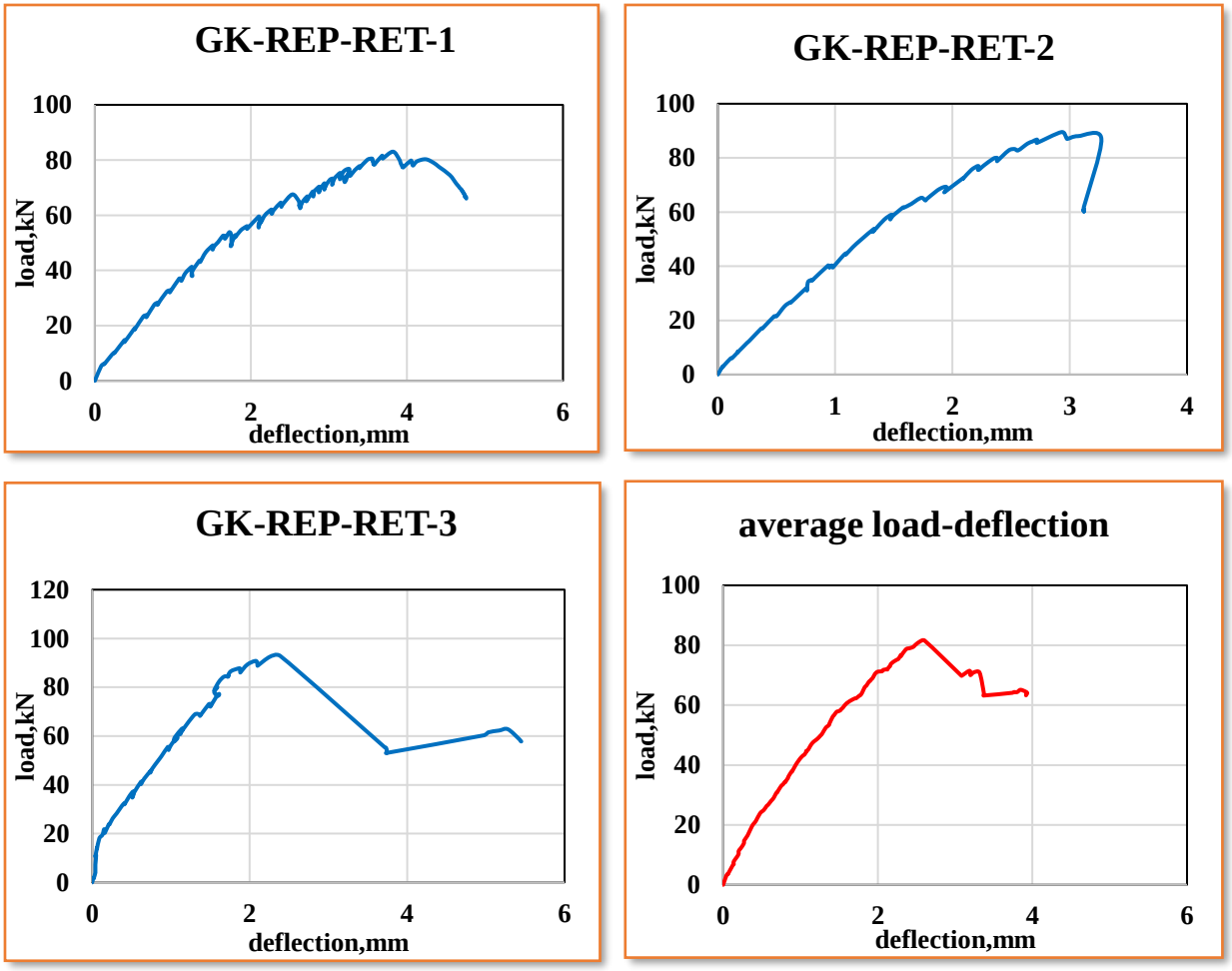

Figure 5-15 load deflection diagram of "GK-REP-RET" series specimens

The repaired specimens behaved more like the strengthened specimens in most ways. The specimens failed in a similar sudden and brittle manner as that of the undamaged members with five layers. However, on one of the specimens, the peeling started at the beam-composite interface and progressed to reinforcement level. The most probable cause for this is due to workmanship errors. It can be due to either cement paste laitance or insufficient pressure around that area during the early bonding age of the composite and the beam (figure 5-16). The aforementioned brittle peeling of the concrete at the bottom reinforcement level occurred at around 81 kN for these specimens, which is a little less than that of the strengthened specimens' results. This is due to the damage of the concrete prior to strengthening.

In general, it can be observed that the preloading did not have that much of effect on the ultimate load that can be carried by the modified specimens. This is due to the fact that, the only part that sustained the damage incurred is the concrete in the tension zone, which does not have a significant contribution in the flexural capacity of the beam when compared with the steel reinforcements. Furthermore, the reinforcement in the beams has not yielded which indicates that any deformation or damage imposed during the preloading stage is reversible. Additionally, due to the pressure imposed to laminate the composite material may result in sealing of part of the cracks with the epoxy; a material with much higher tensile strength than the concrete.

(a)

(b)

Figure 5-16 failure state of GK-REP-RET series specimens

5.2.3 Comparison of repaired specimens and control specimens

Figure 5.17 below represents the comparison between the control specimens and the repaired specimens. Due to the attachment of the wire mesh-epoxy composite and the sealing of the cracks with the epoxy, the repaired beams responded to the load in a much stiffer manner.

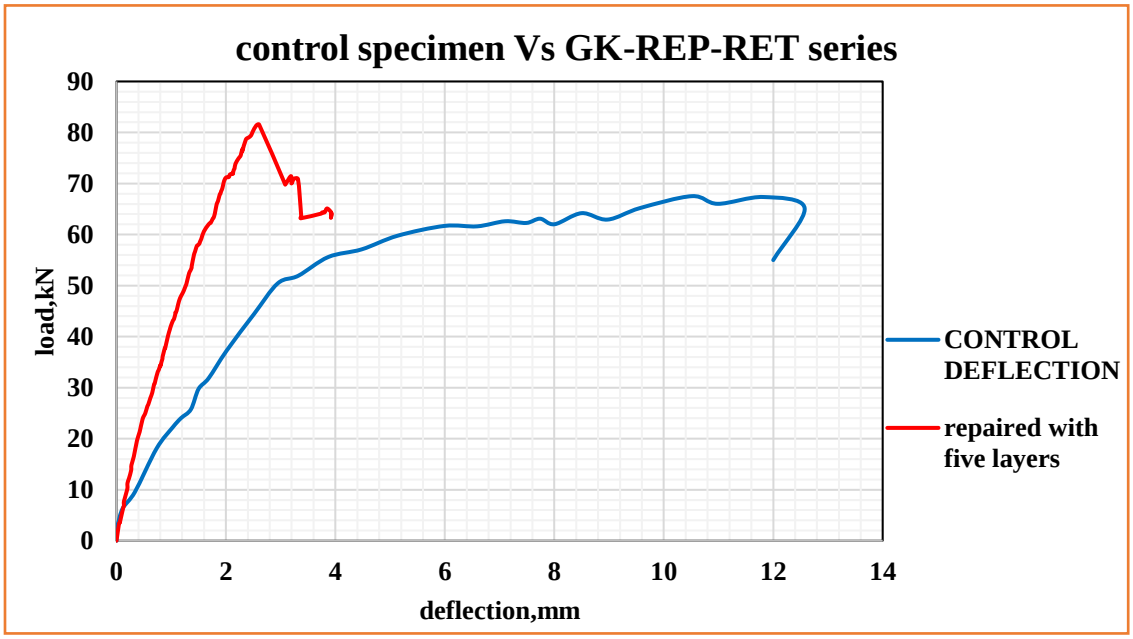

Figure 5-17 comparison between control specimens and repaired specimens with five layers

The control specimens experienced yielding at about 51.9kN.this figure rises to 81.5 kN when it comes the repaired specimens. There is a 57% increment above the original capacity of the beams; a figure that is slightly less than for the strengthened specimens. This means, the technique not only restored the strength of the beam but it strengthened it as well. There is a 57% increment over the control specimens.

Besides the modifications in the flexural performance, alterations in other aspects like ductility and energy absorption capacity is expected and inevitable. Just as the case of the strengthened specimens, the brittleness of the failure has resulted in a less ductile behavior after the peak load. The deflection ductility index is calculated to be 1.5. Compared with the control specimens, it is obvious that there is a considerable loss of ductility in the repaired specimens.

Furthermore, the area under the load-deflection diagram i.e. the total energy absorbed up to the failure point is determined to be 224.6 Joules. The total energy in the control specimens was calculated to be 684.8 Joules. Comparing the two, we can infer that there is a noticeable decrement

in the energy absorption capacity. A total fall of 67.2% can be observed from the comparison. The brittle failure coupled with the energy lost in the preloading stage due to crack formation, are the possible cause for this fall.

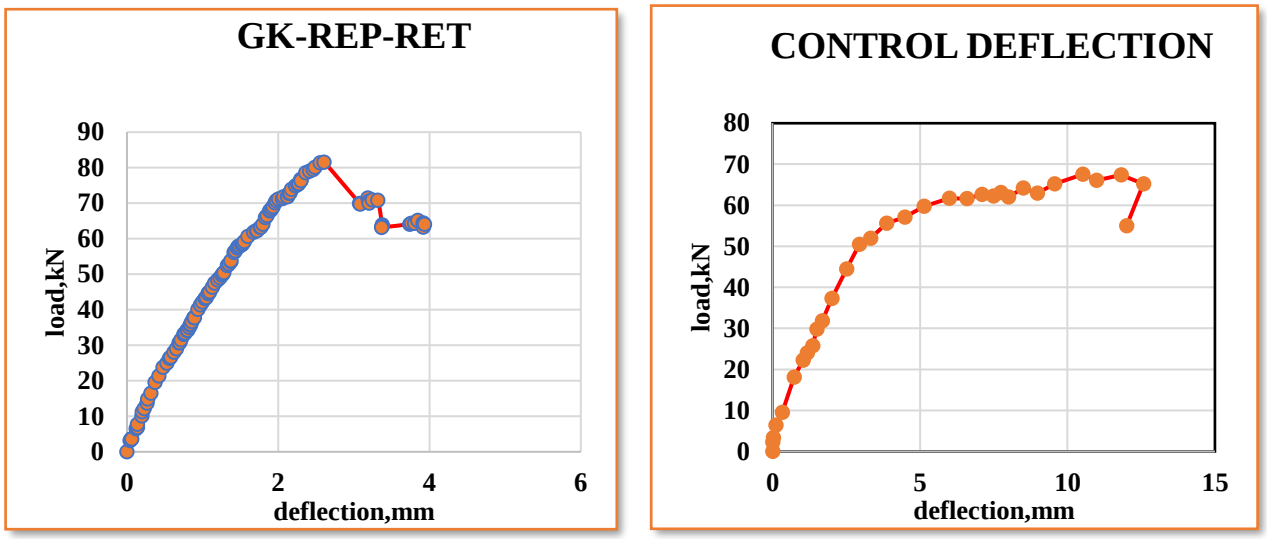

Figure 5-18 area under load-deflection diagram of GK-REP-RET series

5.2.4 Overall summary

The following table summarize the overall results, outputs and comparison carried out over the specimens that passed through preloading, (i.e. damage).

Table 5-2 Summary of test outputs of repairing scheme

specimen	Maximum load kN		Mid-span deflection mm		Deflection ductility index		Total energy absorbed, Joule	
	load	%increase	At yield	failure	value	%change	value	%change
GK-CT-1,2,3	51.9	-	3.32	12.57	3.79	-	684.8	-
GK-REP-RET1,2,3	81.5	57% ↑	2.6	3.92	1.5	60.4 ↓	224.6	67.2% ↓

↑-*increment*
↓-*decrement*

5.3 Results of nonlinear finite element analysis of undamaged specimens

5.3.1 Results of analysis

Figure 5.19 presents the load deflection diagram of the specimens modeled using the discussed behavioral and constitutive models. The figure shows the results of the simulations carried out on all three specimens (Table 4-1).

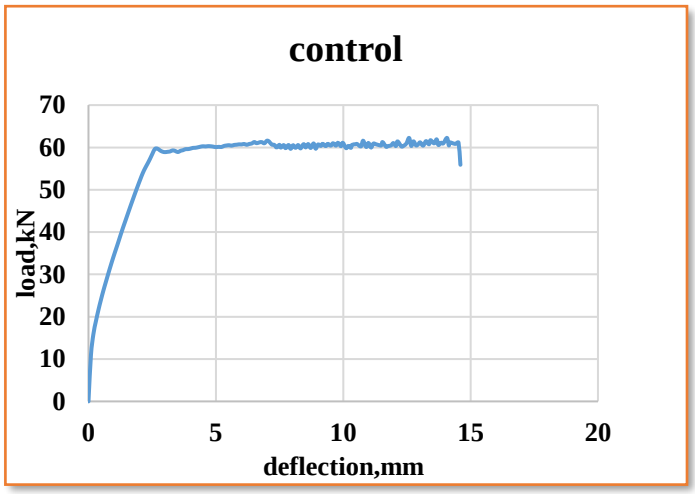

(a)

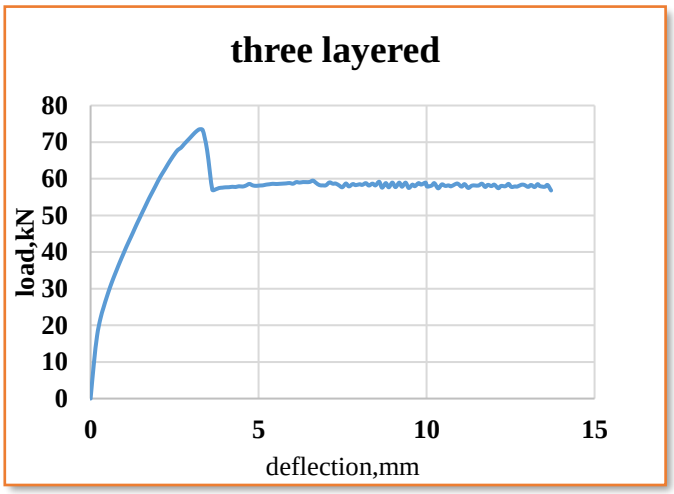

(b)

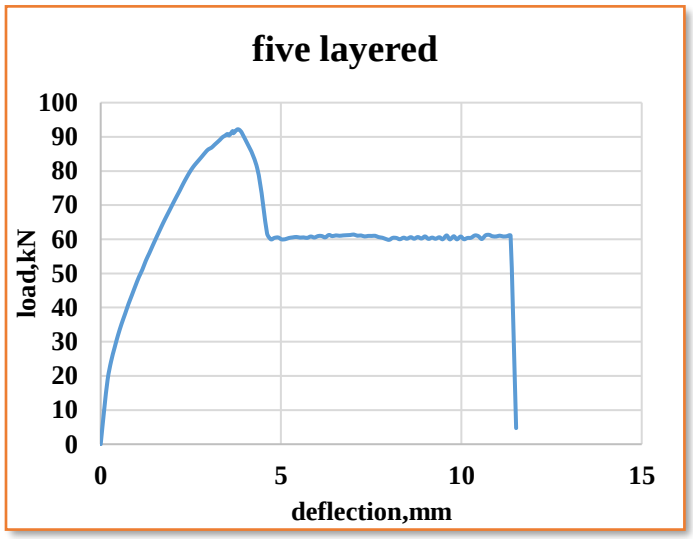

(c)

Figure 5-19 Load-deflection diagram from VecTor2 simulation (a) control specimen (b) retrofitted specimen with three layers of the composite (c) retrofitted specimens with five layers of the composite

As it can be observed in the diagram, the software is capable of capturing the post peak behavior of reinforced concrete element. In addition to that, the unloading point can be clearly seen in the load deflection diagram. Unlike many other simulation software, VecTor2 is capable of determining the failure instant in reinforced concrete beams which makes it a powerful tool to carry out studies related to ductility, failure mechanism, energy absorption etc.

5.3.2 Comparison of NLFEA results and experimental results

Control specimens

The figures below show the comparison between the finite element simulation result of the control specimens and the experimental counterparts.

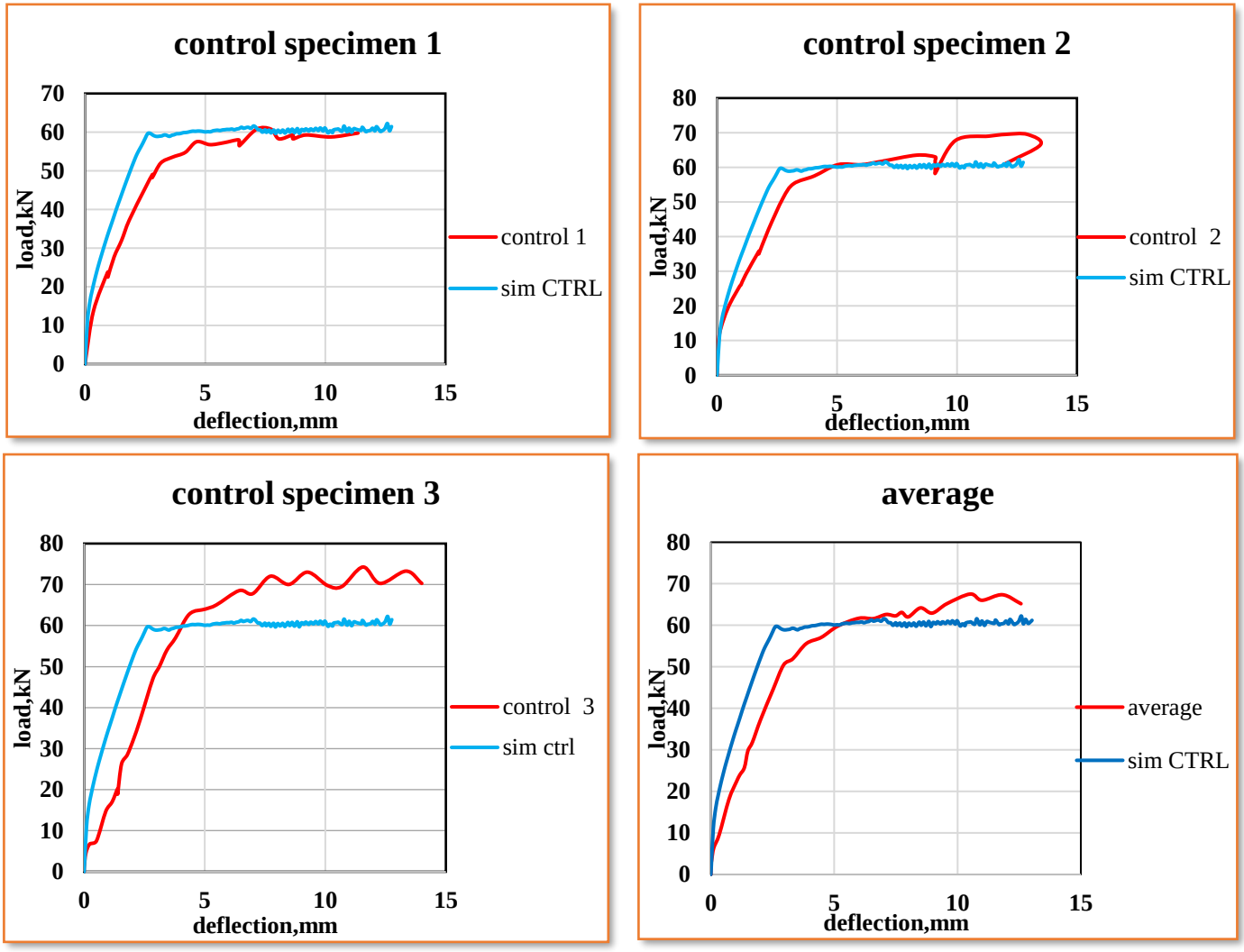

Figure 5-20 comparison of the control specimens with the FEM counterpart

From the comparisons, it can be observed that there is a good agreement between the NLFEA result and the experimental counterparts. The first two control specimens show good agreement with the simulation result. However, it can also be observed that there is a discrepancy in the third control case. The deviation of the third case can be attributed to material property discrepancy occurred in the preparation of the specimens. Using the average of the first two control cases, a better agreement can be obtained as illustrated in Figure 5-21 below.

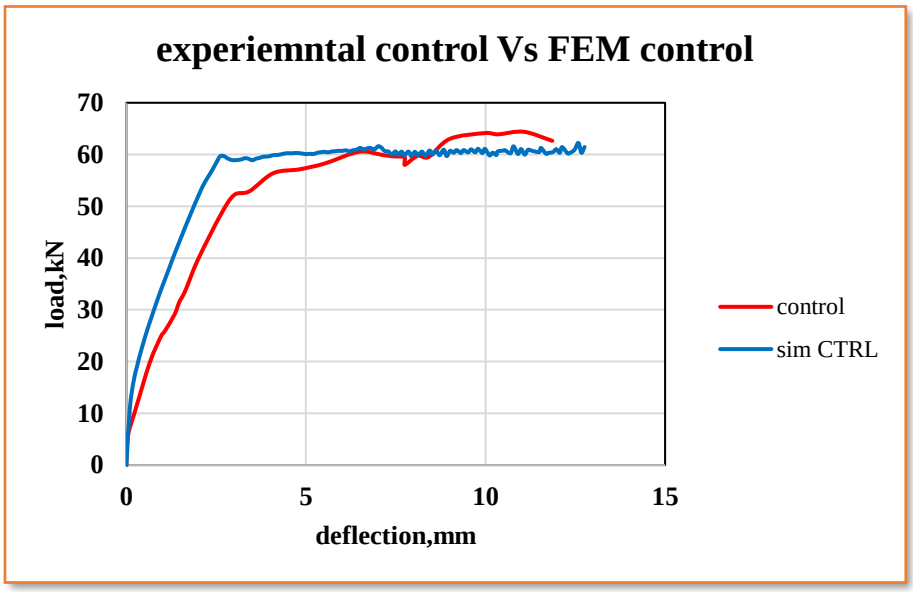

Figure 5-21 comparison between the average of control specimen 1&2 and the FEM counterpart

Three layered specimens

This section presents the comparison between the three layered experimental specimens and their FEM counterpart. From the comparison, it can be observed that there is a good agreement in these cases as well.

In the three layered experimental specimens, an instantaneous drop was observed in the load deflection diagrams as soon as the composite ruptured. The drop is triggered by the loss of the action of the composite due to the rupture. As such drop was also observed in the three layered FEM cases. The subsequent figures illustrate the comparisons.

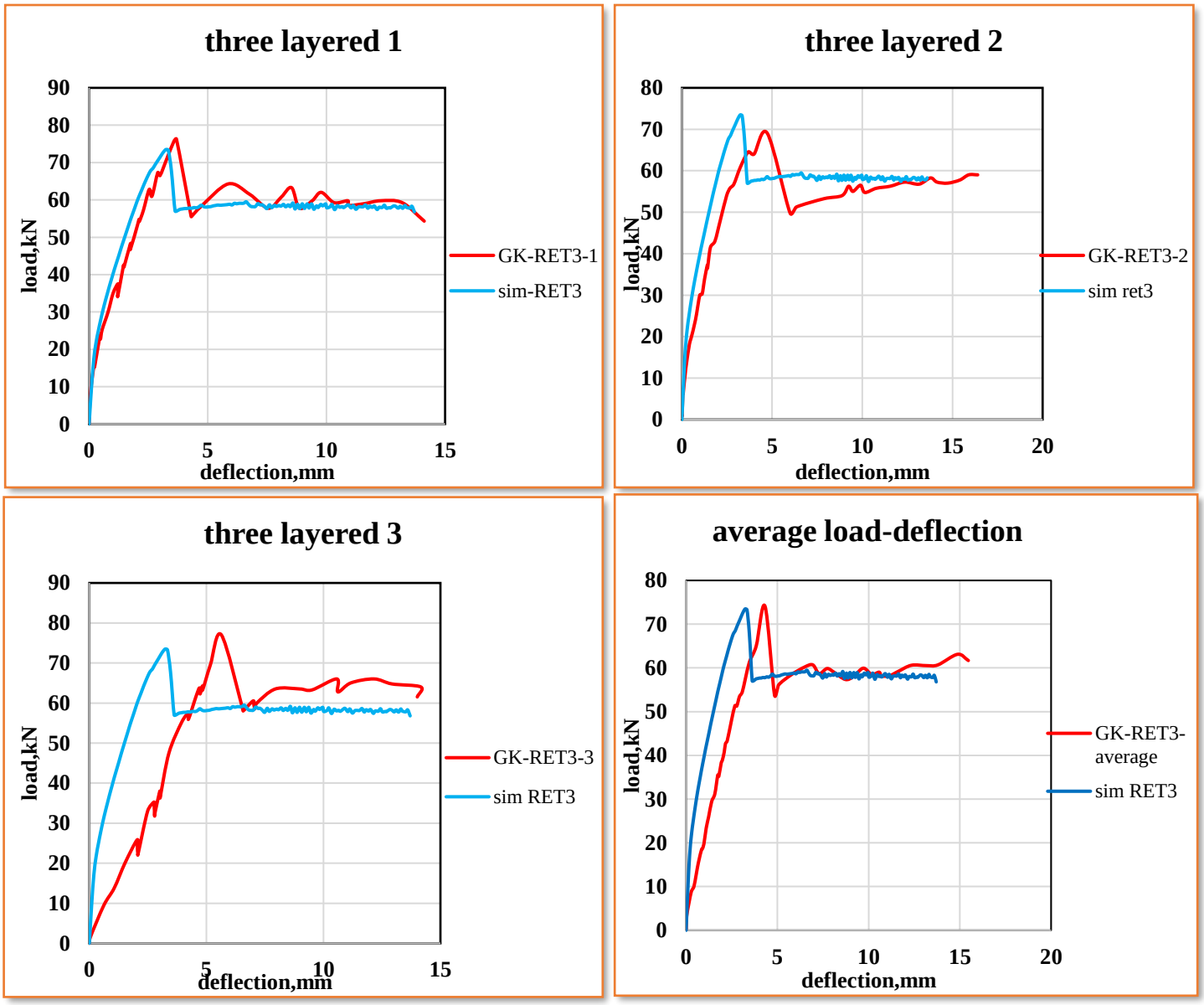

Figure 5-22 comparison of three layered specimens with the FEM counterpart

Similar discrepancy observed in one of the control cases is also observed on one of the three layered cases. A comparison conducted between the average of the first two specimens and the FEM results gives a better agreement.

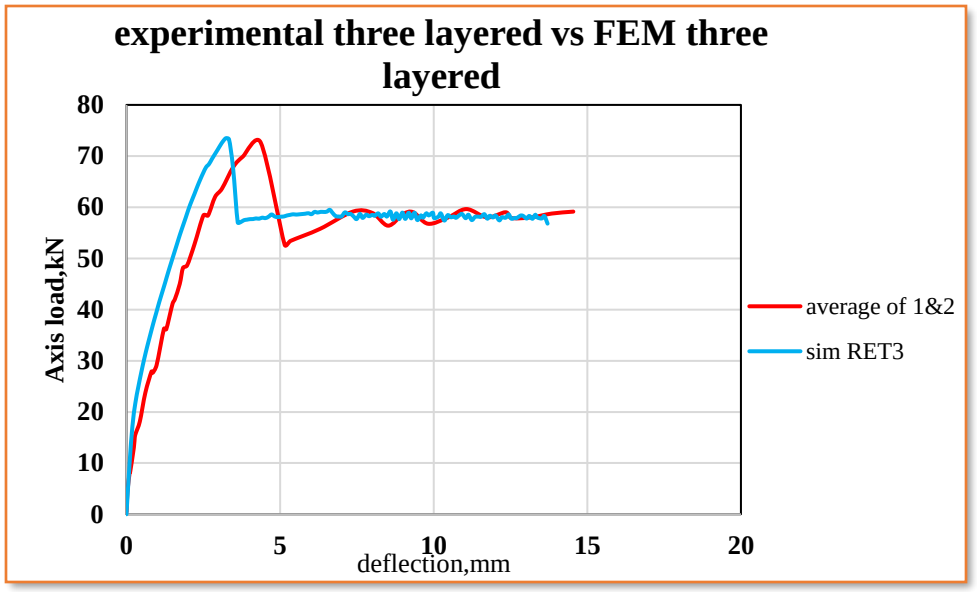

Figure 5-23comparison between average of the three layered specimens 1&2 and FEM counterpart

Five layered specimens

in this case, a comparison is carried out between the simulation result of the five layered specimens and the experimental counterparts. From the comparisons, it can be observed that there is a good agreement between the experimental and the five layered specimens. Unlike the experimental specimens, the simulation results show ductile behavior post-peak. Since the concrete cover peeling is not considered as failure limit, the beam keeps on deflecting until the other failure limits are met. The subsequent figures present the comparison of the experimental and FEM five layered specimens.

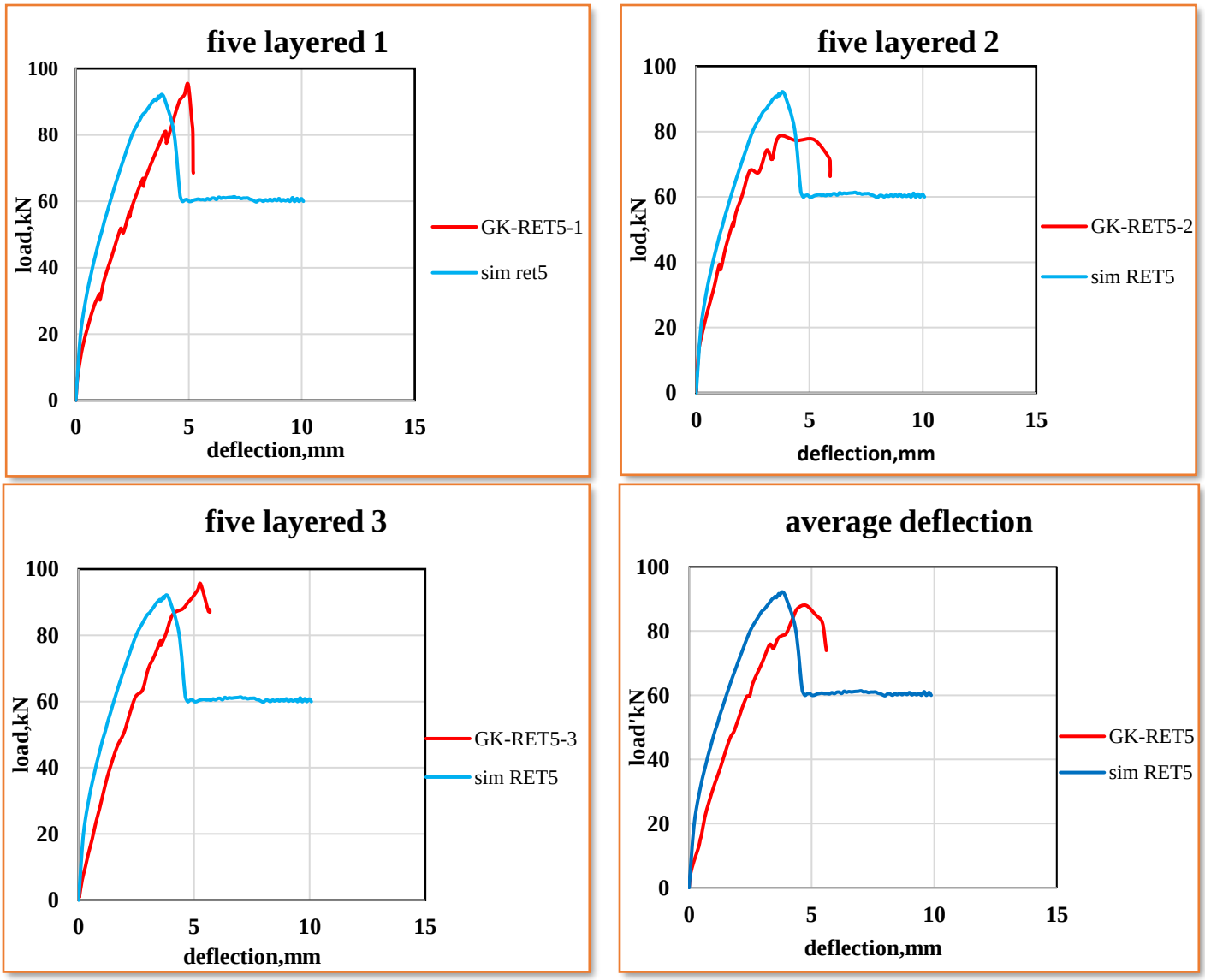

Figure 5-24 comparison between the five layered specimens and the FEM counterpart

5.3.3 failure patterns of NLFEA results

The comparisons conducted on the load deflection diagrams of the experimental specimens and FEM results indicate that there is an acceptable agreement between the outputs. This shows the power of the software in capturing the nonlinear behavior of reinforced concrete elements. The agreement is also observed in the failure patterns of the specimens as well. When it comes to the control and the three layered cases, flexural failure was the governing failure in both the experimental and FEM specimens. Concerning the five layered specimens though, concrete cover rip off was observed in both the experimental and FEM cases.

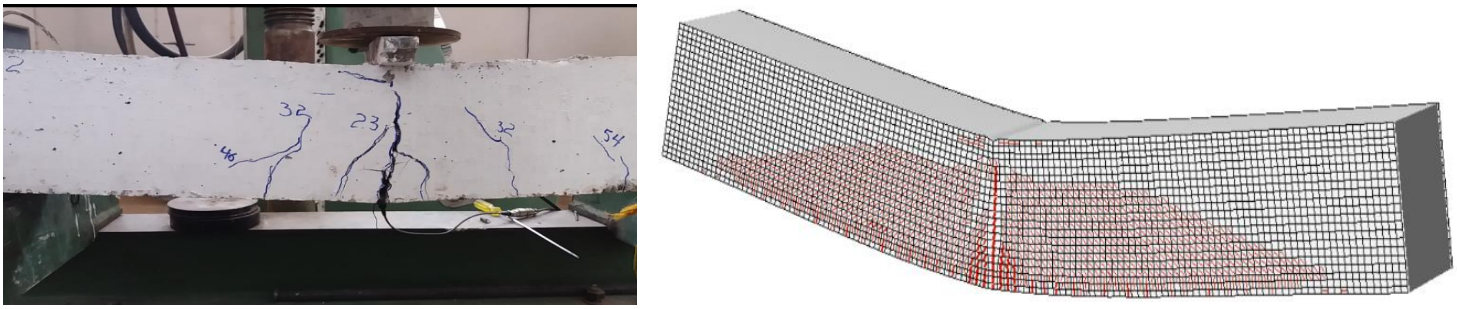

Control specimens

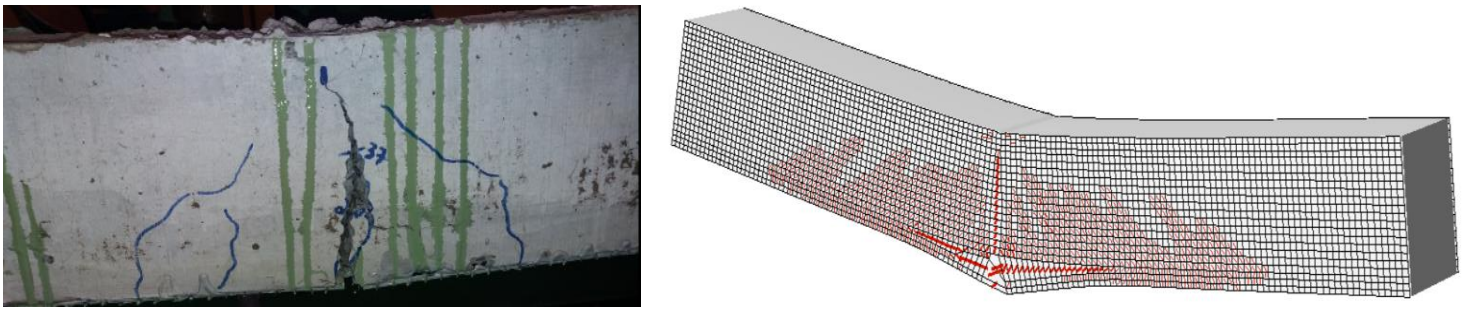

Three layered specimens

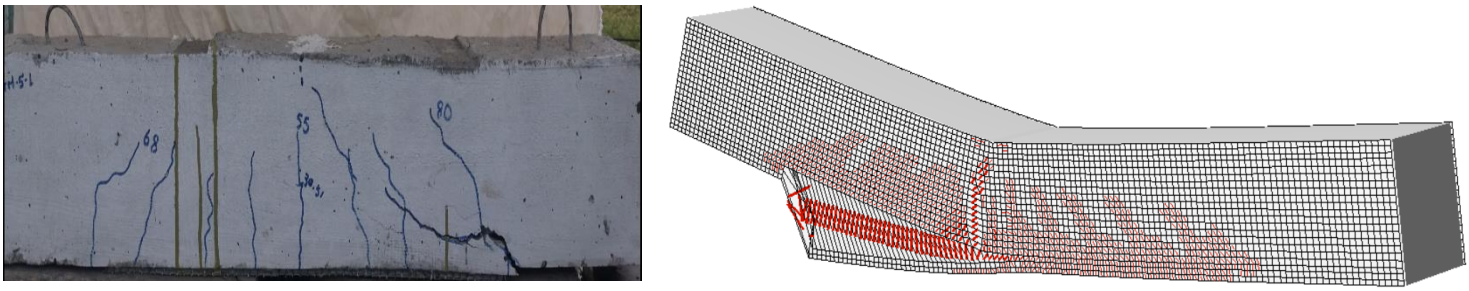

Five layered specimens

Figure 5-25 comparison of failure patterns of experimental and FEM specimens

In general, the comparisons carried out on the load-deflection diagrams and failure patterns of the experimental and FEM specimens revealed the power of the software in capturing the nonlinear behavior of monotonically loaded reinforced concrete beams.

5.4 Results of nonlinear finite element analysis on predamaged specimens

5.4.1 Results of analysis

The subsequent sections represent the results of the simulation carried out depending on the damage modeling technique discussed in section 4.3.

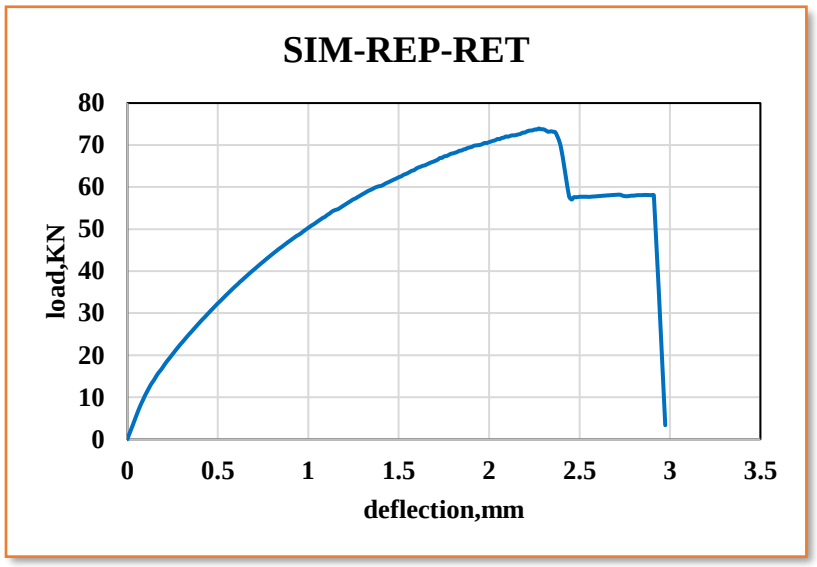

Figure 5-26 load-deflection response of repaired specimen modeled using VecTor2

Unlike the previously discussed simulation results, here, the predamaged specimens displayed a much lower ductile behavior. This is due to the cracks built in the model prior to analysis. In a normal undamaged RC beam element, the way the cracks progress and develop has a major impact on the ductility of the beams; as a result, it is logical that predamaged specimens behave in a brittle manner. The following figures illustrate the state of the specimens at different loading stages and the comparison of failure pattern with the experimental counterpart.

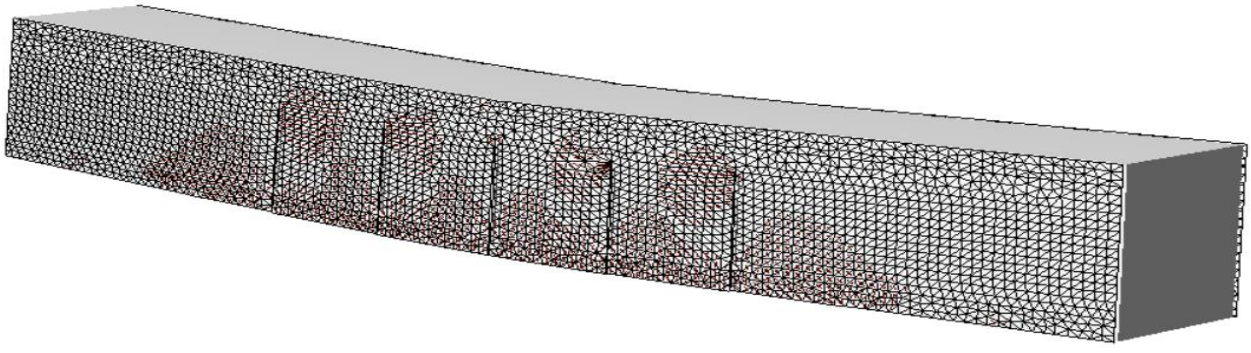

(a)

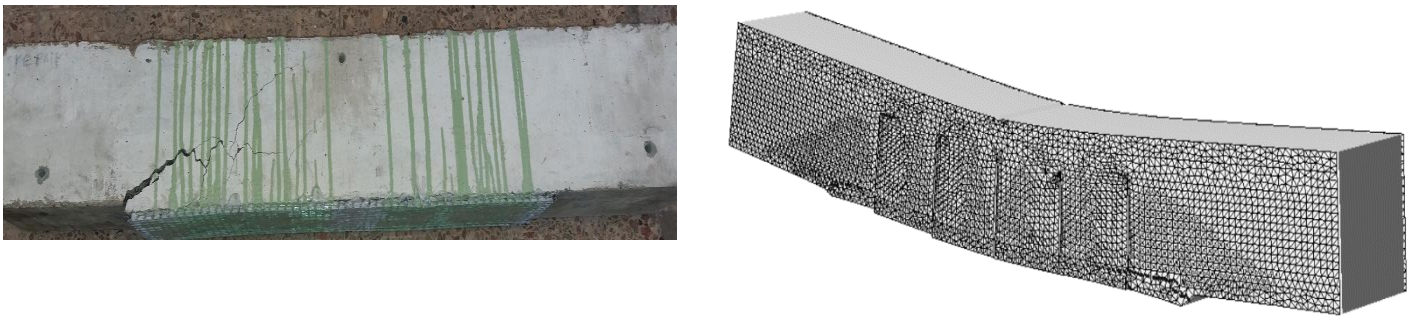

(b)

Figure 5-27 a) state of the repaired specimen at the instant the load is about half of the maximum b) failure pattern comparison of experimental & FEM predamaged specimen

5.4.2 Comparison of predamaged NLFEA results and experiment results

Comparing this diagram with the experimental outputs can provide additional implications in addition to validating the capability of the technique in modeling damage.

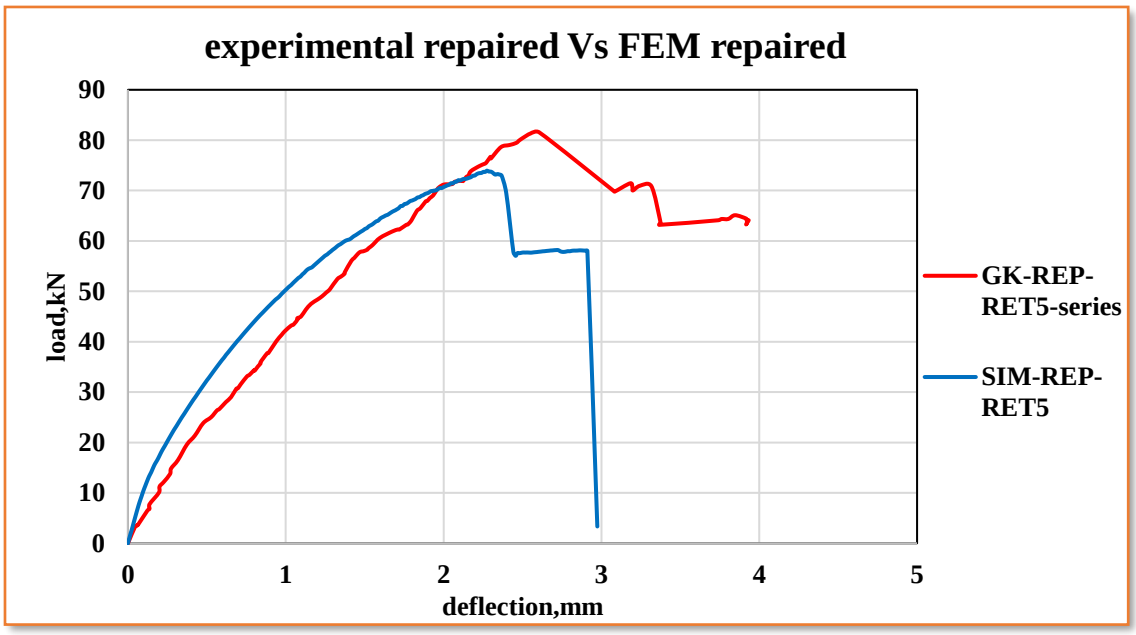

Figure 5-28 comparison of load-deflection response of repaired specimens from experiment and NLFEA

From Figure 5.28, it can be observed that unlike the other cases, the simulation has underestimated the maximum load capacity of the repaired beam to be 73.7 kN. Possible reason is the fact that the damage has been simulated as a built in geometric entity, renders any resistance that can be exploited from concrete non-existent. In addition to this, due to the pressure used to laminate the

wiremesh and bond it to the soffit of the beam, part of the cracks will be sealed with the forced injection of epoxy. This results in the restoration of some of the tensile strength of the concrete which may add up to the flexural resistance of the beams.

In general, VecTor2 has proven to be a very powerful and convenient tool in simulating the behavior of preloaded reinforced concrete beams that have been bonded with external retrofitting reinforcement. Moreover, the simulation results have indicated that modeling cracks as a geometric entity is a viable technique to simulate damage in cracked reinforced concrete beam elements.

6. Analytic model for cover rip off failure

6.1 Synopsis

In this chapter, an analytical composite end shear model is adopted and forwarded to predict the amount of shear load that resulted in concrete cover rip off (peeling of concrete cover) in the specimen with five layers of wire-mesh epoxy composite. When the thesis program was developed, the kind of failure that occurred in the specimens with five layers of the composite was not expected. The occurrence of the rip off failure necessitated the enquiry that led to the analytical model discussed in this chapter.

Cover rip off failure is mostly associated with retrofitting techniques that involve the utilization of steel plates. In few circumstances, it is also observed in FRP retrofitted beams. Numerous experimental and analytical investigations have been carried out on RC beam retrofitted with steel plates to understand the cause of the rip off failure and come up with a solution. These investigations concluded that cover rip off occurs when RC beams are partially plated with steel plates. The plate ends before reaching the support and this results in a shear concentration that ultimately leads to cover rip off. Furthermore, previous researches also discovered that the peeling failure is a function of the shear strength of the beams without shear reinforcement. However, it was not until Jansze w. (1997) that a conclusive analytic model was obtained to determine the shear load that ultimately leads to the peeling. He came up with a "Plate End Shear Model" by developing a fictitious shear span to convert the partially plated beams into a conventionally reinforced concrete beams. The fictitious shear span is integrated with CEB-FIP MC90 expression for flexural shear to predict the shear load that causes the aforementioned rip off failure. Considering the accuracy of Jansze's Plate End Shear Model, FIB adopted the model for the analysis of FRP retrofitted reinforced concrete beam that experience similar cover rip off failure.

Unlike steel plates or FRPs, the technique used in this thesis is a relatively new technique. As a result, it is imperative that an analytic model is forwarded to explain as such cover rip off failures. In this chapter, the Plate End Shear model of Jansze will be compared with another development based on other flexural shear formulation to forward an analytic model that better suits the wiremesh-epoxy technique. In order to create distinction of nomenclature between Jansze's steel

plate and the wiremesh-epoxy composite used in the current investigation, the model is referred to as Composite End Shear model (CESM) henceforth.

6.2 Previously existing model for cover rip off failure

A new failure mode is introduced if additional reinforcment is glued on the (unreinforced) concrete cover namely plate separation. Separation of the plate occurs before the flexural capacity is attained. A lot of effort has been put into solving the problem of this premature type of failure. However, when it comes to conclusive analytical model, none existed until jansze developed his plate end shear model.

6.2.1 Oehlers (1990 and 1992)

Oehlers discussed the various failure modes of plate separation. Refering to figure 6.1, it can be observed that the formation of diagonal shear cracks induced peeling of a plate that terminates at a distance short of the support in a region of high shear forces and low bending moment. This type of peeling occurred rapidly and in a brittle manner and is therefore known as shear peeling. If a shear span was partially plated as in the case of figure 6-1c, a combined shear flexural peeling occurred. All peeling modes occurred at the level of the internal reinforcement hence concrete cover is ripped off. Additionally if plate was bonded only in the constant moment region as in the case of figure 6-1a, increasing curvature induced flexural peeling and separation occurred gradually.After the experiments, Oehlers, concluded that the extent of plating did not affect the shear strength and forwarded formulation 6.1 for flexural peeling failure.

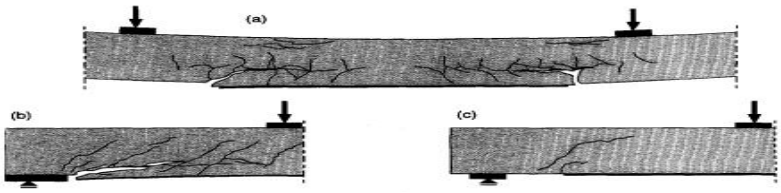

Figure 6-1 Peeling modes of beam with externally bonded plate: (a) flexural peeling (b) shear peeling (c) shear flexural peeling (Oehlers, 1990)

$$M_{up} = \frac{EI_{cp} f_b}{0.9 E_s t_p} \quad (6.1)$$

M_{UP} = flexural peeling moment, EI_{cp} = flexural rigidity,

f_b = brazilian tensile strength of concrete, E_S = young's modulus of plate steel,

t_p = thickness of plate

6.2.2 Jansze W. (1997)

Jansze W. developed a Plate End Shear Model, which is an analytic model that predicts the amount of shear load that initiates a flexural shear cracking that ultimately leads to a peeling or cover rip off failure. This rip off occurs at the bottom reinforcement level. In his study, he was able to prove that the basic mechanism of plate end shear is identical to the mechanism of flexural shear as described by Kim & White (1991)(Appendix A). As a result, Jansze's analytic model is based on the critical crack section analysis of Kim & White. Depending on the analogy between Kim & White's critical crack section for conventionally reinforced beams & the unplated length for partially plated members, Jansze introduced a fictitious shear span. By combining this fictitious shear span with the CEB-FIP MC90 expression for flexural shear, the plate end shear is correctly predicted.

This model is the first and foremost formulation that conclusively developed a way of predicting the shear load that results in cover rip off failure in partially plated RC members. As a result, this model has been included in current analysis as well.

6.3 Composite End Shear Model (CESM)

Figure 6-2 & 6-3 shows the peeling failure occurred in the specimens tested by Jansze and the five layered specimens in the current study. As it can be observed in the figure, there is a kin similarity of failure behavior between Jansze's specimens and the specimens in the current investigation. This similarity is also apparent with the other specimens that exhibited peeling failure and in the finite element simulation results as well. This failure similarity coupled with the plate like nature of the composite led to the inclusion of Jansze's model and his methods in the Composite End Shear Model.

(a) (b)

Figure 6-2 (a) failure of specimens tested by Jansze (b) failure of GK-RET5 series specimens

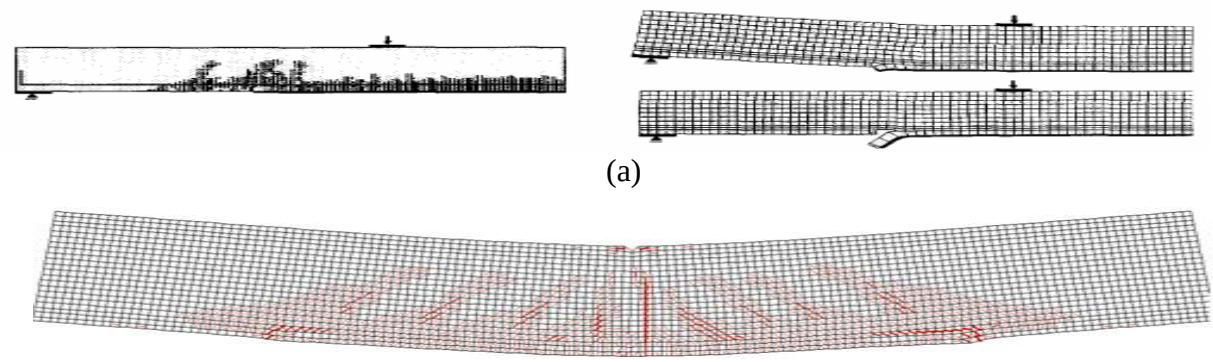

(a)

(b)

Figure 6-3 (a) FEM simulation of partially plated specimen-Jansze (b) FEM simulation of GK-RET5-series in the current investigation

In this formulation, a fictitious shear span is developed to be integrated with flexural shear formulations to predict the shear load that ultimately leads to cover peeling failure.

6.3.1 Formulations for the shear capacity

This section presents two expressions for the mean shear resistance for concrete members without shear reinforcement. These shear resistance forms the basis of the shear formulas & are used in building codes. Hence,

$$V_R = \tau_{cum} bd \tag{6.2}$$

$$\tau_{cum} = C_{m,Rafla}\ \alpha_u \sqrt{f_{cm}}\ \sqrt[3]{100\rho}\, d^{-0.25} \quad \text{[Rafla's expression for flexural shear]} \tag{6.3}$$

Where, $\alpha_u = 6 - 2.2\frac{a}{d}$ $\quad 1 < \frac{a}{d} < 2$ (6.4)

$$\alpha_u = 0.795 + 0.293\left(3.5 - \frac{a}{d}\right)^{2.5} \quad 2 < \frac{a}{d} < 3.5 \tag{6.5}$$

$$\alpha_u = 0.9 - 0.03\frac{a}{d} \quad 3.5 < \frac{a}{d} \tag{6.6}$$

$$\tau_{cum} = C_{m,MC90}\ \sqrt[3]{3\frac{d}{a}}\left(1 + \sqrt{\frac{200}{d}}\right)\sqrt[3]{100\rho f_{cm}} \quad \text{[CEB-FIP MC90 expression of flexural shear]} \tag{6.7}$$

Where, $a = actual\ shear\ span$

$d = effective\ depth$

$f_{cm} = mean\ compressive\ strength\ of\ concrete$

$\rho = reinforcement\ ratio$

The factors $C_{m,MC90}$ and $C_{m,Rafla}$ are constants that need to be determined. CEB-FIP MC90 recomends a value of 0.15 for $C_{m,MC90}$. However, the expression represents an estimation for the shear force causing cracking. As a result, to obtain an equation for the mean maximum nominal shear stress, Jansze carried out a comparison with data of 170 tests obtained from CEB bulletin 224 (2015) to establish an improved factor. His findings revealed that for $C_{m,Rafla}$ = 0.85 and $C_{m,MC90}$ = 0.18 the experimental maximum nominal shear stresses are in good aggreement with the empirically obtained stresses.

These two shear expressions predict shear capacity satisfactorily. However, up on mutual comparison, Jansze found out that Rafla's expression has a better accuracy in prediciting the capacity over a wider range of shear span to depth ratio. He observed that the CEB-FIP MC90 expression underestimates the capacity when the shear span to depth ratio is less than three. bearing this in mind, Rafla's expression has also been taken into consideration for the development of the Composite End Shear Model. These shear formulations will be integrated with the fictitious shear span developed in the subsequent section to predict the shear load that results in cover rip off failure.

6.3.2 Modelling analogy with Kim & White 's critical crack section

Kim & White (1991) developed an expression for conventionally reinforced members to predict the location of the critical flexural-shear cracks. Variables used in the study are those mainly used in shear studies namely longitudinal reinforcement ratio, shear span and effective depth. Based on both equilibrium considerations and experimental observations, a theoretical formulation was derived. (Appendix A)

$$a_c = 3.3\left[\frac{\rho(d/a)^2}{\left(1-\sqrt{\rho}\right)^2}\right]^{1/3} a \qquad (6.8)$$

Where, $\rho = reinforcement\ ratio$ $\quad d = effective\ depth,$

$a = actual\ shear\ span,$ $\quad a_c = critical\ crack\ position$

Up on observation, there is a kin similarity in the mechanism over which the cover rip off failure occurred in the specimens with five layers and Kim and White's flexural shear cracking . In the specimens, an inclined shear crack was forced to develop over a previously existing flexural crack and this inclined cracks were observed at the ending of the composite. However, further development and widening of the diagonal shear cracks was prevented by the virtue of the

transversal reinforcement. As a result, the concrete cover that was not confined within the stirrups got ripped off in a brittle manner. Hence, the unplated distance from the support to the ending of the composite, is analogous to the location of critical crack section in Kim & White's formulation. This is depicted in Figure 6.4. On the left side the critical crack section of Kim & White is illustrated. the right side shows a partially plated specimens with five layers of wiremesh-epoxy composite. As a result of the analogy between a_c and L, the shear span a belonging to a_c is analogous to a fictitious shear span a_f belonging to L. Taken this modelling analogy into account, the following interpretation can be formed:

$$a_c = 3.3\left[\frac{\rho\left(\frac{d}{a}\right)^2}{\left(1-\sqrt{\rho}\right)^2}\right]^{1/3} a \quad \Rightarrow \quad L = 3.3\left[\frac{\rho\left(\frac{d}{a_f}\right)^2}{\left(1-\sqrt{\rho_s}\right)^2}\right]^{1/3} a_f \qquad (6.9)$$

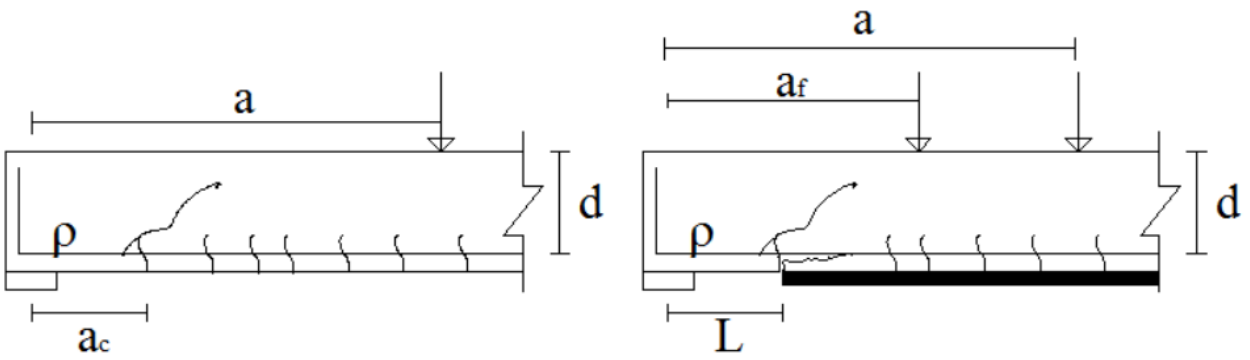

Figure 6-4 modeling analogy between Kim & White's critical cracking section and the specimens with five layers of wiremesh epoxy composite

6.3.3 Caliberation of fictitious shear span

The fictitious shear span a_f is used as an input parameter to compute the shear resistance on the basis of CEB-FIP MC90 and Rafla's expression for flexural shear capacity. The value of the constant in equation 6.8 was determined to be 3.3 from statistical analysis conducted on few available data (Kim & White,1991). Considering this, Jansze compared the results obtained using a_f from equation (6.9) with his experimental and numerical results. In his comparison, he observed that the fictitious shear span obtained from the equation with the constant 3.3 results in erroneous shear load prediction. As a result he deduced that the constant value 3.3 is not satisfactorily defined.

To mitigate this issue, Jansze carried out additional analysis on his outputs to determine that replacing the constant 3.3 with the fictitious shear span to depth ratio, $^{a_f}/_{d}$, provides better prediction of the shear load. Therefore, equation 6.9 becomes;

$$L = \frac{a_f}{d}\left[\frac{\rho\left(\frac{d}{a_f}\right)^2}{\left(1-\sqrt{\rho_s}\right)^2}\right]^{1/3} a_f \tag{6.10}$$

Equation (6.10) can be rewritten into formulation 6.11 that objectively expresses the fictitious shear span.

$$a_f = \sqrt[4]{\frac{\left(1-\sqrt{\rho}\right)^2}{\rho} d\ L^3} \tag{6.11}$$

In subsequent sections, the fictitious shear span obtained from formulation 6.11 is integrated with CEB-FIP MC90 and Rafla's expression of flexural shear capacity to predict the shear load.

6.3.4 Integration of fictitious span with CEB-FIP MC90 Expression (Jansze's formulation)

If shear cracking would occur in the serviceability limit state (i.e. before the yielding of the flexural reinforcements) the amount of shear reinforcement controlling the opening of the diagonal crack may be very small and the criteria of serviceability may be violated. In the absence of a more precise calculation the shear force causing shear cracking may be estimated using formulation (6.1) & (6.6).

$V_R = \tau_{cum} bd$

$$\tau_{cum} = C_{m,MC90}\ \sqrt[3]{3\frac{d}{a}}\left(1+\sqrt{\frac{200}{d}}\right)\sqrt[3]{100\rho f_{cm}}$$

It has been determined in section 6.3.1 that 0.18 can be used for the value of $C_{m,MC90}$. By replacing the actual shear span a in equation 6.6 with the fictitious shear span a_f, an expression (equation 6.12) is obtained to predict the shear stress that causes concrete cover rip off.

$$\tau_{com} = 0.18\sqrt[3]{3\frac{d}{a_f}}\left(1+\sqrt{\frac{200}{d}}\right)\sqrt[3]{100\rho f_{cm}} \tag{6.12}$$

6.3.5 Integration of fictitious shear span with Rafla's expression

Rafla's expression for shear capacity is considered in this analytic model formulation for its better accuracy on a wide range of shear span to depth ratio. Up on comparison, Jansze was able to observe that when the shear span to depth ratio is less than three, Rafla's expression has a better accuracy on predicting shear load. Rafla recommended equations (6.1) to (6.5) to determine shear load capacity.

$$\tau_{cum} = C_{m,Rafla}\ \alpha_u \sqrt{f_{cm}}\ \sqrt[3]{100\rho}d^{-0.25}$$

Where, $\alpha_u = 6 - 2.2\frac{a}{d}$ $\quad 1 < \frac{a}{d} < 2$

$\alpha_u = 0.795 + 0.293\left(3.5 - \frac{a}{d}\right)^{2.5}$ $\quad 2 < \frac{a}{d} < 3.5$

$\alpha_u = 0.9 - 0.03\frac{a}{d}$ $\quad 3.5 < \frac{a}{d}$

Jansze recommends 0.85 to be used as the value of $C_{m,Rafla}$. In Rafla's formulation, additional coefficient, α_u, exists. This specific coefficient is dependent on the actual shear span to depth ratio. Here again, the actual shear span is replaced with the fictitious shear span to give a second formulation (Eq. 6.13) to come up with an expression capable of predicting the shear load.

$$\tau_{cum} = 0.85\ \alpha_{uf} \sqrt{f_{cm}}\ \sqrt[3]{100\rho}d^{-0.25} \tag{6.13}$$

Where, $\alpha_{uf} = 6 - 2.2\frac{a_f}{d}$ $\quad 1 < \frac{a_f}{d} < 2$

$\alpha_{uf} = 0.795 + 0.293\left(3.5 - \frac{a_f}{d}\right)^{2.5}$ $\quad 2 < \frac{a_f}{d} < 3.5$

$\alpha_{uf} = 0.9 - 0.03\frac{a_f}{d}$ $\quad 3.5 < \frac{a_f}{d}$

6.4 Summary of Composite End Shear Formulation

Two formulations have been presented for the prediction of the shear load that resulted in cover rip off failure in the specimens with five layers of wire mesh-epoxy composite. These formulations were developed on the basis of the analogy between Kim & White's mechanism of flexural shear crack and the cover rip off failure occurred in the specimens with five layers of the wiremesh-epoxy composite. These formulations are validated with experimental and FEM results to investigate their accuracy as well as compare and select the better formulation to predict the composite end shear.

Table 6-1 summary of composite end formulations

Composite end shear model: based on CEB-FIP MC90 & Rafla's expression for flexural shear	
Fictitious shear span	$a_f = \sqrt[4]{\frac{\left(1-\sqrt{\rho}\right)^2}{\rho} d\, L^3}$
Maximum nominal shear stress (CEB-FIP MC90)	$\tau_{com} = 0.18 \sqrt[3]{3\frac{d}{a_f}} \left(1+\sqrt{\frac{200}{d}}\right) \sqrt[3]{100\rho f_{cm}}$
Maximum nominal shear stress (Rafla's expression)	$\tau_{com} = 0.85\ \alpha_{uf} \sqrt{f_{cm}} \sqrt[3]{100\rho} d^{-0.25}$ $\alpha_{uf} = 6 - 2.2\frac{a_f}{d}$ $\quad 1 < \frac{a_f}{d} < 2$ $\alpha_{uf} = 0.795 + 0.293\left(3.5 - \frac{a_f}{d}\right)^{2.5}$ $\quad 2 < \frac{a_f}{d} < 3.5$ $\alpha_{uf} = 0.9 - 0.03\frac{a_f}{d}$ $\quad 3.5 < \frac{a_f}{d}$
Maximum shear force	$V_{com} = \tau_{com} b d$
	ρ reinforcement ratio (-) d effective depth of internal bars (mm) L distance from the support to cmposite end (mm) a_L fictitious shear span (mm) f_{cm} uniaxial meancompressive strength (N/mm^2) b width of concrete section (mm)

6.5 Verification of the formulations with experimental and NLFEA results

6.5.1 Analytical model versus experimental results

The number of results that can be obtained from the experimental tests carried out in this investigations is limited. Furthermore, additional data can not be found from literatures as there are none that are conducted on the technique and displayed a similar failure behavior. As a result, multiple simulation results are going to be deployed in order to validate the capability of the model in predicting the maximum shear load. Table 6.2 summarizes the comparison between the experimental results of the specimens with five layers and the analytical model formulated on the two flexural shear expressions. The FEM simulation result of the specimens with five layers has also been included in the comparison.

Table 6-2 Comparison of shear loads between the results from experimental tests and the analytical model

Test series	***Actual load,kN***	***CEB-FIP MC90,kN***	***Rafla,kN***
GK-RET5-1	95.23	62.25	64.13
GK-RET5-2	78.53	62.25	64.13
GK-RET5-3	95.54	62.25	64.13
FEM	88.01	62.25	64.13
Calculated using fcm=26MPa, a_f=427mm, ρ= 0.01292			

It can be seen that both formulations underestimate the results from both the experiment and finite element simulations at an exaggerated level. CEB-FIP MC90 expression has the tendecy to predict the shear capacity insufficiently when the shear span to depth ratio of beams is less than three. This was observed on jansze's mutual comparison of The two expressions (i.e. Rafla' and CEB-FIP MC90). Since the shear span to depth ratio of the specimens with five layers is 2.5, it is understandable that the CEB-FIP MC 90 underestimated the shear load. When it comes to Rafla's expression, it predicted the shear load slightly higher than the CEB-FIP expression.

The only available experimental data is the one obtained from the current investigation. as a result, it is imperative to carry out additional verification works using simulation results. Hereunder, both shear capacity expressions are compared against a series of simulation results with shear span to depth ratio, a/d of 3.75 and 5.

6.5.2 Analytical model versus simulation of 1500mm beams $\left({}^{a}/_{d} = 3.75\right)$

In the comparison between the experimental results and the analytical prediction, unsatisfactory results were obtained. Both formulations predicted the shear load insufficiently. This is due to the incapability of the CEB-FIP MC90 formulation to predict shear capacity if the shear span to depth ratio is less than three. In order to mitigate this issue, a series of simulations were carried out on beams with shear span to depth ratio of 3.75. in these series of simulations, the span length is kept the same size of 1500mm, along with the geometric properties, reinforcement ratio and concrete grade. The only changing parameter was the unplated length (the distance from support to the end of the composite). This helps to understand the effect of the unplated length on the failure behavior of the beams.

Note: In the simulation series designations, the first value indicates the unplated length while the second value represents the total span length.

Table 6-3 Summary of results of FEM and analytical model on the 1500mm span series.

Simulation series designation	**Fictitious shear span,mm**	**Simulation results,kN**	**CEB-FIP MC90,kN**	**Rafla,kN**	**Type of failure**
Fully plated	-	61.73	-	-	flexure
Unplated 75-1500	253.89	61.73	74.1	54.8	flexure
Unplated 150-1500	426.99	61.73	62.1	52.74	flexure
Unplated 225-1500	578.74	61.42	56.52	50.92	flexure
Unplated 300-1500	718.11	59.66	52.6	49.26	Cover rip off
Unplated 375-1500	848.23	56.55	49.8	47.72	Cover rip off
Unplated 450-1500	973.32	55.46	47.5	46.23	Cover rip off
Control 1500		37.8	-	-	flexure
Calculated with fcm=26 MPa,ρ=0.012922,true shear span=1500mm					

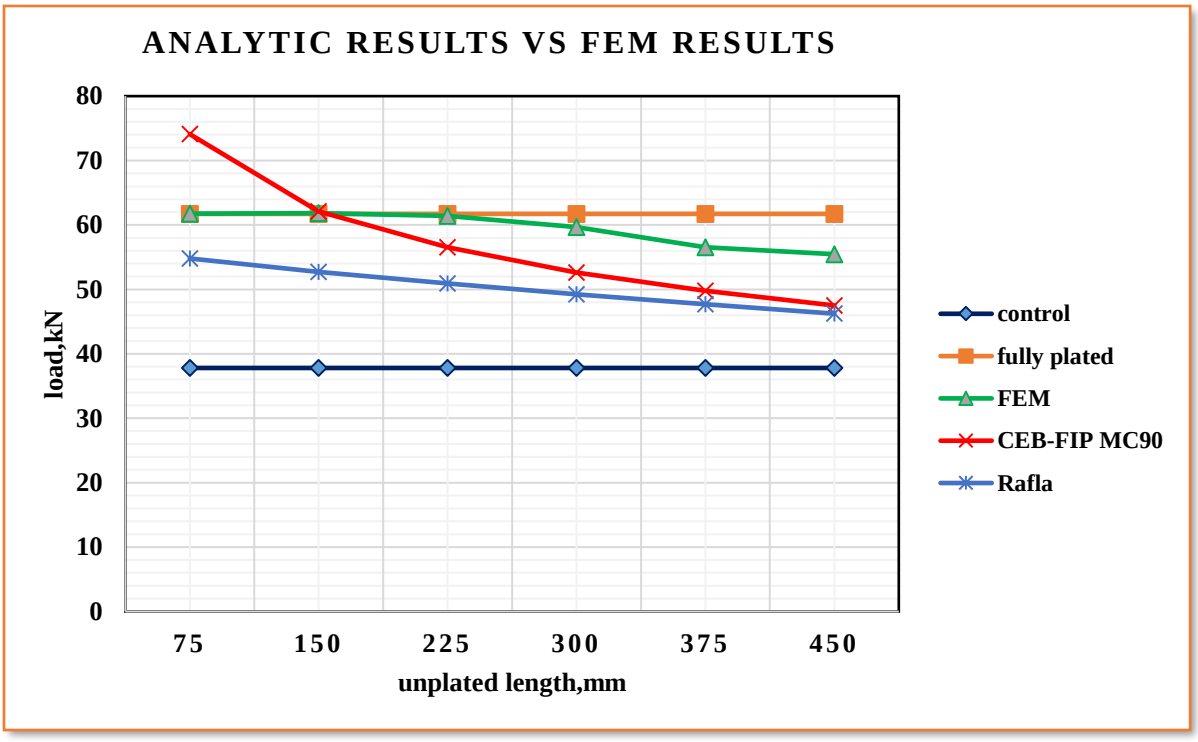

Figure 6-5 comparison between shear values from FEM analysis and analytical model on 1500mm beam

The comparison carried out on the results from the Non Linear Finite Element Analysis and the analytical formulations shows that the model performs well in predicting the shear load. Two limit cases have been used in the comparison. The first limit case is a normal reinforced concrete member without any external reinforcement attached to it while the other limit is a case where the beam is plated with the composite over its entire span length.

From figure 6-5, it is apparent that the CEB-FIP MC90 expression predicts the shear load more accurately than Rafla's expression. In the simulations, when the unplated length is 300mm and above, the beams failed from concrete cover rip off (appendix B). In all these cases where peeling occured, the CEB-FIP expression predicted the shear load to be 85% to 88% of the simulation results. Rafla's expression provided results that are 82% to 84% of the simulation results.

Peeling of the concrete cover was not observed in the simulations where the unplated length is less than 300mm. Instead, a conventional flexural failure was observed. In these circumstances, it is expected that the flexural failure loads are less than the shear failure loads. Rafla's expression provided results that are lower than the simulation results in all the cases. This is illogical

considering the fact that cover rip off didn't occur when the unplated length is less than 300mm. when it comes to the CEB-FIP MC90 expression, it provided results that are higher than the loads that caused flexural failure. This, occurred on two out of three cases where cover rip off did not occur. On one case, a result that is less than the flexural load was obtained.

6.5.3 Analytical model versus simulation of 2000mm beams $\left({}^{a}/_{d} = 5\right)$

In this scenario, minor modifications have been done to the structural specifications besides the span length. The reinforcement ratio has been increased to 0.0162 in order to investigate the versatility of the model.Peeling occurred on the beams where the unplated length is 400mm and above. Table 6-4 summarizes the results obtained from the FEM simulations and the two formulations on flexural shear. In the simulation series designations, the first value indicates the unplated length while the second value represents the total span length.

Table 6-4 Summary of results of FEM and analytical model on the 2000mm span series.

Simulation series	**Fictitious shear span,mm**	**FEM results,kN**	**Rafla,kN**	**CEB-FIP MC90,kN**	**Type of failure**
Fully plated	-	58.72	-	-	flexure
Unplated 100-2000	295.67	58.94	58.5	76.6	flexure
Unplated 200-2000	497.25	58.85	55.89	64.4	flexure
Unplated 300-2000	673.98	58.87	53.63	58.2	flexure
Unplated 400-2000	836.28	57.08	51.55	54.2	Cover rip off
Unplated 500-2000	988.67	52.04	49.6	51.2	Cover rip off
Unplated 600-2000	1133.4	46.42	47.74	48.9	Cover rip off
Control 2000	-	40.3	-	-	flexure
Calculated with fcm=26 MPa, ρ=0.0161523, true shear span=2000mm					

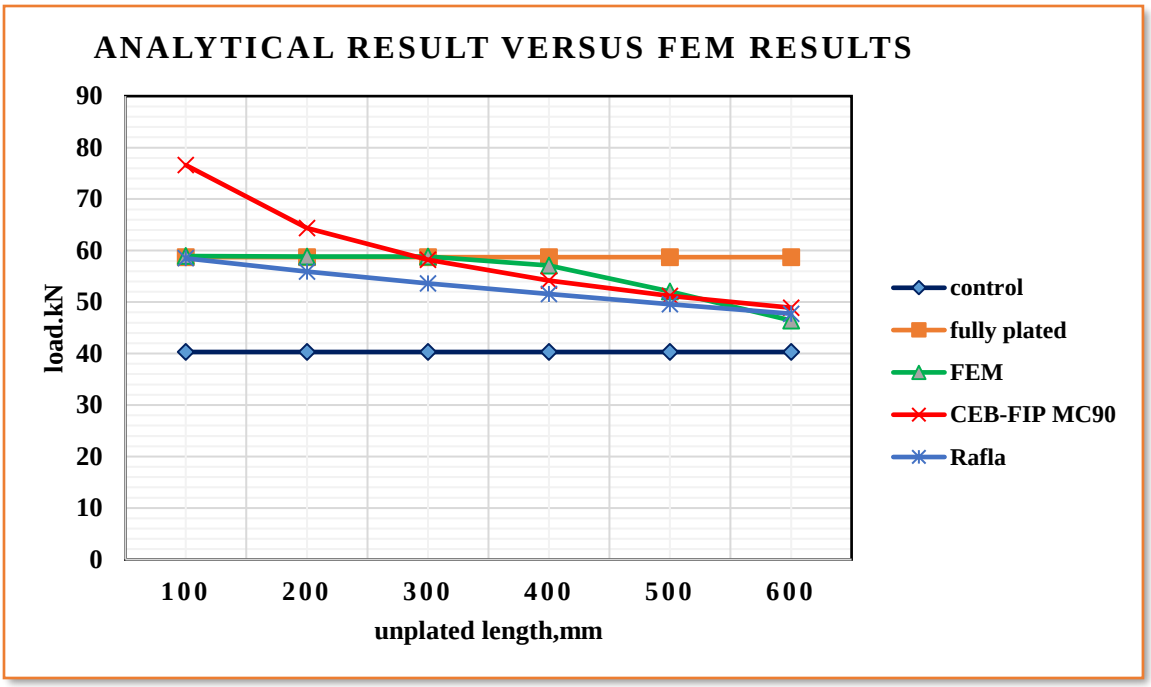

Figure 6-6 comparison between FEM results and analytical results on 2000mm beams

Peeling of cover occurred in three cases where the unplated length is 400mm and above. In these, the CEB-FIP MC90 expression provided shear loads that are 95% and 98% under and 105% over the simulation results. Among the three cases where flexural failure occured, the model provided higher shear loads in two cases at 109% and 130% above the failure loads of the simulations. In one case it underestimated the shear load at 99% which is almost an exact result. This is logical on the basis that flexural failure occurs when the shear capacity of the beam is higher than the flexural capacity. Concerning Rafla's expressions, for the cases where cover rip off occurred, it predicted in a closely accurate manner as that of the CEB-FIP MC90 expression. However, in the cases where flexural failure occurred, it provided shear capacity which is less than the flexural capacity. This shows that the CEB-FIP MC90 has better accuracy and is also theoretically logical. The simulation results of the 2000mm beams are found on appendix C.

6.6 Summary of verification and comparison

the comparison carried out on the two flexural shear formulations (i.e. CEB-FIP MC90 & Rafla's) revealed that the CEB-FIP MC90 has a better accuracy as well as conceptually logical prediction of the shear loads that resulted in peeling (cover rip off) failure. Despite the discrepancies observed in the comparison between the experimental results of the GK-RET5 series and the analytical

prediction of the shear load, the simulations conducted indicate that the model is capable of predicting the shear loads if the actual shear span to depth ratio is greater than three.

It was also observed that the extent of plating (i.e. unplated length) has a decisive role on the failure behavior of the beams. Furthermore, the failure loads were decreasing as the unplated length was increasing. This was observed in both the FEM simulations and analytical investigations.

In general, it can be inferred that by integrating the developed fictitious shear span with the CEB-FIP MC90 expression for flexural shear, a composite end shear model can be formulated that can predict the shear load that ultimately leads to peeling of concrete cover. As a result, it can be concluded that Jansze's plate end shear model can predict the composite end shear that results in cover rip off as well.

Composite end shear model: based on CEB-FIP MC90	
Fictitious shear span	$a_f = \sqrt[4]{\frac{\left(1-\sqrt{\rho}\right)^2}{\rho} d\, L^3}$
Maximum nominal shear stress	$\tau_{com} = 0.18\sqrt[3]{3\frac{d}{a_f}}\left(1+\sqrt{\frac{200}{d}}\right)\sqrt[3]{100\rho f_{cm}}$
Maximum shear force	$V_{com} = \tau_{com} b d$
	ρ reinforcement ratio (-) d effective depth of internal bars (mm) L distance from the support to cmposite end (mm) a_L fictitious shear span (mm) f_{cm} uniaxial meancompressive strength (N/mm^2) b width of concrete section (mm)

7. Conclusion and recommendation

7.1 Conclusion

In this thesis, an experimental, non-linear finite element and analytic investigations have been carried out to obtain an insight on the capability of wire mesh-epoxy composite on flexural retrofitting of reinforced concrete beams. The investigations are carried out from two perspectives. The first perspective is strengthening of beams where unloaded specimens are retrofitted with the wire-mesh epoxy composite. The second perspective is rehabilitation of damaged specimens where preloaded specimens are retrofitted with the composite. The investigations revealed that there is a substantial enhancement of flexural capacity due to the attachment of the composite. The enhancement is observed in both the undamaged and predamaged specimens.

The experimental investigation that was carried out in two schemes provided the first insight on the capability of the wire mesh-epoxy composite to increase flexural strength of RC beams. In the strengthening scheme, undamage specimens were strengthened using three and five layers of the composite. from the three layers, a 42% increment of flexural strength was observed. The specimens with five layers of the wiremesh-epoxy composite showed enhancement up to 69%. The specimens under the rehabilitation scheme showed a full restoration on their capacity. However, further study conducted on the load-deflection diagrams revealed that there is a considerable loss of ductility due to the attachment of the composite.

The non linear finite element analysis carried out using VecTor2 showed a good agreement with the outputs of the experimental investigation. In doing so, the software proved to be a very powerful tool in capturing the nonlinear behavior of reinforced concrete members. For the preloaded specimens, a simplistic technique of modeling damage was used. The damage was modeled by integrating the cracks developed due to preloading into the model as a geometric entity. The agreement of the results obtained from VecTor2 and the experimental investigation showed that it is a viable technique of modeling a damage incurred from loading.

The adopted analytical model i.e. Composite End Shear Model, was verified to be a functional model in predicting the shear load that ultimately leads to the brittle peeling of concrete cover. The model also indicated that the extent of the length from the support to the end of the composite has a determinant role on the failure behavior of reinforced concrete beams that are retrofitted with wire-mesh epoxy composite.

7.2 Recommendation

the following areas can be investigated further in future works.

- the possibility of using wire mesh-epoxy composite for other retrofitting schemes like shear retrofitting can be investigated.
- the attachement of the composite has resulted in a considerable loss of ductility. As a results, future works can explore the possibility of enhancing flexural capacity without posing adverse effect on the ductility of specimens.
- In the rehabilitation scheme, it was observed that monotonic loading doesn't pose noticeable damage. Therefore, the rehabilitation capability shall be investigated in relation to other kinds of loadings like cyclic loads.
- The response of the repaired beams towards different level and degree of damage can be explored.
- Versatility of the crack modeling technique need to be studied further. Additionally Other possible modeling techniques can also be explored towards the damage modeling.
- The Composite End Shear Model has proven to be capable of predicting the shear concentrated at the end of the composite. However, the effect of thickness or layers is not included in the development of the model. from the results of the experimental investigation though, it was observed that the number of layers has an effect on whether peeling occurs or not. As a result, the model can further be developed to incorporate these aspects.
- If the technique is to be used, due care must be taken since the attachment of the composite reduces the ductility considerably.

References

Alam, A. & Jumaat, M.Z. , (2014), *effective method of repairing reinforced concrete beams using externally bonded steel plates*, research gate.

Alam, A. & Jumaat, M.Z. , (2014), *strengthening of reinforced concrete structure*, Kuala Lampur, University of Malaya.

Nilson, A. H., Darwin, D., Dolan, C.W., (2010), *design of concrete structures 14th ed*, Newyork,Mcgraw Hills

Ealias, A. M. & Binu, P., (2015), *strengthening of reinforced concrete beam using wire mesh-epoxy composite*, structural journal, International Journal of Science & Research.

Khan, A.R. & Fareed, S., (2013), *behavior of reinforced concrete beams strengthened by CFRP wraps with and without end anchorage*, structural journal, Science Direct.

Satput, A.S. & Varma, M.B., (2017), *retrofitting of beams using glass fiber reinforced polymer (GFRP) wraps, structure journal*, IOSR-journal of mechanical and civil engineering.

Aalto University, (2016), *strengthening of building structures*, Aalto University

Dinku, A., (2002), *construction material laboratory manual*, Addis Ababa University, Addis Ababa, Ethiopia.

Neeladharan, C. & Anharayan, M. , (2018), *retrofitting of reinforced concrete beams by using phenolic & ferrocement*, International Journal of Advanced Research Trends in Engineering & Technology (IJARTET)

Neeladharan, C., (2018), *repair & strengthening of a damaged reinforced concrete beam using carbon FRP sheets*, Research Gate.

Oehlers, D. J. & Moran, J.P. , (1990), *premature failure of externally plated reinforced concrete beams*, journal of structural engineering, ASCE.

Oehlers, D.J. , (1992), *reinforced concrete beams with plates glued to their soffits, journal of structural engineering*, ASCE.

Sevuk,F. & Arslan, G., (2005), *retrofitting of damaged reinforced concrete beams by using steel plates*, ASCE, University of Leeds.

FIB, (1993), *CEB-FIP model code 1990:design code*, Thomas Telford services Ltd, Lausanne, Switzerland.

FIB, (1999), *structural concrete text book on behavioud-design & performance:CEB/FIP*, model code 1990.

FIB, (2001), *externally bonded FRP reinforcement for reinforced structures*, (CEB-FIP) technical report

Arslan, G., Sevuk, F., Ekiz,I., (2008), *steel plate contribution to load-carrying capacity of retrofitted reinofrced concrete beams*, Science Direct, Elsevier.

Qeshta, I. M. I., Shafigh, Jumaat, M. Z., (2015), *flexural behavior of rinforced concrete beams strengthened with wire mesh-epoxy composite*, structure journal, elsevier.

Wight, J. K. & MacGregor, J.G., (2012), *reinforced concrete mechanics & design*, New Jersey, Pearson Education,inc.

Eswaran, K., Sridhar, J., Karunya, N., Ranee, A. , (2016), *study on strengthening of predamaged concrete beams using ferrocement laminates*, International Research Journal of Engineering & Technology (IRJET)

Heiza, K., Nabil, A., Tayel, M., (2014), *state of the art review: strengthening of reinforced cocnrete structures-different strengthening techniques*, Research Gate.

Saad, M. H., (2009), *Elasticity: theory, applications & numerics*, Burlington:USA, Elsevier,inc.

Danraka, M.N. , Mahmed, H.M., Olumatosin,O.K.J., (2017), *strengthening of reinforced concrete beams using FRP technique: A review*, IJESC, Research Gate.

Siraj, M., (2018), *strengthening torsion critical reinforced concrete beam by externally bonded carbon fiber reinforced polymer: analytical to experimental investigation*, Addis Ababa University, Addis Ababa, Ethiopia.

Bansal,P. P., Kumar, M., Kaushik, S. K., *effect of wiremesh orientation on strength of beams retrofitted using ferrocement jackets*, international journal of engineering

Wong, P. S., Vecchio, F. J., Trommel, H., (2013), *VecTor2 & Formwork user's manual*, University of Toronto, Canada.

Almahadi, R.A., (2005), *finite element modeling of reinforced concrete beams retrofitted with CFRP fabrics*, research publication, Research Gate.

Merid, R., (2016), *retrofitting of reinforced concrete beam using fiber reinforced polymer*, Addis Ababa University, Addis Ababa, Ethiopia.

Hsu, T. T. C. & Mo, Y. L., (2010), *unified theory of concrete structures*, John Wiley & Sons, Ltd, United Kingdom.

Jansze, W., (1997), *strengthening of reinforced concrete members in bending by externally bonded steel plates*, Delft University of Technology.

Kim, W. & White, R. N. , (1991), *initiation of shear cracking in reinforced concrete beams with no web reinforcement*, structural journal, ACI-structural journals.

Summer, Y. & Aktas,M., (2014), *finite element modeling of existing cracks on preloaded reinforced concrete beams*, research article.

Obaidat, Y. T., (2010), *structural retrofitting of reinforced concrete beams using carbon fiber reinforced polymer*, Lund, Sweden

APPENDICES

APPENDIX A

Kim & White's formulation on critical location of flexural shear crack (Kim & White,1991)

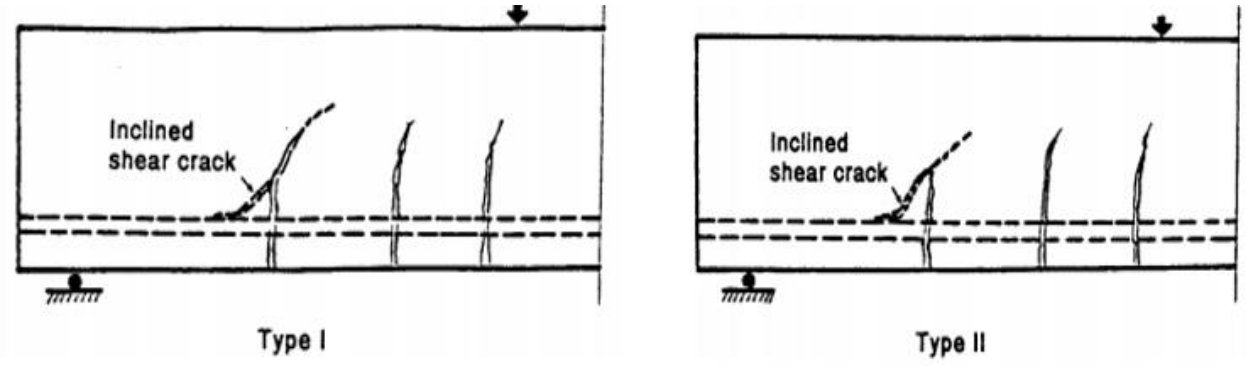

Figure A1-experimentally observed flexural shear cracks, (Kim & White, 1991)

In a homogeneous beam, the average distribution of the shear stress over the surface in a horizontal cross section is constant. The distribution of the shear stress τ in a vertical cross section is parabolic and can be written in the well known formula as;

$$\tau = \frac{VQ}{Ib} \tag{A1}$$

Where V is the external force, Q is the first moment of area, I is moment of inertia of the section and b is the width. Figure below shows a reinforced concrete beam with a flexural crack at the critical shear crack distance a_c. equilibrium of an element p p'm'n' is considered, with the reinforcement tension force T acting in the flexural crack.

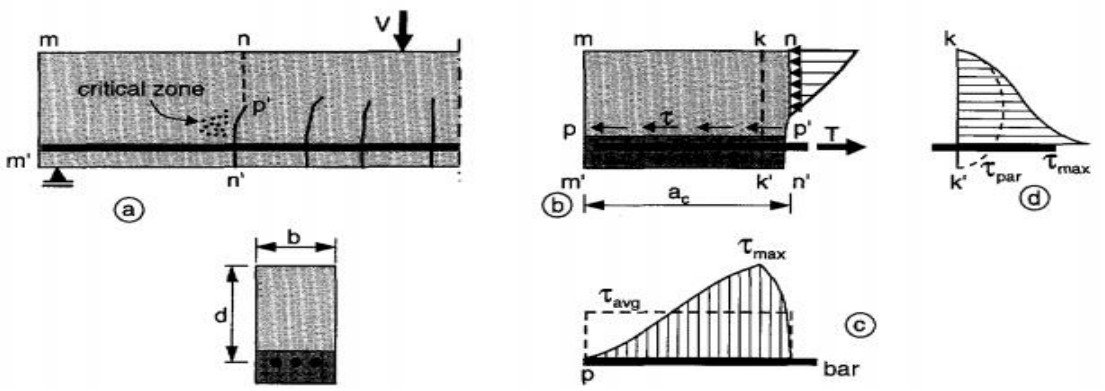

Figure A2- shear stress in reinforced concrete beams, (Kim & White,1991)

The average shear stress τ acting on the horizontal plane p p' is;

$$\tau = \frac{T}{ba_c} \tag{A2}$$

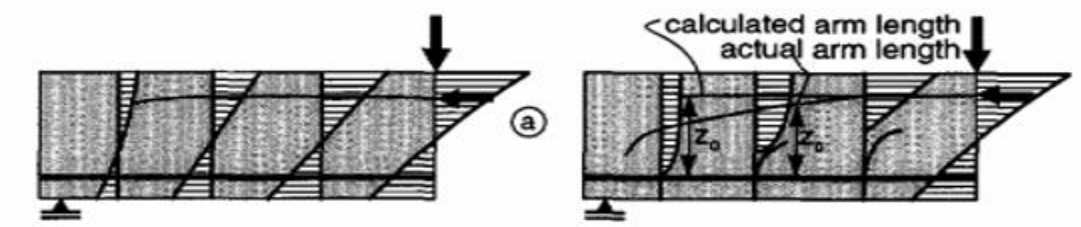

reduction of internal moment arm length due to the development of arch action by flexural cracks based on finite element analysis, before flexural cracking (left) & after flexural cracking (right): Kim & White (1991)

In simply supported RC beams under point loading, the bending moment at the critical section distance a_c from the support section is expressed by Va_c in which V is the applied shear force. Then the calculated steel force at the critical section is,

$$T_0 = \frac{Va_c}{Z_0} \tag{A3}$$

Substituting equation A3 along with the magnification factors for effect of bond and arch action into equation, the shear stress at the critical section can be expressed as,

$$v_c = m_{arch}m_{bond}\left[\frac{V}{bZ_0}\right] \tag{A4}$$

When v_c reaches a limiting tensile stressf'_t, an inclined shear crack may initiate at a point in the critical zone, and the corresponding shear force is an inclined- shear cracking load $V_{cr,s}$, which can be derived from (A4)

$$V_{cr,s} = \frac{1}{m_{arch}m_{bond}}(f'_t bZ_0) \tag{A5}$$

The shear stress magnification factors have meaning only after flexural cracking has occurred. The corresponding shear force $V_{cr,f}$ at the critical section located a_c from the support can be determined from the flexural cracking moment M_{cr} as follows.

$$V_{cr,f} = \frac{M_{cr}}{a_c} \tag{A6}$$

A5 & A6 are the two cracking criteria over which Kim & White developed an equation to predict the critical section over which the flexural shear crack occurs.

By equilibrating and calibrating criteria A5 & A6, the following equation for critical crack position emerges.

$$a_c = k_3 \left[\frac{\rho(d/a)^2}{\left(1-\sqrt{\rho}\right)^2}\right]^{1/3} a$$

The constant K_3 is determined analytically to be 3.3.

$$a_c = 3.3 \left[\frac{\rho(d/a)^2}{\left(1-\sqrt{\rho}\right)^2}\right]^{1/3} a$$

Where, $\rho = reinforcement\ ratio$ $d = effective\ depth,$

$a = actual\ shear\ span,$ $a_c = critical\ crack\ position$

APPENDIX B

Simulation results of 1500 mm beams

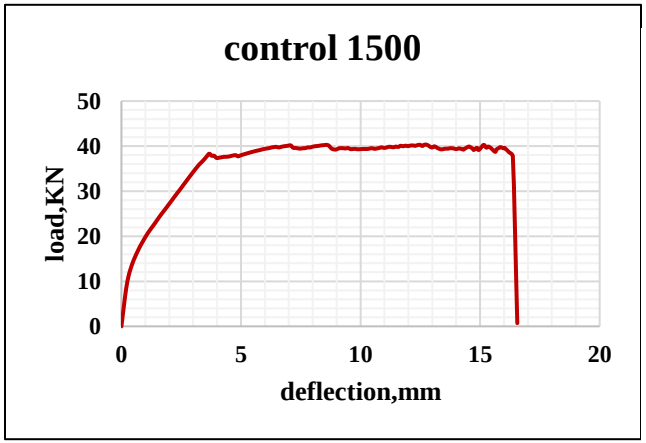

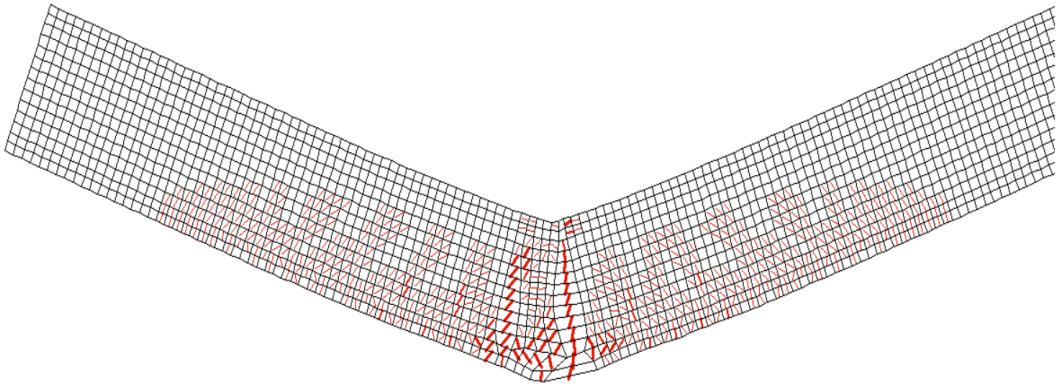

Figure B- 1; control 1500

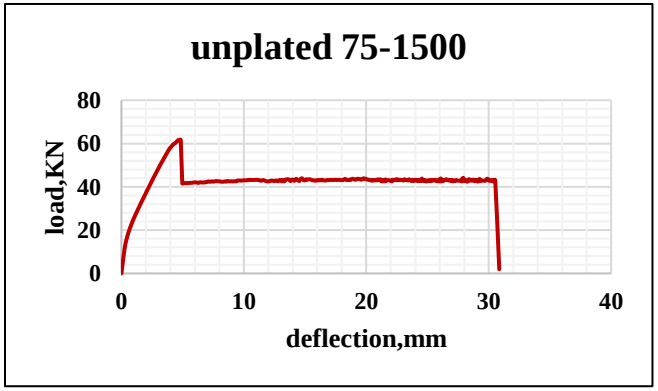

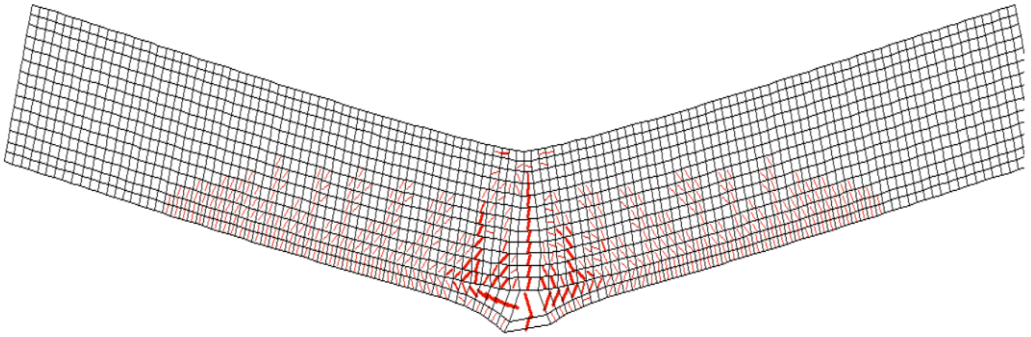

Figure B- 2; Unplated 75-1500

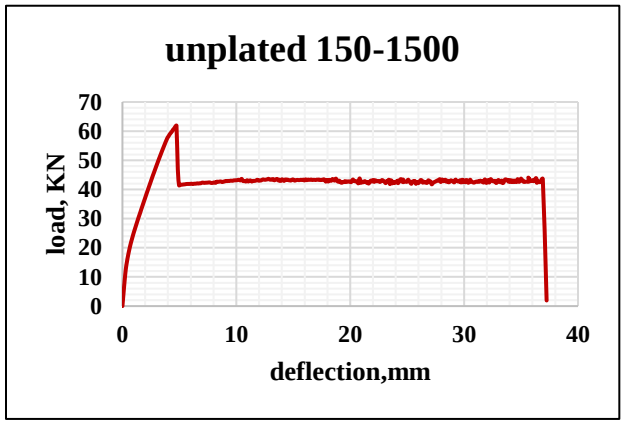

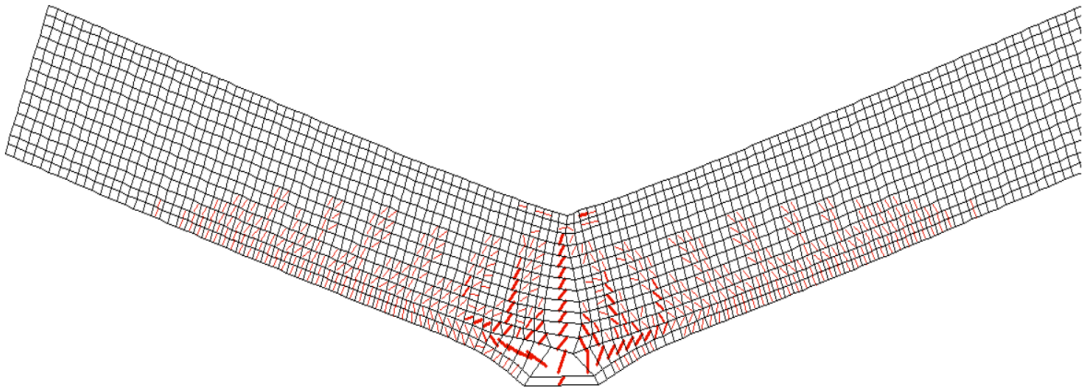

Figure B- 3; Unplated 150-1500

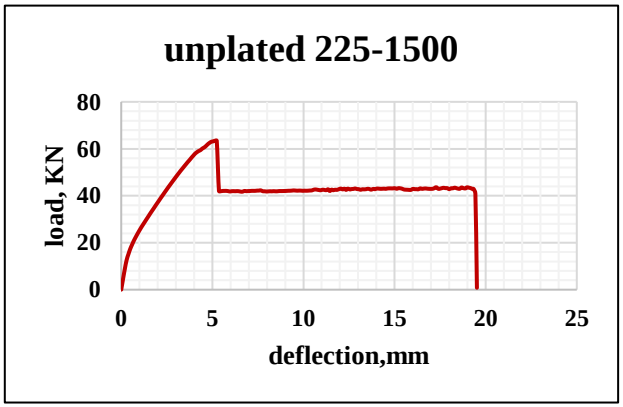

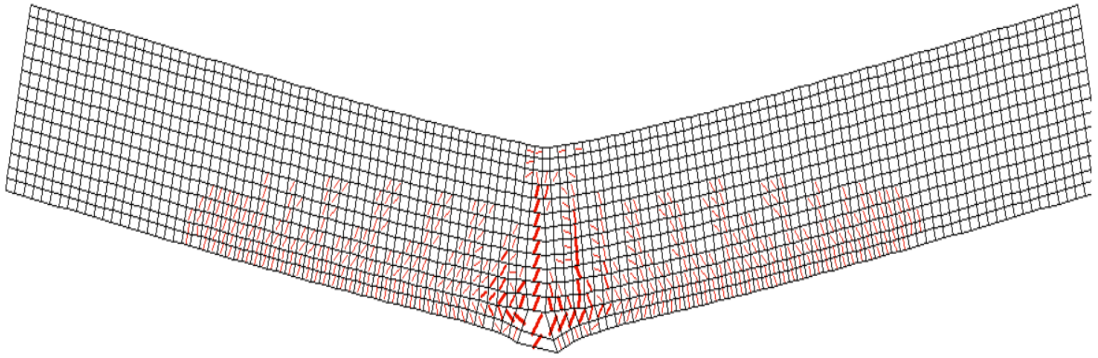

Figure B- 4; Unplated 225-1500

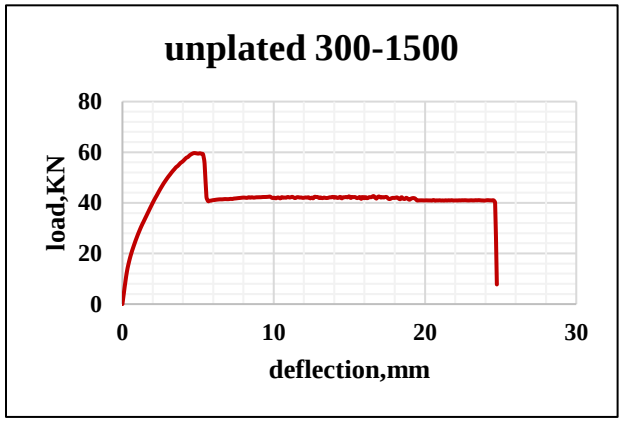

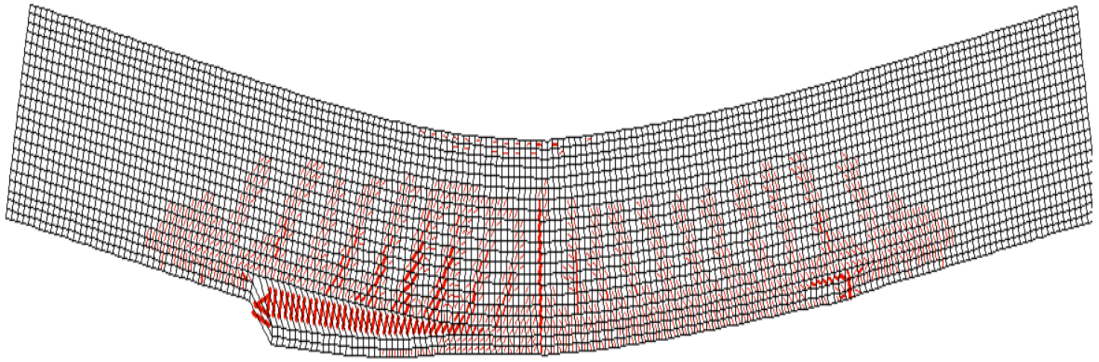

Figure B- 5; Unplated 300-1500

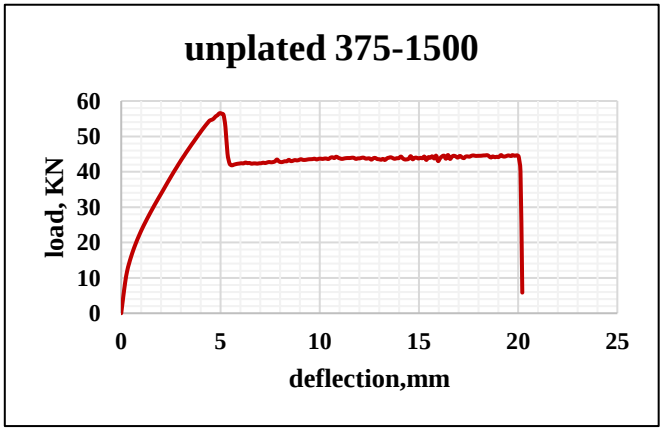

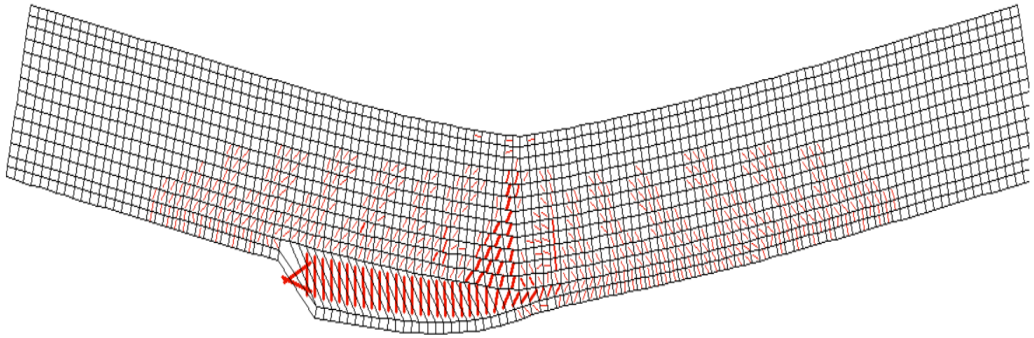

Figure B- 6; Unplated 375-1500

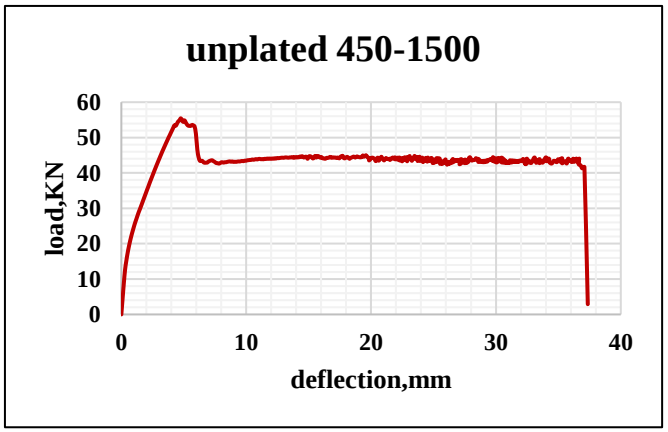

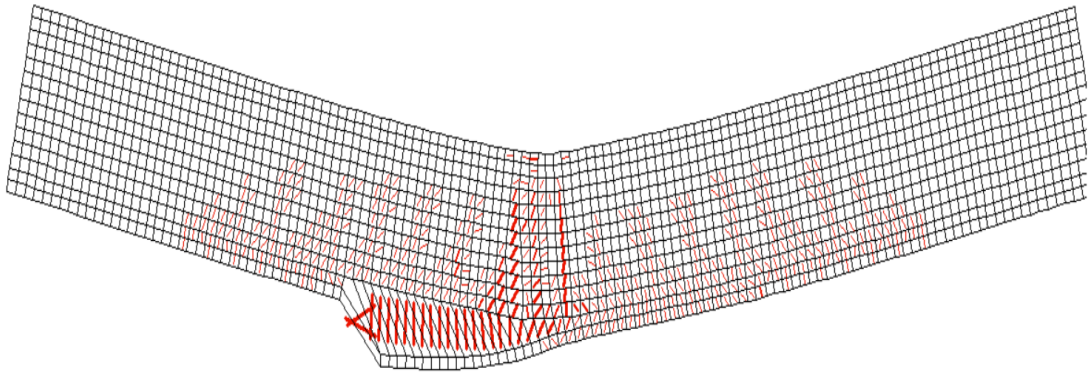

Figure B- 7; Unplated 450-1500

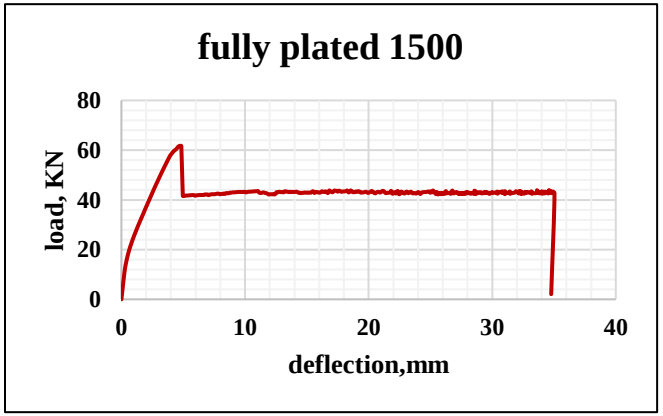

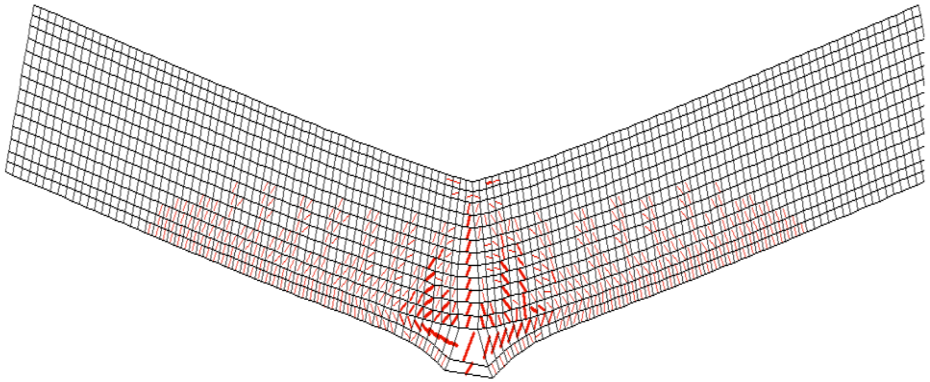

Figure B- 8; fully plated 1500

APPENDIX C

Simulation results of 2000mm beams

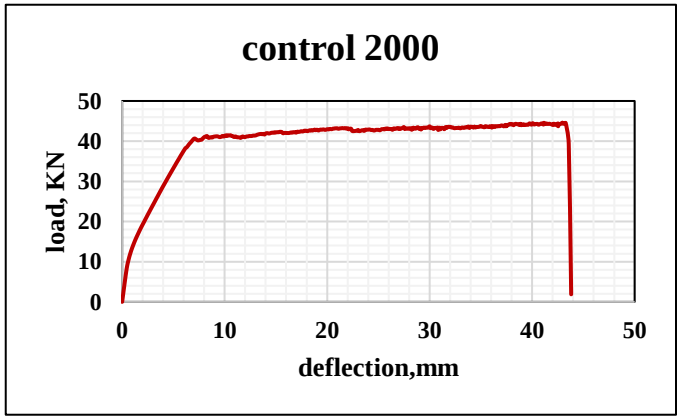

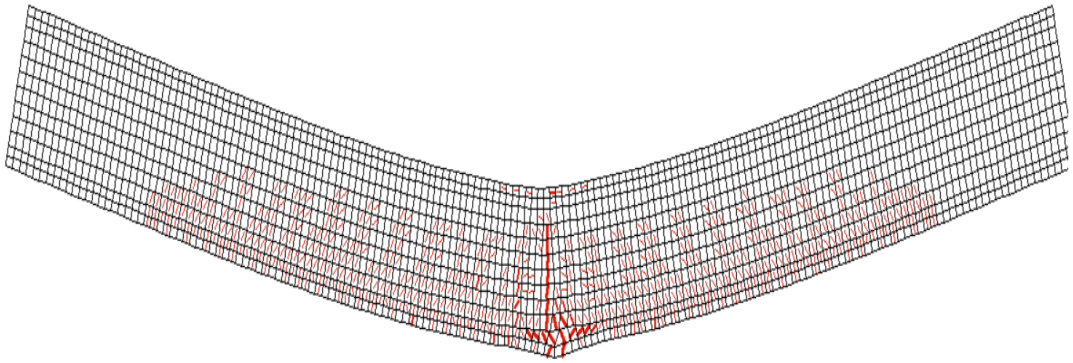

Figure C- 1; control 2000

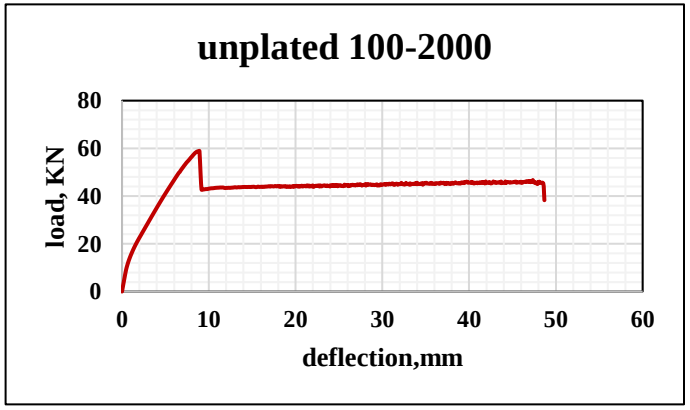

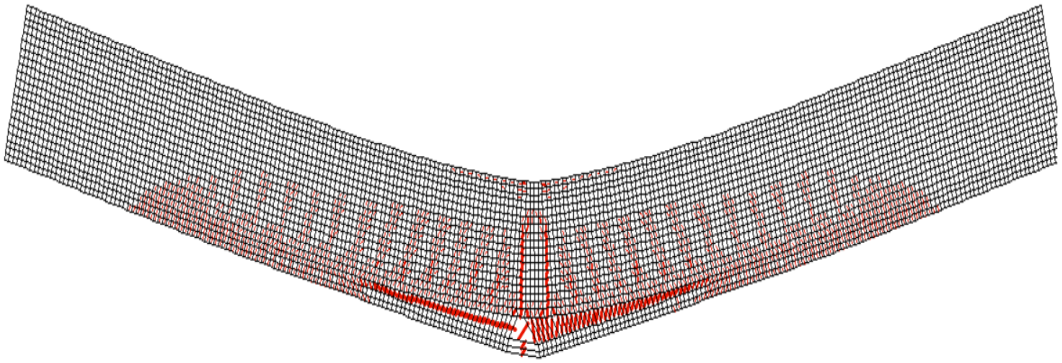

Figure C- 2; Unplated 100-2000

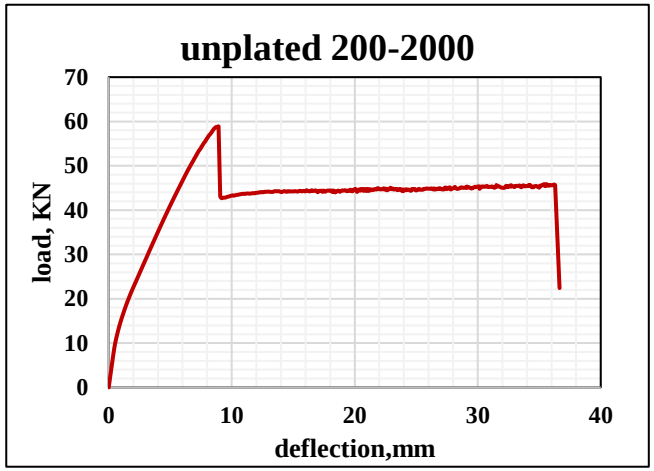

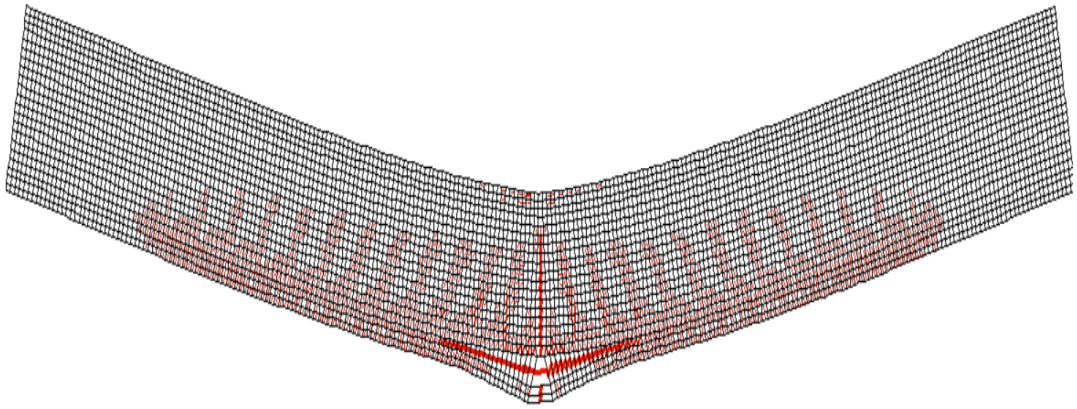

Figure C- 3; Unplated 200-2000

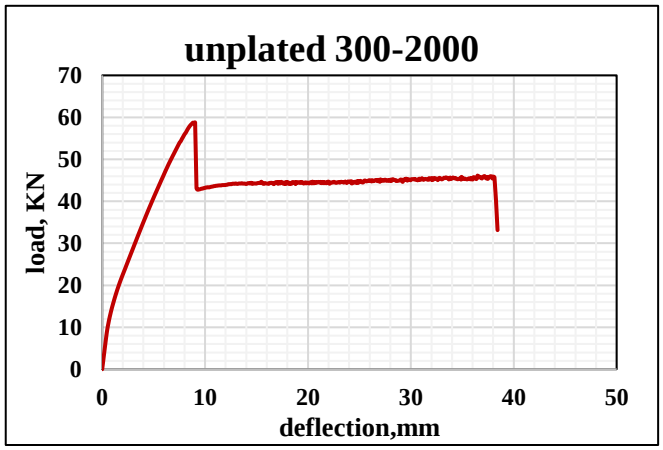

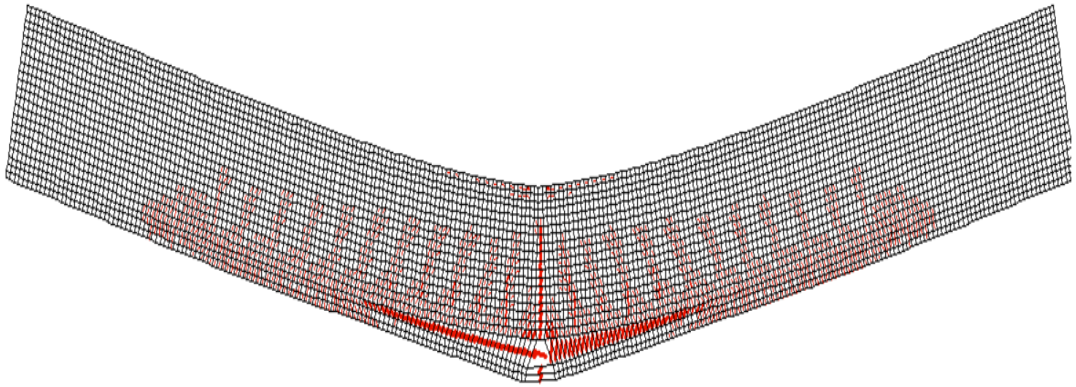

Figure C- 4; Unplated 300-2000

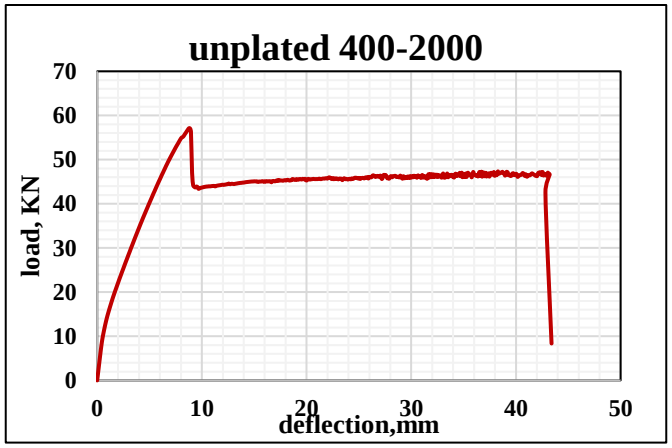

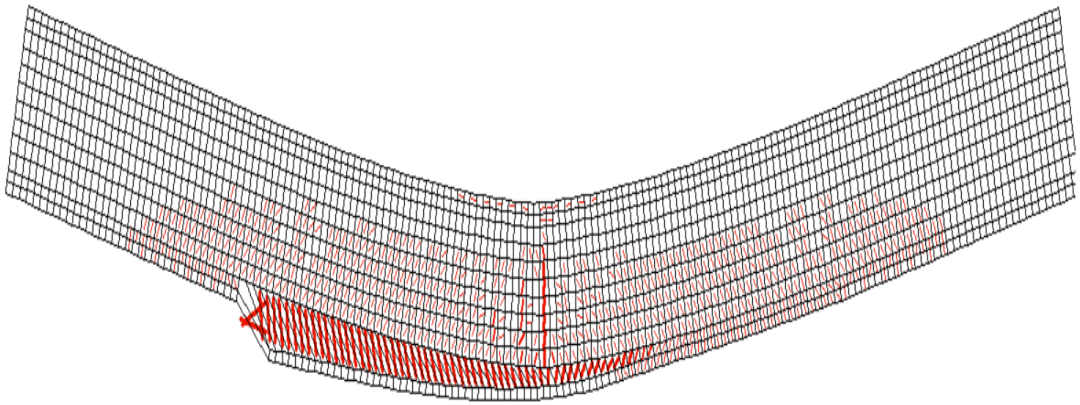

Figure C- 5; Unplated 400-2000

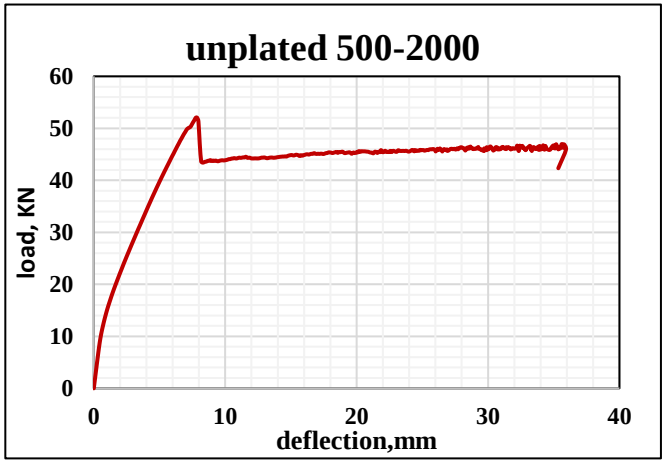

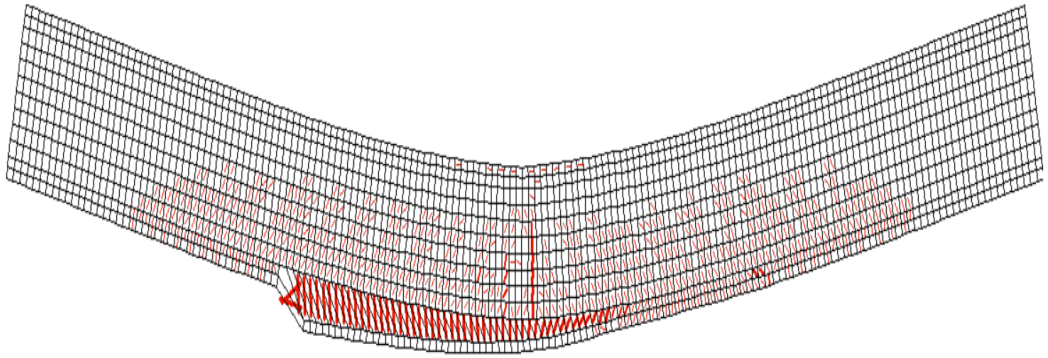

Figure C- 6; Unplated 500-2000

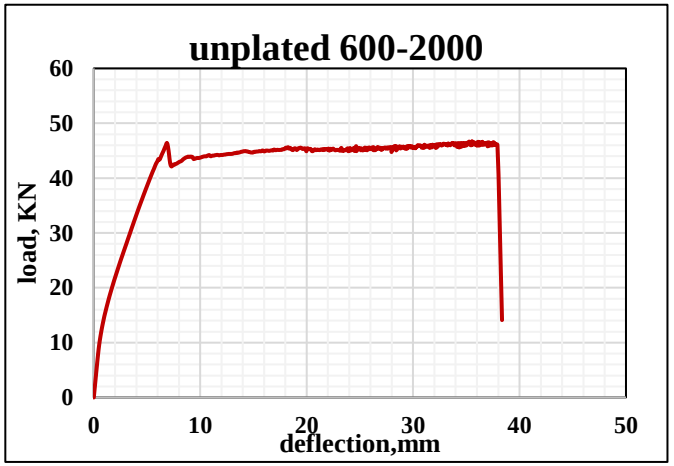

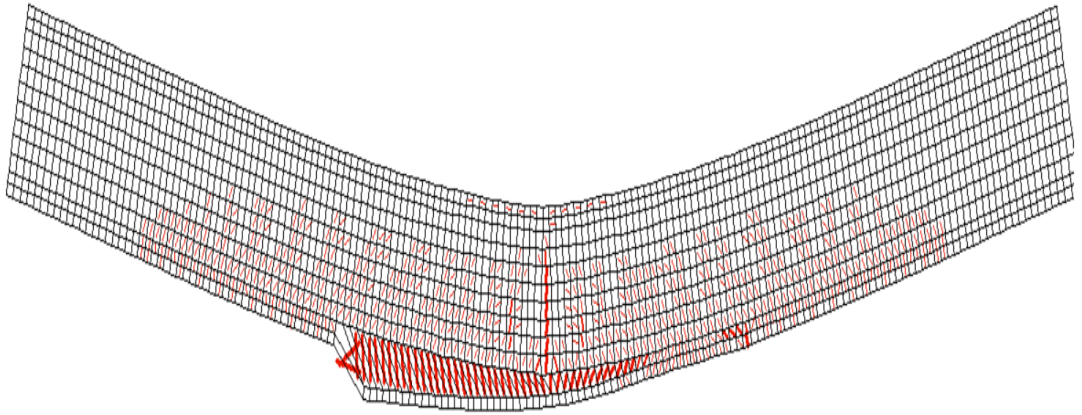

Figure C- 7; Unplated 600-2000

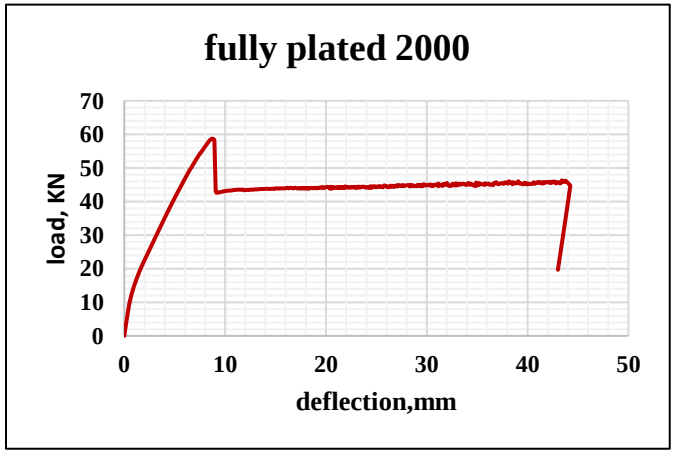

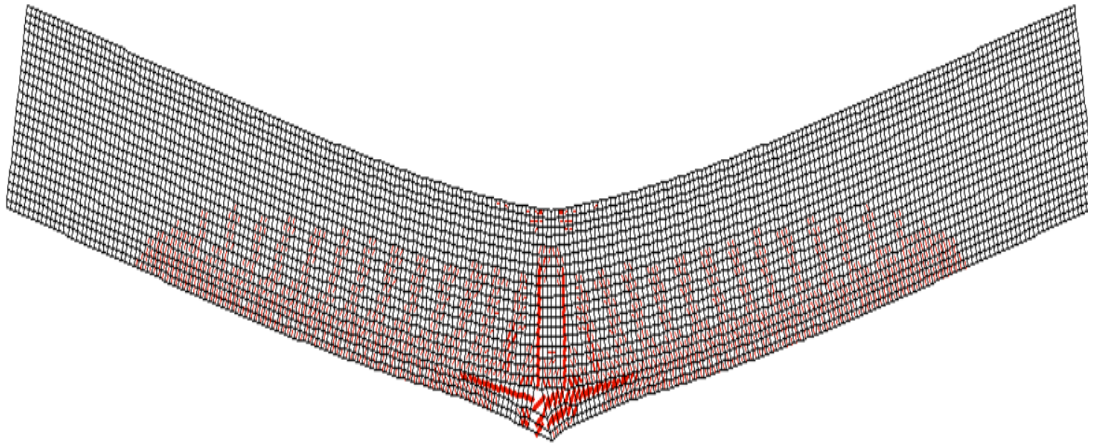

Figure C- 8; fully plated 20

Appendix-D

Analysis of specimen beams

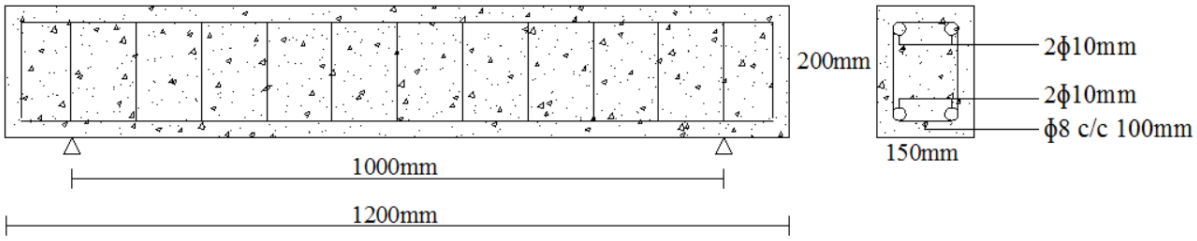

Material property

$fcd = \frac{0.85fck}{1.5} = \frac{0.85*18}{1.5}$ =10.2 MPa

$fyd = \frac{fyk}{1.15} = \frac{545}{1.15}$ = 473.9MPa

Assumption of failure

- Bottom steel yielding and outer most concrete reaching usable strain

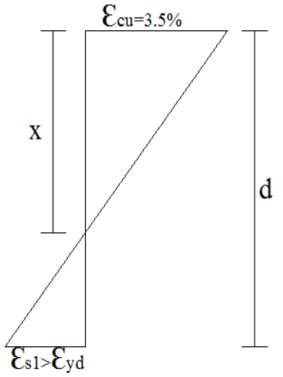

Similarity 1

$$\frac{x}{d-x} = \frac{3.5}{\varepsilon_{s1}} \Rightarrow \frac{d-x}{x} = \frac{\varepsilon_{s1}}{3.5} = \frac{\varepsilon_{s1}}{3.5} \Rightarrow \frac{d}{x} = \frac{\varepsilon_{s1}}{3.5} + 1$$

$$\frac{x}{d} = \frac{3.5}{\varepsilon_{s1}+3.5} \quad \text{(Similarity I)}$$

Similarity 2

$\frac{x}{3.5} = \frac{x-25}{\varepsilon_{s2}} \Rightarrow \varepsilon_{s2} = \frac{3.5(x-25)}{x}$ (Similarity II)

Equilibrium

$C_C = T_S$

$C_c = \alpha f c d b d + E_s \varepsilon_{s2} A_{s2}$

$T_S = A_{S1} f y d$

From this equivalence, we can rearrange to get the following equation.

$\alpha_c = 0.3 - 126.68\varepsilon_{s2}$ **(Equation 1)**

Using the parabolic rectangular stress-strain relationship;

For $\varepsilon_{c2} \leq \varepsilon_{cm} \leq \varepsilon_{cu2}$

$\alpha_c = k_x \left(\frac{3\varepsilon_{cm}-2}{3\varepsilon_{cm}}\right) \Rightarrow \alpha_c = \frac{29.75}{10.5\varepsilon_{s1}+36.75}$ **(Equation 2)**

By relating these two equation, we obtain a third equation of the following form.

$0.3 - 126.68\varepsilon_{s2} = \frac{29.75}{10.5\varepsilon_{s1}+36.75}$ **(Equation 3)**

Using the above similarity equations and the third equation, the following equivalence is attained which leads to the succeeding quadratic equation.

$(-374.7 + 19.5\varepsilon_{s1}) = \frac{29.75}{10.5\varepsilon_{s1} + 36.75}$

$\varepsilon_{s1}{}^2 - 15.72\varepsilon_{s1} - 67.4 = 0$

$\varepsilon_{s1} = 19.23 > \varepsilon_{yd} = \frac{545}{200{,}000} = 2.73$ …….coherent with initial assumption!

Substituting this value in similarity 1, x=25mm

Using this x value in similarity 2, $\varepsilon_{s2} = 0 < \varepsilon_{yd} = 2.7$ ……ok!

$M = \alpha_c f c d b d^2 (1 - \beta_c) + A_{s2} f y d (d - d_2)$

$\alpha_c \approx 0.125$

$\beta_c = \frac{x}{d}\left(\frac{\varepsilon_{cm}(3\varepsilon_{cm}-4)+2}{2\varepsilon_{cm}(3\varepsilon_{cm}-2)}\right) = 0.06422$

Inserting these, **M=14.89KN.m**